2mit

NASA TECHNICAL NOTE **NASA TN D-7444**

NASA TN D-7444

COMPUTED LATERAL POWER SPECTRAL DENSITY RESPONSE OF CONVENTIONAL AND STOL AIRPLANES TO RANDOM ATMOSPHERIC TURBULENCE

by Jacob H. Lichtenstein

Langley Research Center

Hampton, Va. 23665

NATIONAL AERONAUTICS AND SPACE ADMINISTRATION • WASHINGTON, D. C. • MARCH 1974

1. Report No.	2. Government Accession No.	3. Recipient's Catalog No.
NASA TN D-7444		

4. Title and Subtitle	5. Report Date
COMPUTED LATERAL POWER SPECTRAL DENSITY RESPONSE OF CONVENTIONAL AND STOL AIRPLANES TO RANDOM ATMOSPHERIC TURBULENCE	March 1974
	6. Performing Organization Code
7. Author(s)	8. Performing Organization Report No.
Jacob H. Lichtenstein	L-9035
	10. Work Unit No.
9. Performing Organization Name and Address	501-26-05-04
NASA Langley Research Center Hampton, Va. 23665	11. Contract or Grant No.
	13. Type of Report and Period Covered
12. Sponsoring Agency Name and Address	Technical Note
National Aeronautics and Space Administration Washington, D.C. 20546	14. Sponsoring Agency Code

15. Supplementary Notes

16. Abstract

A method of computing the power spectral densities of the lateral response of airplanes to random atmospheric turbulence has been adapted to an electronic digital computer. By use of this program, the power spectral densities of the lateral roll, yaw, and sideslip angular displacement of several conventional and STOL airplanes were computed. The results showed that for the conventional airplanes, the roll response was more prominent than that for yaw or sideslip response. For the STOL airplanes, on the other hand, the yaw and sideslip responses were larger than the roll response. The response frequency of the STOL airplanes generally was higher than that for the conventional airplanes. This combination of greater sensitivity of the STOL airplanes in yaw and sideslip and the frequency at which they occur could be a factor causing the poor riding qualities of this class of airplanes.

17. Key Words (S ed by Author(s))	18. Distribution Statement
Power spectral density response of airplanes Airplane response to gusts STOL airplane response	Unclassified – Unlimited STAR Category 02

19. Security Classif. (of this report)	20. Security Classif. (of this page)	21. No. of Pages	22. Price*
Unclassified	Unclassified	~~89~~ 91	$4.00

*For sale by the National Technical Information Service, Springfield, Virginia 22151

COMPUTED LATERAL POWER SPECTRAL DENSITY RESPONSE OF CONVENTIONAL AND STOL AIRPLANES TO RANDOM ATMOSPHERIC TURBULENCE

By Jacob H. Lichtenstein
Langley Research Center

SUMMARY

A method of computing the power spectral densities of the lateral response of airplanes to random atmospheric turbulence has been adapted to an electronic digital computer. By use of this program, the power spectral densities of the lateral roll, yaw, and sideslip angular displacement of several conventional and STOL airplanes were computed. The results showed that for the conventional airplanes, the roll response was more prominent than that for yaw or sideslip response. For the STOL airplanes, on the other hand, the yaw and sideslip responses were larger than the roll response. The response frequency of the STOL airplanes generally was higher than that for the conventional airplanes. This combination of greater sensitivity of the STOL airplanes in yaw and sideslip and the frequency at which they occur could be a factor causing the poor riding qualities of this class of airplanes.

INTRODUCTION

Air transportation between the centers of major metropolitan areas has been severely threatened in both adequacy and convenience by the rapidly increasing urban population growth. The growth is seen both in the total population as well as in the sprawl into the outlying suburban areas. As a result, airport facilities for the large commercial jet transports, already overloaded by a constantly increasing traffic density, can only be expanded in regions far from the inner city. These developments have sharpened the air transportation industries' interest in short take-off and landing vehicles (STOL). These aircraft could utilize new airports with greatly reduced runway lengths located closer to the population centers. Consequently, short-haul air transportation could be made more convenient while, at the same time, congestion at airports designed primarily for the large long-haul transport airplanes could be alleviated.

One of the requirements for a STOL operation to date has been that of a relatively light wing loading for the vehicle at least during the landing phases of the flight. Unfortunately, the response of an airplane to atmospheric turbulence is inversely related to its

wing loading. Thus, the large response of an airplane with light wing loading could result in poor riding qualities. An evaluations test report (ref. 1) on the suitability of an airplane, which is typical of the STOL type of aircraft, for airline operation discusses its unsatisfactory riding qualities in rough air, particularly in the lateral-directional mode.

The subject of riding qualities of aircraft has been investigated and a synopsis of the current knowledge of the subject can be found in reference 2. At present, there are few generally accepted criteria for defining good or acceptable riding qualities. Moreover, the specific aircraft characteristics which contribute to good riding qualities are not clearly understood. It is apparent, however, that the motion of the airplane in response to atmospheric turbulence is one of the contributing factors.

Since atmospheric turbulence is most appropriately treated analytically as a random quantity, predicted aircraft motion resulting from turbulence excitation will also be random and can only be described in a statistical manner. An overall discussion of the dynamic response of airplanes to atmospheric turbulence is given in reference 3. Three measures of the response are the response power spectrum, the response root-mean-square (rms) value, and the expected number of exceedances of a given response level. Of these, the output power spectrum will yield information most directly related to configuration differences. A correlation of the frequencies at which maximum response occurs with those that cause the most discomfort in airplane passengers may indicate areas in which the airplane behavior should be altered. In the present paper, the lateral-directional power spectral response of a group of twelve airplanes, of various configurations including potential STOL vehicles, has been computed by use of the method presented in reference 4. The power spectra are presented both for use in future studies relating to ride qualities and as a basis for the observations made herein.

SYMBOLS

Values are given in both SI and U.S. Customary Units. The measurements and calculations were made in U.S. Customary Units.

A aspect ratio

b wing span, m (ft)

$C_{D,0}$ drag coefficient at zero lift

C_L lift coefficient, $\frac{\text{Lift}}{qS}$

C_l rolling-moment coefficient, $\frac{\text{Rolling moment}}{qSb}$

C_n yawing-moment coefficient, $\frac{\text{Yawing moment}}{qSb}$

C_Y side-force coefficient, $\frac{\text{Side force}}{qS}$

D nondimensional operator, $\frac{b}{U}\frac{d}{dt}$

G matrix containing stability derivatives relating airplane moments and forces to gust velocities

h altitude, m (ft)

h_Z height of center of pressure of vertical tail above X-axis, m (ft)

K_X nondimensional radius of gyration about X-axis, k_X/b

K_Z nondimensional radius of gyration about Z-axis, k_Z/b

K_{XZ} nondimensional product of inertia, k_{XZ}/b^2

k_X, k_Z radii of gyration, m (ft)

k_{XZ} product of gyration, m^2 (ft^2)

L integral scale of turbulence, m (ft)

l_T tail length measured from center of gravity to center of pressure of vertical tail, m (ft)

p rolling velocity, $\dot{\phi}$, rad/sec

q dynamic pressure, $\frac{1}{2}\rho U^2$, N/m^2 (lb/ft^2)

r yawing velocity, $\dot{\psi}$, rad/sec

S wing area, m^2 (ft^2)

s profile height (refer to sketch (a)), m (ft)

t time, sec

U	relative velocity between airplane and general air mass, m/sec (ft/sec)
u	velocity along X-axis (U on figures), m/sec (ft/sec)
v	velocity along Y-axis (V on figures), m/sec (ft/sec)
W	mass of airplane, kg (lb)
w	velocity along Z-axis (W on figures), m/sec (ft/sec)
X,Y,Z	three orthogonal axes of airplane
x,y,z	coordinates with reference to X-, Y-, and Z-axes, m (ft)
α_0	trim (steady-state) angle of attack, deg (rad)
β	angle of sideslip, rad
Γ	dihedral angle, deg
γ	flight-path angle, rad
Δ	matrix of airplane equations of motion in still air (see ref. 1)
ζ	damping ratio between actual damping and critical damping
μ	relative density factor, $\frac{\text{Mass}}{\rho Sb}$
ρ	density of atmosphere, kg/m^3 ($slugs/ft^3$)
σ	sidewash angle, rad
$\sigma_\phi,\sigma_\psi,\sigma_\beta$	root-mean-square value of roll, yaw, and sideslip angle per unit root-mean-square gust velocity, rad/(m/sec) (rad/(ft/sec))
Φ_f	power spectral density of function f
ϕ	angle of roll, rad
ψ	angle of yaw, rad

ω circular frequency, rad/sec

ω_n undamped natural frequency, rad/sec

$| \; |$ absolute value of a quantity (determinant of a matrix)

$[\;]$ rectangular matrix

$\{ \}$ column matrix

Stability derivatives of airplane are indicated by subscript notation; for example,

$$C_{l_r} = \frac{\partial C_l}{\partial\left(\frac{rb}{2U}\right)} \qquad C_{n_p} = \frac{\partial C_n}{\partial\left(\frac{pb}{2U}\right)} \qquad C_{Y_\beta} = \frac{\partial C_Y}{\partial\left(\frac{v}{U}\right)}$$

Subscripts:

F fuselage

g gust

T vertical tail

W wing

0 initial conditions

A bar over a quantity denotes a mean value.

PROCEDURE

Power Spectra of Airplane Response

The airplanes considered in this investigation are assumed to be rigid bodies with fixed control surfaces in straight and level flight. Quasi-steady aerodynamic forces are employed. The gust input consists of three orthogonal velocity components which are uncorrelated and each represented with a one-dimensional power spectrum. Spanwise variations in gust velocity are assumed to be negligible. The airplane is executing small motions in sideslip, yaw, and roll described by the linear equations of motion normally employed in stability analyses. The governing equations are developed in detail in reference 4. Expressions for the response power spectra which have been numerically evaluated for the various airplane configurations given in this paper are described in outline form in the following discussion.

The lateral-directional equations of motion as given in reference 4 are

$$[\Delta]\begin{Bmatrix} D\phi_0 \\ D\psi_0 \\ \beta_0 \end{Bmatrix} = [G]\begin{Bmatrix} D\phi_g \\ D\psi_g \\ \beta_g \end{Bmatrix} \tag{1}$$

where the terms ϕ_0, ψ_0, and β_0 are with respect to the general air mass and the matrix $[\Delta]$ is the familiar "still air" rigid airframe characteristic equation and the matrix $[G]$ gives the relationship between the aerodynamic moments and forces resulting from the gust velocities encountered. Linear and angular velocity components of the airplane relative to the still air and the gust constitute the elements of the vectors $D\phi_0$ and $D\phi_g$, respectively. A solution in the frequency domain ω, that is, the frequency response function, is defined by

$$\begin{Bmatrix} \phi_0(\omega) \\ \psi_0(\omega) \\ \beta_0(\omega) \end{Bmatrix} = [\Delta(\omega)]^{-1}[G(\omega)]\begin{Bmatrix} D\phi_g(\omega) \\ D\psi_g(\omega) \\ \beta_g(\omega) \end{Bmatrix} \tag{2}$$

The frequency dependent forms of the $[\Delta]$ and $[G]$ matrices are

$$[\Delta(\omega)] = \begin{bmatrix} \left(-2\mu K_x{}^2 \frac{b^2}{U^2}\omega^2 - \frac{1}{2}C_{l_p}i\omega\right) & \left(+2\mu K_{xz}\frac{b^2}{U^2}\omega^2 - \frac{1}{2}C_{l_r}i\omega\right) & \left(-C_{l_\beta}\right) \\ \left(2\mu K_{xz}\frac{b^2}{U^2}\omega^2 - \frac{1}{2}C_{n_p}i\omega\right) & \left(-2\mu K_z{}^2\frac{b^2}{U^2}\omega^2 - \frac{1}{2}C_{n_r}i\omega\right) & \left(-C_{n_\beta}\right) \\ \left(-\frac{1}{2}C_{Y_p}i\omega - C_L\right) & \left[\left(2\mu - \frac{1}{2}C_{Y_r}\right)i\omega - C_L\tan\gamma\right] & \left(2\mu i\omega - C_{Y_\beta}\right) \end{bmatrix}$$

and

$$[G(\omega)] = \begin{bmatrix} \left(\frac{1}{2}C_{l_p}\right)_W & \left(\frac{1}{2}C_{l_r}\right)_W & \left[C_{l_\beta}(\omega)\right]_{WT} \\ \left(\frac{1}{2}C_{n_p}\right)_W & \left(\frac{1}{2}C_{n_r}\right)_W & \left[C_{n_\beta}(\omega)\right]_{FT} \\ 0 & 0 & \left[C_{Y_\beta}(\omega)\right]_{FT} \end{bmatrix}$$

The frequency-dependent expressions for $C_{l_\beta}(\omega)$, $C_{n_\beta}(\omega)$, and $C_{Y_\beta}(\omega)$ are given in appendix C of reference 4. The s and x dimensions given in table I and used in obtaining these derivatives are illustrated in sketch (a).

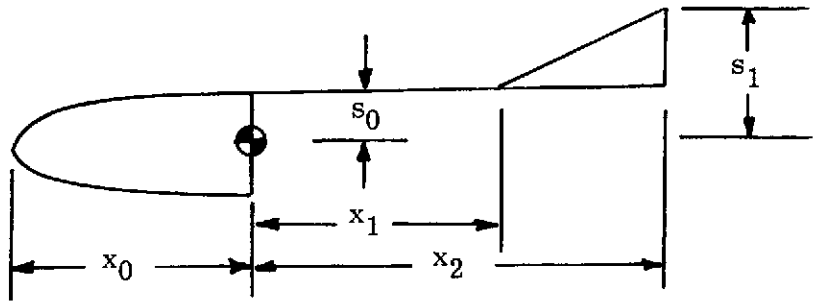

Sketch (a)

For linear second-order systems, the output power spectrum is equal to the product of the square of the amplitude of the frequency-response function and the input power spectrum. An analogous expression is derived for the three-degree-of-freedom lateral-directional motion in reference 4 in which it is assumed that any cross power between the gust-velocity components is negligible. The following relationships for the gust spectra and gust velocities:

$$\Phi_{v_g}(\omega) = \Phi_{w_g}(\omega) = U^2\Phi_{\beta_g}(\omega)$$

$$\overline{u_g^2} = \overline{v_g^2} = \overline{w_g^2}$$

which result from the assumptions of homogeneous isotropic turbulence permit the gust inputs to be specified in terms of a single quantity, the side gust spectrum Φ_{β_g}. The final equations are given by

$$\begin{Bmatrix} \Phi_\phi \\ \Phi_\psi \\ \Phi_\beta \end{Bmatrix} = \begin{bmatrix} \left|\frac{\phi}{D\phi_g}\right|^2 & \left|\frac{\phi}{D\psi_g}\right|^2 & \left|\frac{\phi}{\beta_g}\right|^2 \\ \left|\frac{\psi}{D\phi_g}\right|^2 & \left|\frac{\psi}{D\psi_g}\right|^2 & \left|\frac{\psi}{\beta_g}\right|^2 \\ \left|\frac{\beta}{D\phi_g}\right|^2 & \left|\frac{\beta}{D\psi_g}\right|^2 & \left|\frac{\beta}{\beta_g}\right|^2 \end{bmatrix} \begin{Bmatrix} \left|\frac{D\phi_g}{\beta_g}\right|^2 \\ \left|\frac{D\psi_g}{\beta_g}\right|^2 \\ 1 \end{Bmatrix} \Phi_{\beta_g} \tag{3}$$

All numerical results presented in a later section were obtained through application of equation (3) together with the appropriate form for the input gust spectra Φ_{β_g} discussed in the next section.

Gust Velocity Power Spectrum

Numerous analytical representations of atmospheric turbulence spectra have been proposed. Of these, the two which have won greatest acceptance are the Dryden (used for fitting wind-tunnel turbulence data) and the von Karman (based on the theory of isotropic turbulence). A comprehensive discussion of the relative merits of the two spectra is given in reference 3 wherein it is concluded that the von Karman spectrum is more representative of atmospheric turbulence. Nevertheless, the Dryden spectrum is more amenable to theoretical studies because certain integrals encountered in the analysis may be readily evaluated in closed form. The quantities in equation (3), $\left|\frac{D\phi_{\xi}}{\beta_g}\right|^2$ and $\left|\frac{D\psi_g}{\beta_g}\right|^2$, that is, the ratio of the rolling gust spectrum and yawing gust spectrum to the side gust spectrum, as given in reference 4, are both based on the Dryden spectrum. Therefore, for the purposes of this paper, the accuracy required does not warrant incorporating the von Karman spectrum.

A theoretical treatise on turbulence (ref. 5) and flight measurements (ref. 6) have shown that for the turbulence in the atmosphere spanning the frequency range that affects the airplane dynamic response, the power spectra can be expressed as

$$\frac{\Phi_{v_g}}{\overline{v_g^2}} = \frac{\Phi_{w_g}}{\overline{w_g^2}} = \frac{L}{\pi U} \frac{1 + 3(k')^2}{\left(1 + (k')^2\right)^2} \tag{4}$$

for the lateral components, and for the longitudinal components

$$\frac{\Phi_{u_g}}{\overline{u_g^2}} = \frac{2L}{\pi U} \frac{1}{1 + (k')^2} \tag{5}$$

where $k' = \frac{\omega L}{U}$.

In addition, the data in reference 5 indicate that the scale length of the turbulence L should be on the order of 304.8 m (1000 ft) to 609.6 m (2000 ft), but closer to 304.8 m (1000 ft). Consequently, for this paper, a value of 335.3 m (1100 ft) and a root-mean-square gust velocity of 1.8288 m/sec (6 ft/sec) were used.

PRESENTATION OF RESULTS

The power spectral densities of the lateral angular response (ϕ, ψ, and β), given by equation (3), have been computed for 12 airplanes. A listing of the aircraft, pertinent geometric and aerodynamic characteristics, and flight conditions is given in table I.

The airplanes are grouped together in the following manner: the three conventional airplanes are called C-A, C-B, and C-C; the five airplanes classified as large STOL airplanes are called LS-A, LS-B, LS-C, LS-D, and LS-E; and the four relatively small STOL airplanes are called SS-A, SS-B, SS-C, and SS-D.

In addition to the data presented, computations also were made for airplanes A, B, and C of reference 4. Agreement of the results was good, as would be expected, the difference being mainly due to the mechanics of computation. The results, therefore, are not repeated in the present paper.

The first group of data presented consists of sets of data for the conventional airplanes. The data for the first airplane (C-A) are for the stability derivatives obtained by using the method presented in reference 7; the second set of data (C-B) are for the same airplane but for the stability derivatives generally obtained by the Datcom method presented in reference 8, the wing-alone derivatives being obtained by the method presented in reference 9; the third set (C-C) is for an enlarged version of the same airplane, the derivatives generally being obtained by the Datcom method. These results are presented in figures 1 to 3.

The next group consists of airplanes currently representative of large STOL vehicles. There are two versions of the first airplane designated LS-A and LS-B. The first was represented with stability derivatives obtained in a manner similar to the conventional airplane; the second used aerodynamic derivatives obtained during a riding qualities investigation conducted on an NASA moving-base simulation of the airplane. The derivatives were developed by modifying the initial derivatives used in the simulator until the pilots judged that the flight characteristics of the simulator closely matched those of the actual airplane. The derivatives are used in the present paper in order to compare the responses of the same airplane described with data obtained by two alternate procedures. The results are presented in figures 4 and 5. The results for LS-C, LS-D, and LS-E (both the Mach 0.36 and Mach 0.75 results) presented in figures 6, 7, and 8, respectively, were obtained by using the derivatives developed generally by the Datcom procedures with the wing-alone derivatives being computed by the method given in reference 9.

The last group consists of small STOL airplanes. Three sets of data for the first airplane are shown. The aerodynamic derivatives were the same and were obtained by the Datcom method. Two versions (original and modified inertias) differed only in their moments of inertia; the third set was computed for a different flight altitude which was

comparable with most of the other airplanes. These results are shown in figures 9, 10, and 11. The results for the other airplane (LS-D) are presented in figure 12 and the aerodynamic derivatives were obtained from reference 10.

The data presented in figures 13, 14, and 15 are comparisons of the airplanes arranged in three convenient groups (conventional, large STOL, and small STOL). These data are for the square root of the dimensional power spectral density which is indicative of the magnitude of the angular displacement.

One airplane representative of each of the groups of airplanes in figures 13, 14, and 15 is presented together in figure 16 for comparison.

The root-mean-square values of the various roll, yaw, and sideslip angles per unit root-mean-square gust velocity are presented on the initial figure of the set for each airplane. These values were obtained by integrating the response power spectral densities over the frequency range from 0.01 rad/sec to 60 rad/sec.

DISCUSSION

The power spectral densities developed in this investigation did not reveal a major reason for the fact that the STOL-type airplanes had poor riding qualities compared with a conventional airplane. However, there were several minor differences which, when taken together, could point up some conditions that lead to the different riding qualities.

Conventional Airplanes

The power spectral densities of the conventional airplanes were computed as representative of typical contemporary transports. The pattern of the results for all three airplanes (figs. 1 to 3) is nearly the same and their magnitudes are quite close. They exhibit a peak in the response at a frequency that corresponds to that for the Dutch roll. The main differences between the various power spectral densities for the airplanes are that the Datcom versions peak at a slightly higher frequency (see table in next section) and their magnitude is smaller.

The frequency difference is due to the larger value of C_{n_β} of the Datcom version (-0.17 as compared with -0.14). The magnitude difference is due to the somewhat greater damping $\left(C_{n_r} = -0.30 \text{ compared with } C_{n_r} = -0.23\right)$ of the Datcom version. In all three cases the roll angle seemed to be the most sensitive in that its power spectral density was about one-half an order of magnitude larger than the yaw or sideslip angle.

The roll response of the airplane to the various gust components is very dependent upon the values of the stability derivatives. For instance, if figures 1(b) and 2(b) are compared, it can be seen that for the C-A, the vertical (w) gust component is the most effective in inducing the roll response; however, for the Datcom version (C-B), both the

vertical (w) and side (v) components are nearly equally effective. A comparison of figures 1(c) and 1(d) for the yaw response shows a similar result. The longitudinal gust component (u) shows relatively little effect on any of the responses.

This effect of the various components on yaw response is due mainly to the different values in the derivatives C_{n_r} and C_{n_β}. (See preceding discussion, table I, and the values used for the tail parameters $\left(C_{Y_{\beta,T}}, \sigma_{\beta_T}, \text{etc.}\right)$.) This result illustrates the importance of using the best possible methods of estimating the stability derivatives in order to insure the most representative response picture.

STOL Airplanes

The power spectral density data for the STOL-type airplanes as a group (figs. 4 to 12) except for the blown-flap configurations (LS-D and LS-E) exhibit a different pattern from the previously discussed conventional airplanes. These STOL airplanes do not exhibit the sharp peak in power spectral density at the Dutch roll frequency and, in addition, the yaw and sideslip response is generally greater in this region than the roll response. The response of the larger STOL airplanes (LS-A, etc.) is slightly larger than that for the conventional aircraft, as can be seen from the values of σ_ϕ, σ_ψ, and σ_β (SS-A, etc.); however, for the small STOL airplanes, the response is considerably larger. (Compare figs. 9 to 12 with figs. 1 to 3.) The magnitude of the response, in general, could be expected to be related to the airplane wing loading and, since the larger STOL airplanes and the conventional airplanes are about the same, their responses also are similar in magnitude. For the small STOL airplanes, the wing loading was much lower and the response appreciably larger.

Looking at two versions of the same airplane, the LS-A and the LS-B simulator, shows that the simulator version (LS-B) has a somewhat higher peak in the response (near the natural frequency) and at a slightly lower frequency than the regular version. (Compare figs. 4 and 5.) The difference in response is entirely due to the difference in aerodynamic data. The simulator version has smaller damping in yaw $\left(C_{n_r}\right.$ of -0.46 compared with -0.58$\left.\right)$, which permits larger magnitudes of the perturbations, and a lower C_{n_β} $\left(C_{n_\beta}\right.$ of 0.27 compared with 0.46$\left.\right)$ which results in a lower frequency.

The effect of velocity changes is shown in the data for the LS-D and LS-E airplanes. (See figs. 7 and 8.) Here the velocity has been changed by a factor of 2 and the dynamic pressure consequently by a factor of 4. It can be seen by comparing figures 7(e) and 8(e) that the magnitude of the peak response is inversely proportional to the velocity, and the frequency at which the peak response occurs is proportional to the velocity.

The data for the various versions of the same airplane (SS-A to SS-C) show only minor changes in either pattern or magnitude even though the inertias have changed about 100 percent from the Datcom version to the modified inertia version. This result indi-

cates that changes in the magnitude of the moment of inertia on the order of 2 do not have a significant effect on the overall power spectral response of the airplane. The effect of the relatively small change in altitude (2591 m to 1524 m or 8500 ft to 5000 ft) was nearly undetectable.

Comparison of the STOL and Conventional Airplanes

An interesting fact is that for these STOL airplanes, even the roll response generally is influenced mainly by the lateral gusts rather than by the vertical gusts as for the conventional airplanes. Thus, the full effects of turbulence can influence the airplane response even at low altitudes during a landing approach where the proximity of the ground seriously restricts the vertical gust components. This result may be a part of the explanation for this class of airplanes being described as having very poor riding qualities during the landing-approach phase of a flight.

The data in the following table show that although the STOL airplanes generally have higher damping, their natural frequency is also higher and approaches 0.5 Hz. This frequency may put the airplane response into the frequency range where it would be annoying to the passengers.

Airplane	Computed natural frequency, ω_n, rad/sec	Damping ratio, ζ
Conventional airplane		
A	1.57	0.110
B	1.81	.112
C	1.79	.073
Large STOL airplane		
A	3.24	.237
B	2.49	.221
C	1.09	.547
D	2.26	.052
E	4.50	.107
Small STOL airplane		
A	2.29	.370
B	2.68	.256
C	2.67	.258
D	3.04	.257

The information of figure 16 comparing the various types of airplanes shows that the light wing-loaded STOL (SS-A) has considerably larger responses for all three lateral angles than the other airplanes. Except for the peak at the Dutch roll frequency (airplane C-A) the roll response is similar for both the LS-B and C-A. However, the yaw and sideslip responses are generally larger for the LS-B (again except for the peak) than for the C-A. (See fig. (15).) This combination of larger sideslip and yaw would result in larger lateral accelerations. Since people exhibit a lower acceptance level for the lateral acceleration than in the other directions, this condition may be a source of passenger discomfort.

CONCLUDING REMARKS

A method of computing the power spectral densities of the lateral angular response of airplanes to random atmospheric turbulence has been adapted to an electronic digital computer. By use of this program, the power spectral densities of the lateral angular displacement of several conventional and STOL airplanes were computed. The results of the computations showed that the conventional airplanes had a sharp peak in the response at the Dutch roll frequency, the roll response being more prominent than the yaw or sideslip response. The STOL type of airplanes, on the other hand, generally did not have much of a peak at the Dutch roll frequency, but the yaw and sideslip response was larger than the roll response.

The large STOL airplanes which sizewise were comparable to the conventional airplane generally had somewhat larger response and at a higher frequency which put their behavior closer to the region of possible passenger discomfort. A more definitive reason for the poorer ride qualities was not apparent from the present calculations.

Langley Research Center,
National Aeronautics and Space Administration,
Hampton, Va., December 12, 1973.

REFERENCES

1. Anon.: Inter-Metropolitan STOL Evaluation (Phase X). Develop. Engineer. Rep. 50, American Airlines, Jan. 1970.

2. Anon.: Symposium on Vehicle Ride Quality. NASA TM X-2620, 1972.

3. Houbolt, John C.; Steiner, Roy; and Pratt, Kermit G.: Dynamic Response of Airplanes to Atmospheric Turbulence Including Flight Data on Input and Response. NASA TR R-199, 1964.

4. Eggleston, John M.; and Phillips, William H.: The Lateral Response of Airplanes to Random Atmospheric Turbulence. NASA TR R-74, 1960. (Supersedes NACA TN 3954 by Eggleston and TN 4196 by Eggleston and Phillips.)

5. Batchelor, G. K.: The Theory of Homogeneous Turbulence. Cambridge Univ. Press, 1959.

6. Crane, Harold L.; and Chilton, Robert G.: Measurements of Atmospheric Turbulence Over a Wide Range of Wavelength for One Meterological Condition. NACA TN 3702, 1956.

7. Lina, Lindsay J.; and Canavos, George C.: Influence of Angle of Glide Slope on the Accuracy of Performing Instrument Approaches in a Simulator. NASA TN D-4835, 1968.

8. Anon.: USAF Stability and Control Datcom. Contracts AF 33(616)-6460, AF 33(615)-1605, F33615-67-C-1156, F33615-68-C-1260, and F33615-70-C-1087, McDonnell-Douglas Corp., Oct. 1960. (Revised Sept. 1970.)

9. Queijo, M. J.: Theory for Computing Span Loads and Stability Derivatives Due to Sideslip, Yawing, and Rolling for Wings in Subsonic Compressible Flow. NASA TN D-4929, 1968.

10. Anon.: STOL Airplane Characteristics Documentation for a 12,500 Pound Turbo-Prop Airplane. DHC Rep. 71-6, De Havilland Aircraft of Canada, Ltd., Sept. 16, 1971.

TABLE I.- FLIGHT CONDITIONS, PHYSICAL DIMENSIONS, AND STABILITY DERIVATIVES OF THE AIRPLANES CONSIDERED IN THE INVESTIGATION

Quantity	Conventional			Large STOL					Small STOL			
	A	B	C	A	B	C	D	E	A	B	C	D
Flight conditions												
h, m (ft)	1 524 (5 000)	1 524 (5 000)	7 620 (25 000)	1 524 (5 000)	1 524 (5 000)	1 524 (5 000)	1 524 (5 000)	1 524 (5 000)	2 591 (8 500)	2 591 (8 500)	1 524 (5 000)	1 524 (5 000)
U, m/sec (ft/sec)	134.78 (442.2)	134.78 (442.2)	241.40 (792)	120.70 (396)	120.70 (396)	121.92 (400)	121.92 (400)	250.85 (823)	73.76 (242)	73.76 (242)	73.76 (242)	77.18 (253.2)
W, kg (lb)	27 751 (61 180)	27 751 (61 180)	38 029 (83 840)	22 226 (49 000)	20 412 (45 000)	16 982 (37 439)	24 993 (55 100)	24 993 (55 100)	1 542 (3 400)	1 315 (2 900)	1 315 (2 900)	5 216 (11 500)
W/S, kg/m^2 (lb/ft^2)	319.7 (65.48)	319.7 (65.48)	409.4 (83.84)	269.1 (43.31)	243.6 (42.68)	342.0 (70.02)	319.2 (65.36)	319.2 (65.36)	71.9 (14.72)	61.3 (12.55)	61.3 (12.55)	133.7 (27.38)
μ	11.163	11.163	26.2	10.99	9.99	15.746	12.721	12.72	6.477	5.50	4.88	6.397
C_L	.33	.33	.251	.343	.343	.429	.4	.0946	.2765	.2765	.2765	.4174
tan γ	0	0	0	0	0	0	0	0	0	0	0	0
α_0, rad	.031	.0318	.0310	-.0349	-.0349	.1101	.086	.01	.0614	.0614	.0614	.0227
Dimensions												
b, m (ft)	27.13 (89)	27.13 (89)	28.47 (93.4)	23.20 (76.1)	23.16 (76.0)	20.57 (67.5)	23.77 (78)	23.77 (78)	11.89 (39)	11.89 (39)	11.89 (39)	19.81 (65)
S, m^2 (ft^2)	86.80 (934.3)	86.80 (934.3)	92.90 (1,000)	82.59 (889)	83.80 (902)	49.65 (534.4)	78.31 (843)	78.31 (843)	21.46 (231)	21.46 (231)	21.46 (231)	39.02 (420)
S_{vT}, m^2 (ft^2)	18.09 (194.7)	19.56 (210.5)	19.46 (209.5)	20.35 (219)	20.35 (219)	12.08 (130.0)	16.62 (178.9)	16.62 (178.9)	2.40 (25.8)	2.40 (25.8)	2.40 (25.8)	9.20 (99)
A	8.25	8.25	8.72	6.52	6.52	8.53	7.75	7.75	6.58	6.58	6.58	10
Γ, deg	3	3	3	4	4	-2.12	-3.5	-3.5	0	0	0	3
h_z, m (ft)	3.712 (12.18)	3.712 (12.18)	4.243 (13.92)	3.000 (9.84)	3.000 (9.84)	2.990 (9.81)	3.575 (11.73)	3.575 (11.73)	2.179 (7.15)	2.179 (7.15)	2.179 (7.15)	1.829 (6.1)
l_T, m (ft)	11.08 (36.34)	11.08 (36.34)	15.00 (49.20)	11.29 (37.05)	11.29 (37.05)	6.52 (21.40)	7.78 (25.53)	7.78 (25.53)	5.79 (19)	5.79 (19)	5.79 (19)	7.96 (26.1)
x_0, m (ft)	14.48 (47.50)	14.48 (47.50)	17.53 (57.50)	7.39 (24.26)	7.39 (24.26)	6.72 (22.04)	11.04 (36.23)	11.04 (36.23)	2.33 (7.63)	2.33 (7.63)	2.33 (7.63)	5.94 (19.5)
x_1, m (ft)	8.36 (27.43)	8.36 (27.43)	11.92 (39.10)	9.48 (31.09)	9.48 (31.09)	4.97 (16.31)	5.42 (17.77)	5.42 (17.77)	5.19 (17.04)	5.19 (17.04)	5.19 (17.04)	6.71 (22.0)
x_2, m (ft)	15.94 (52.30)	15.94 (52.30)	18.36 (60.25)	14.81 (48.59)	14.81 (48.59)	8.69 (28.52)	9.61 (31.53)	9.61 (31.53)	6.72 (22.06)	6.72 (22.06)	6.72 (22.06)	9.97 (32.7)
s_0, m (ft)	1.82 (5.96)	1.82 (5.96)	2.47 (8.10)	1.50 (4.92)	1.50 (4.92)	1.88 (6.18)	1.22 (4.01)	1.22 (4.01)	0.63 (2.07)	0.63 (2.07)	0.63 (2.07)	1.22 (4)
s_1, m (ft)	5.63 (18.47)	5.63 (18.47)	6.39 (20.95)	6.22 (20.52)	6.22 (20.42)	6.50 (21.33)	6.11 (20.06)	6.11 (20.06)	2.86 (9.39)	2.86 (9.39)	2.86 (9.39)	4.11 (13.5)

TABLE I.- FLIGHT CONDITIONS, PHYSICAL DIMENSIONS, AND STABILITY DERIVATIVES OF THE AIRPLANES CONSIDERED IN THE INVESTIGATION - Concluded

Quantity	Conventional			Large STOL					Small STOL			
	A	B	C	A	B	C	D	E	A	B	C	D
Stability derivatives for airplane												
K_x^2	0.0137	0.0137	0.0128	0.0325	0.0315	0.0327	0.0234	0.0234	0.0075	0.0175	0.0175	0.0103
K_z^2	.0656	.0656	.0700	.0578	.0604	.0504	.0443	.0443	.0156	.0328	.0328	.0247
K_{xz}	.00468	.00468	.0043	-.004	.00022	.0045	.00195	.00195	-.00103	.00241	.00241	.00085
C_{l_p}	-.4783	-.388	-.4783	-.443	-.4974	-.73	-.438	-.51	-.4875	-.4875	-.4875	-.548
C_{l_r}	.1623	.168	.1623	.1965	-.0671	.20	.1436	.10	.1034	.1034	.1034	.107
C_{l_β}	-.1419	-.1489	-.1419	-.1397	-.0952	-.175	-.2443	-.20	-.0651	-.0651	-.0651	-.113
C_{n_p}	.00322	-.0584	.00322	-.0733	-.1519	.050	-.092	-.05	-.0209	-.0209	-.0209	.0132
C_{n_r}	-.2277	-.2973	-.328	-.5833	-.456	-.73	-.203	-.20	-.149	-.149	-.149	-.1827
C_{n_β}	.1383	.1709	.1657	.463	.267	.060	.200	.20	.0605	.0605	.0605	.1247
C_{Y_p}	.0568	.039	.0568	-.079	-.079	.500	.044	.10	-.0637	-.0637	-.0637	0
C_{Y_r}	.5365	.706	.5365	1.17	1.17	.400	.70	.70	.2549	.2549	.2549	0
C_{Y_β}	-.899	-1.16	-1.081	-1.486	-1.35	-1.65	-1.146	-1.146	-.460	-.460	-.460	-.8457
C_{L_α}, per/rad	5.872	5.872	5.872	6.55	6.55	3.896	4.68	4.68	4.5	4.5	4.5	5.79
Stability derivatives for wing or tail												
$C_{l_{p_w}}$	-.4676	-.4676	-.4676	-.42	-.42	-.5185	-.452	-.524	-.123	-.123	-.123	-.548
$C_{l_{r_w}}$	.437	.437	.437	.0803	.0803	.0627	.067	.0235	.0419	.0419	.0419	.107
$C_{l_{\beta_w}}$	-.056	-.072	-.056	-.0703	-.0703	-.0165	-.0166	-.0166	-.0177	-.0177	-.0177	-.0441
$C_{n_{p_w}}$	-.40	-.40	-.40	-.0382	-.0382	-.0553	-.0544	-.0129	-.0368	-.0368	-.0368	.0132
$C_{n_{r_w}}$	.023	.023	.023	-.0061	-.0061	-.0074	-.0074	-.00436	-.0240	-.0240	-.0240	-.126
$C_{D,0}$	.018	.0052	.018	.00656	.00656	.0071	.01	.01	.0073	.0073	.0073	.01
α_w, rad	.031	.0318	.0310	-.0349	-.0349	.1101	.01	.01	.0614	.0614	.0614	.0227
$C_{Y_{\beta_T}}$	-.607	-.8512	-.607	-1.185	-1.185	-.647	-.537	-.537	-.575	-.575	-.575	-.6921
σ/β_T	.2	.332	.2	.489	.489	.0068	.3455	.3455	-.241	-.241	-.241	.0849
Source reference	7	8	8	8	(a)	8	8	8	8	8	8	10

[a]Aerodynamic coefficients modified for use on a NASA moving base simulator in order to give realistic handling qualities.

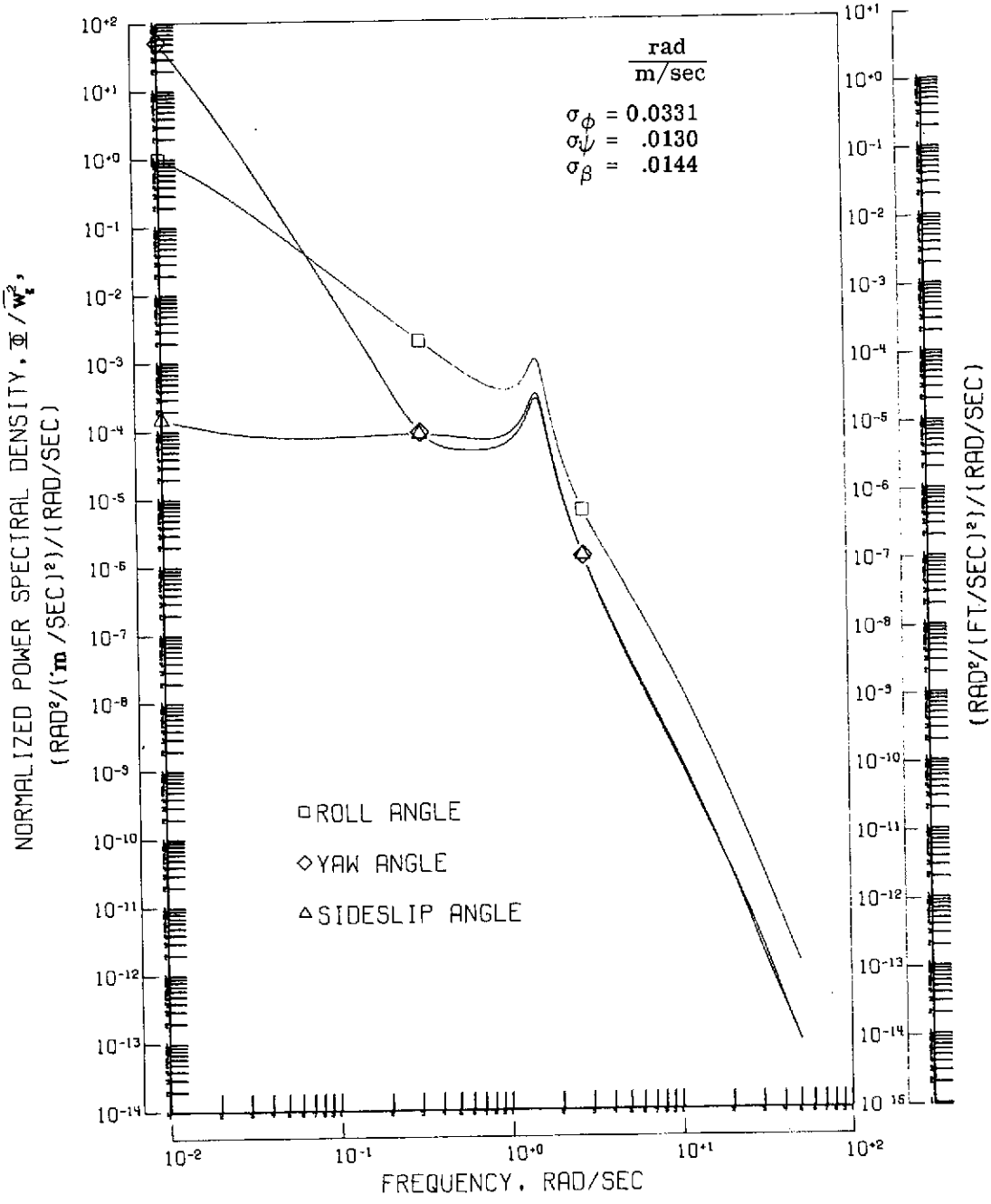

(a) Normalized total power spectral density response for each of the lateral displacements.

Figure 1.- Response of "conventional A" airplane to random gusts for an assumed scale length of 335.28 m (1100 ft).

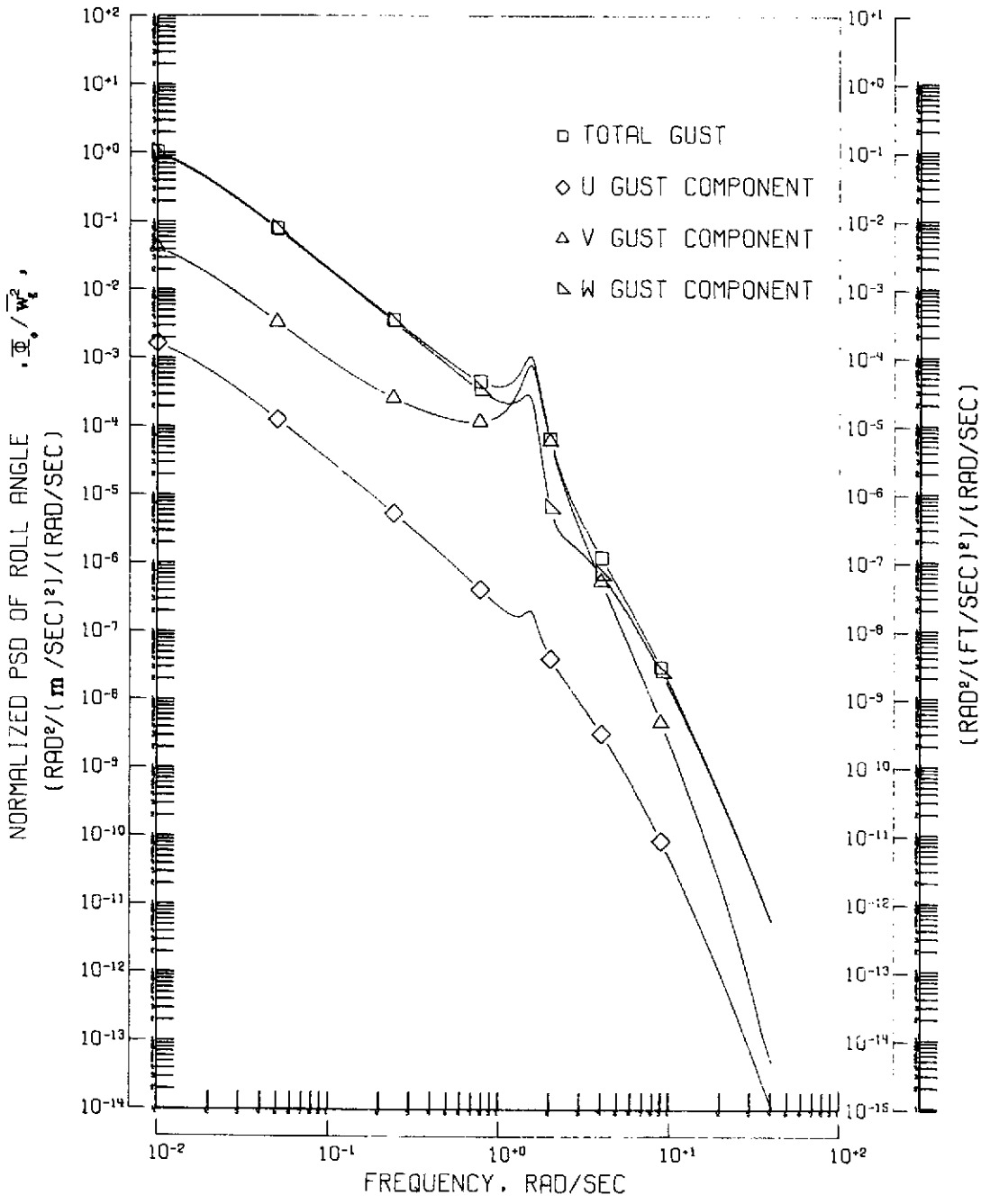

(b) Normalized total and individual component power spectral density response in roll for each of the gust components.

Figure 1.- Continued.

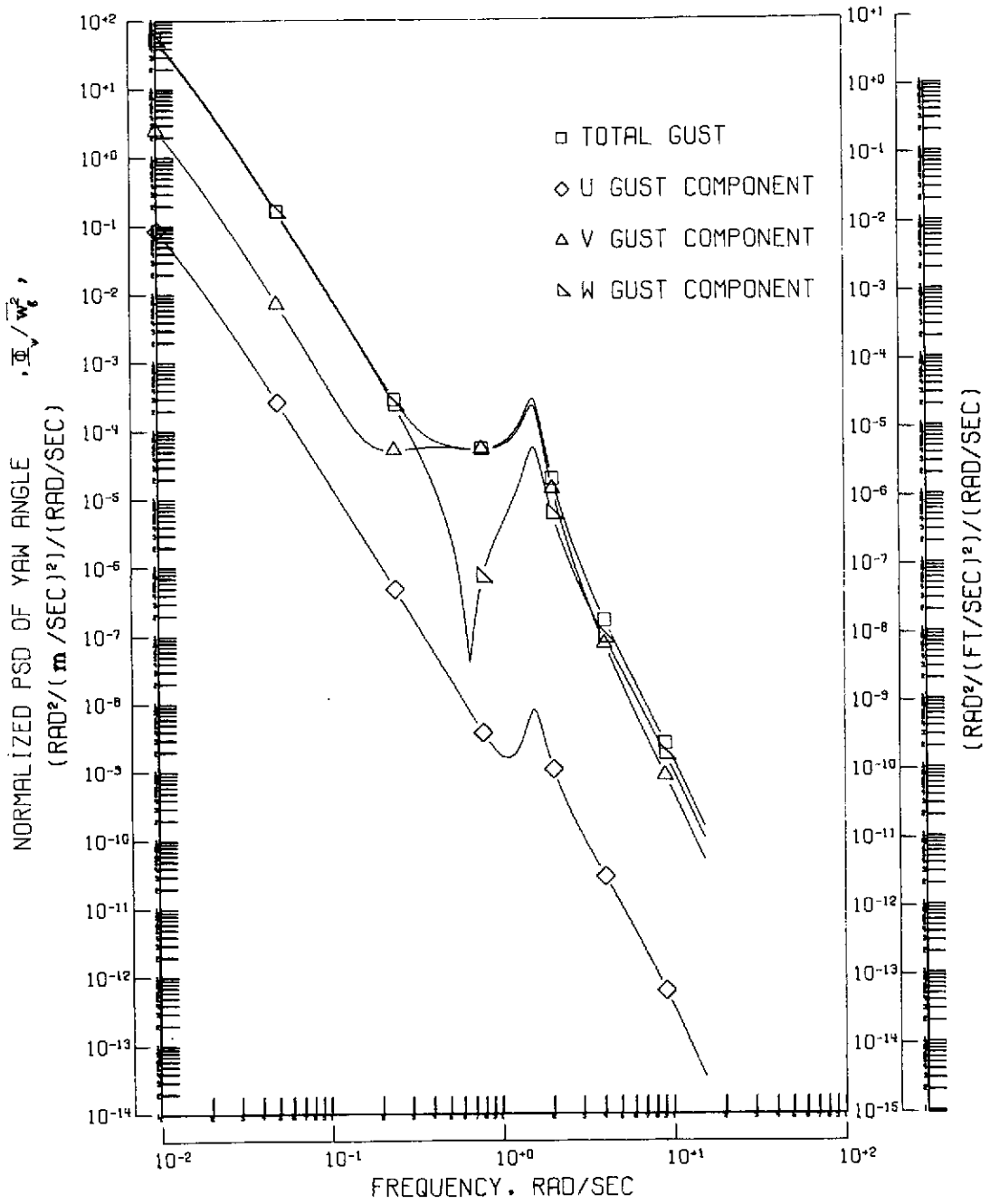

(c) Normalized total and individual component power spectral density response in yaw for each of the gust components.

Figure 1.- Continued.

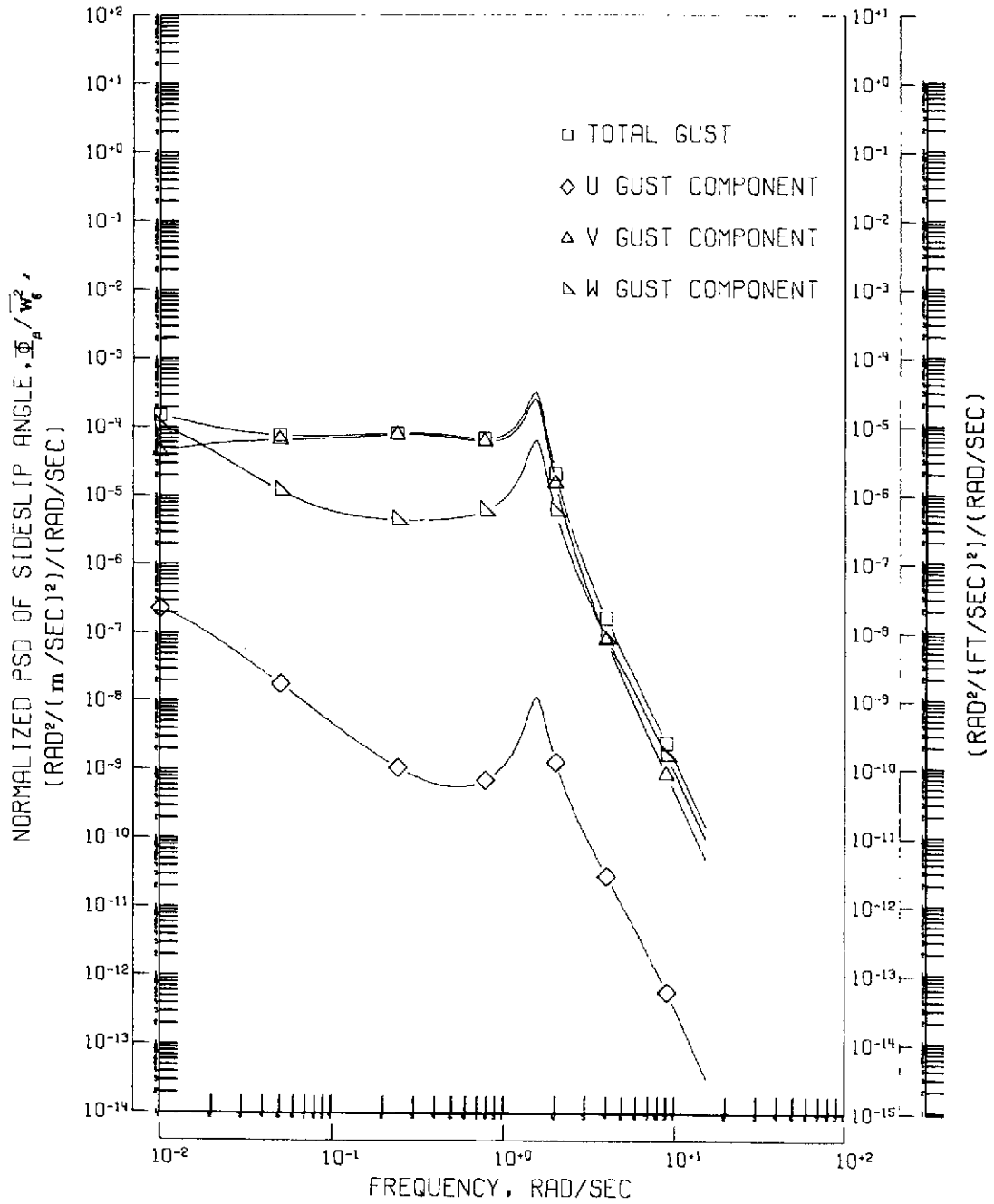

(d) Normalized total and individual component power spectral density response in sideslip for each of the gust components.

Figure 1.- Continued.

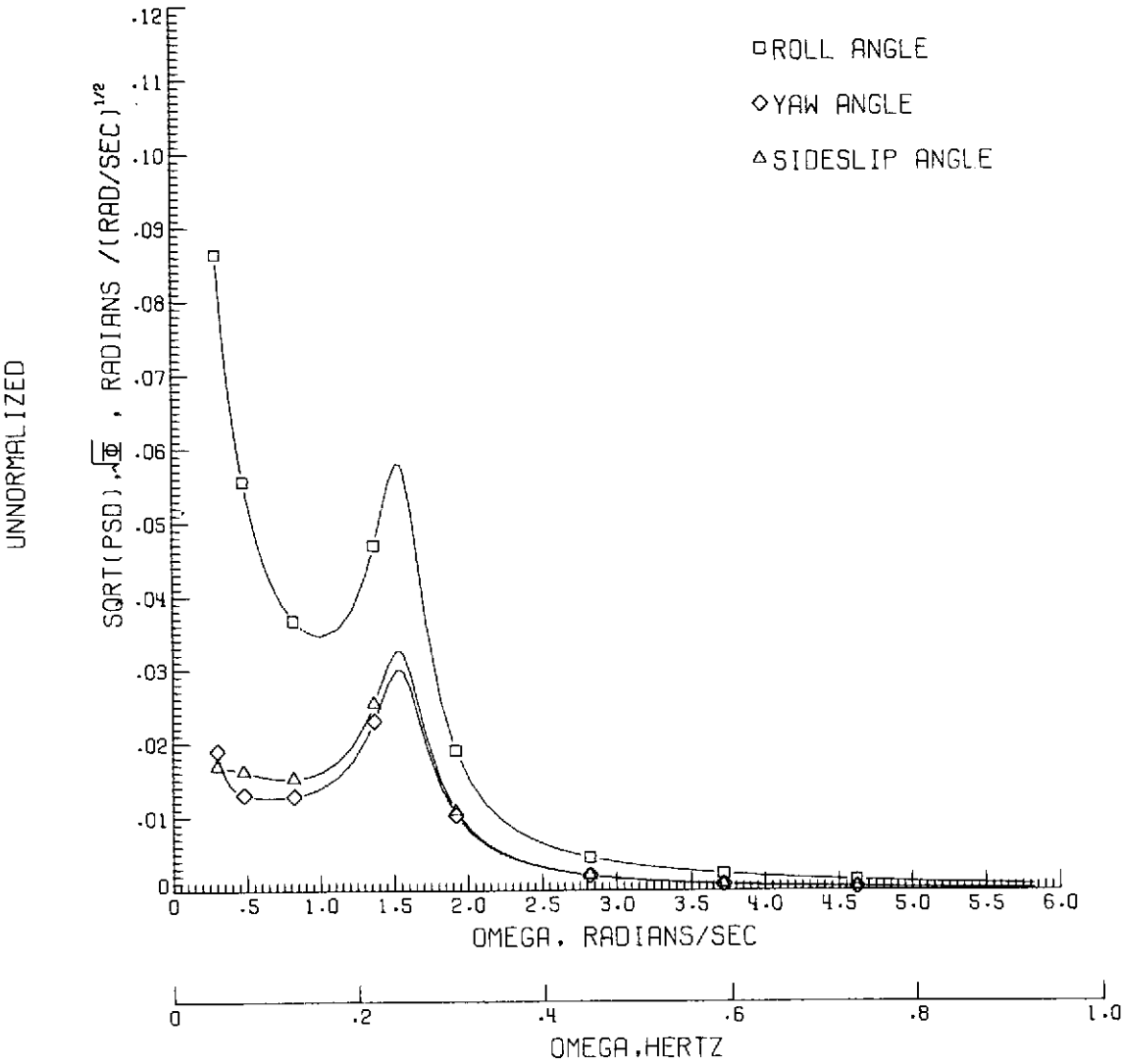

(e) Square root of the dimensional power spectral density response for each of the lateral displacements. The average gust intensity was 1.83 m/sec (6 ft/sec).

Figure 1.- Concluded.

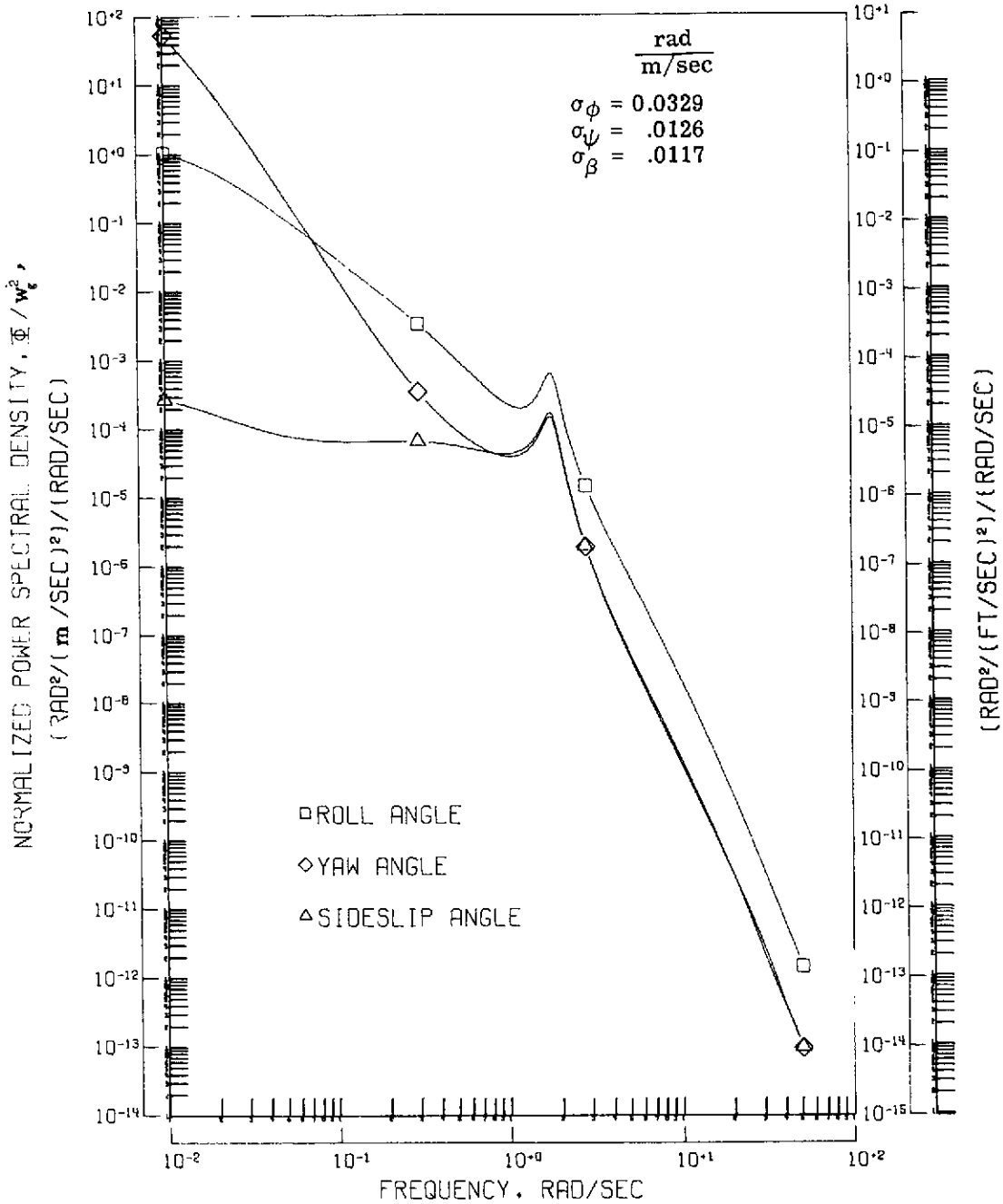

(a) Normalized total power spectral density response for each of the lateral displacements.

Figure 2.- Response of "conventional B" airplane to random gusts for an assumed scale length of 335.28 m (1100 ft).

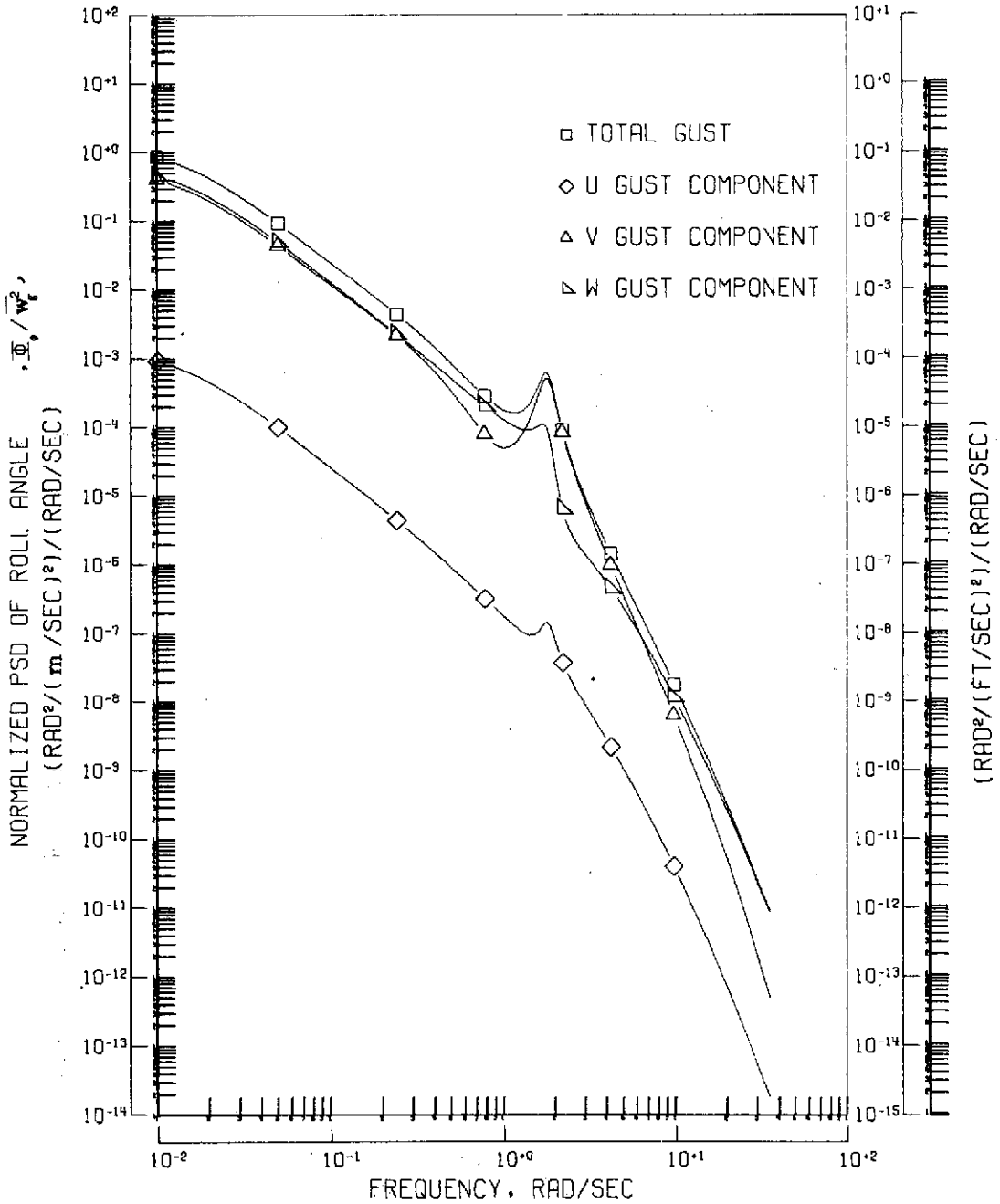

(b) Normalized total and individual component power spectral density response in roll for each of the gust components.

Figure 2.- Continued.

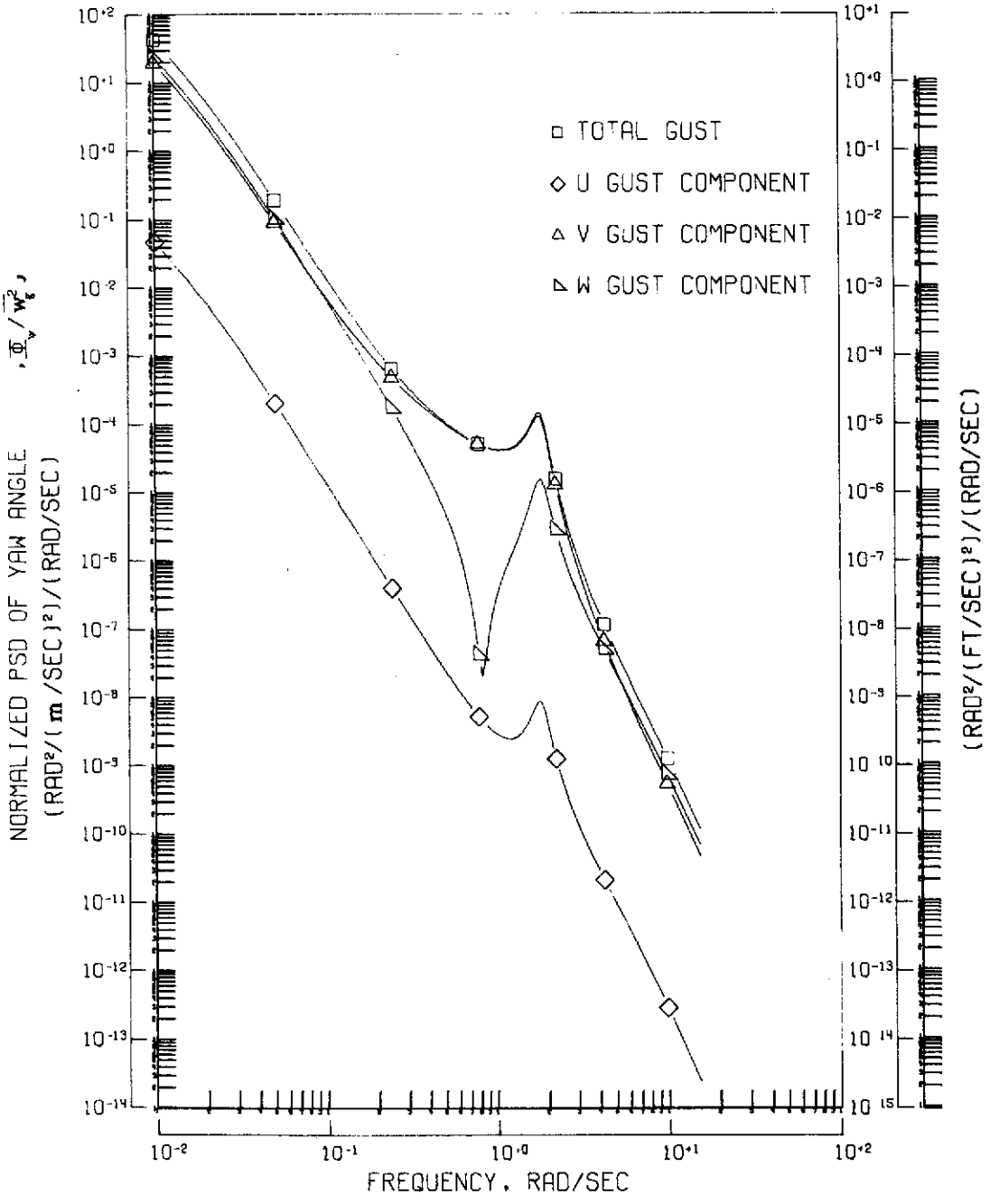

(c) Normalized total and individual component power spectral density response in yaw for each of the gust components.

Figure 2.- Continued.

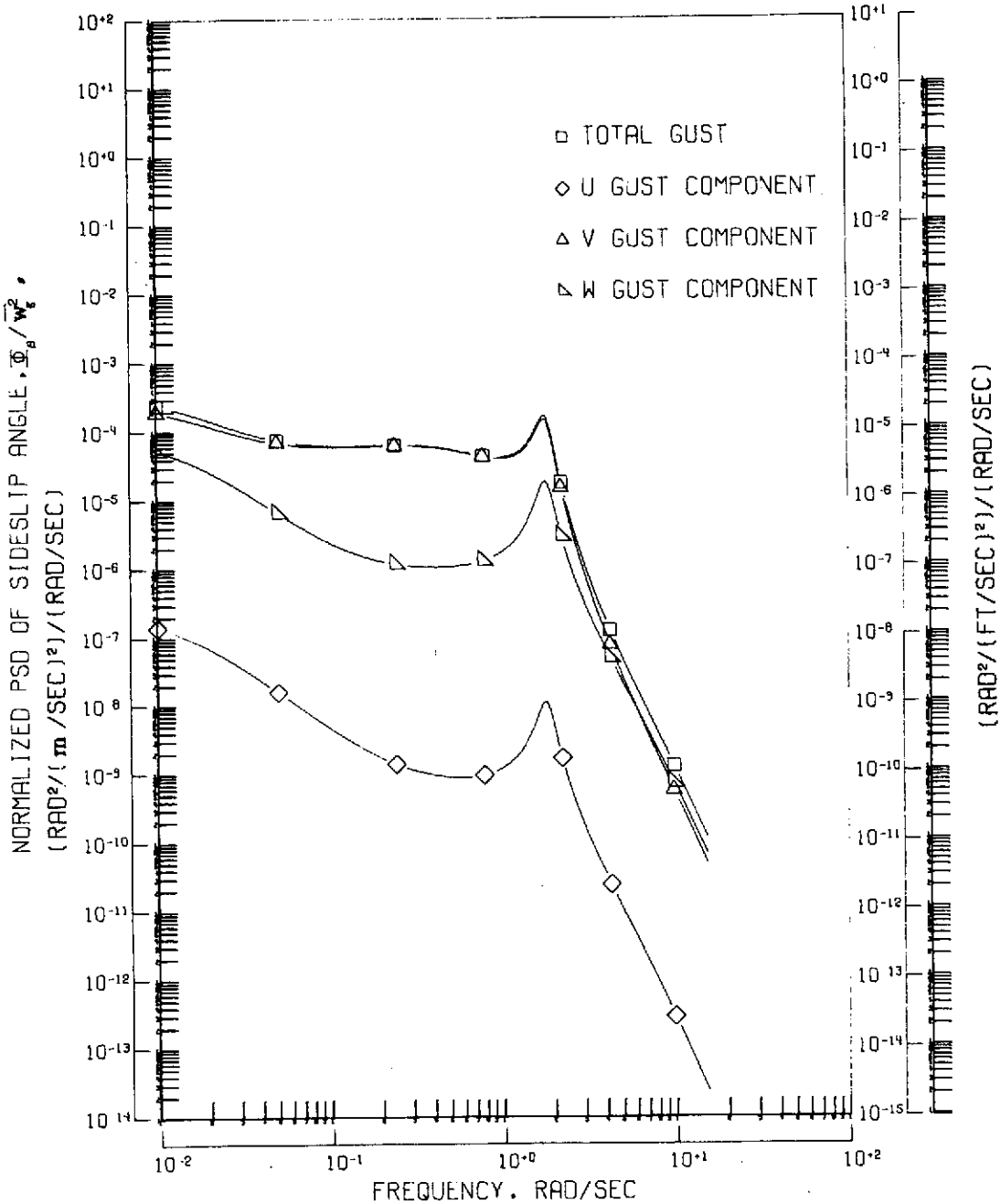

(d) Normalized total and individual component power spectral density response in sideslip for each of the gust components.

Figure 2.- Continued.

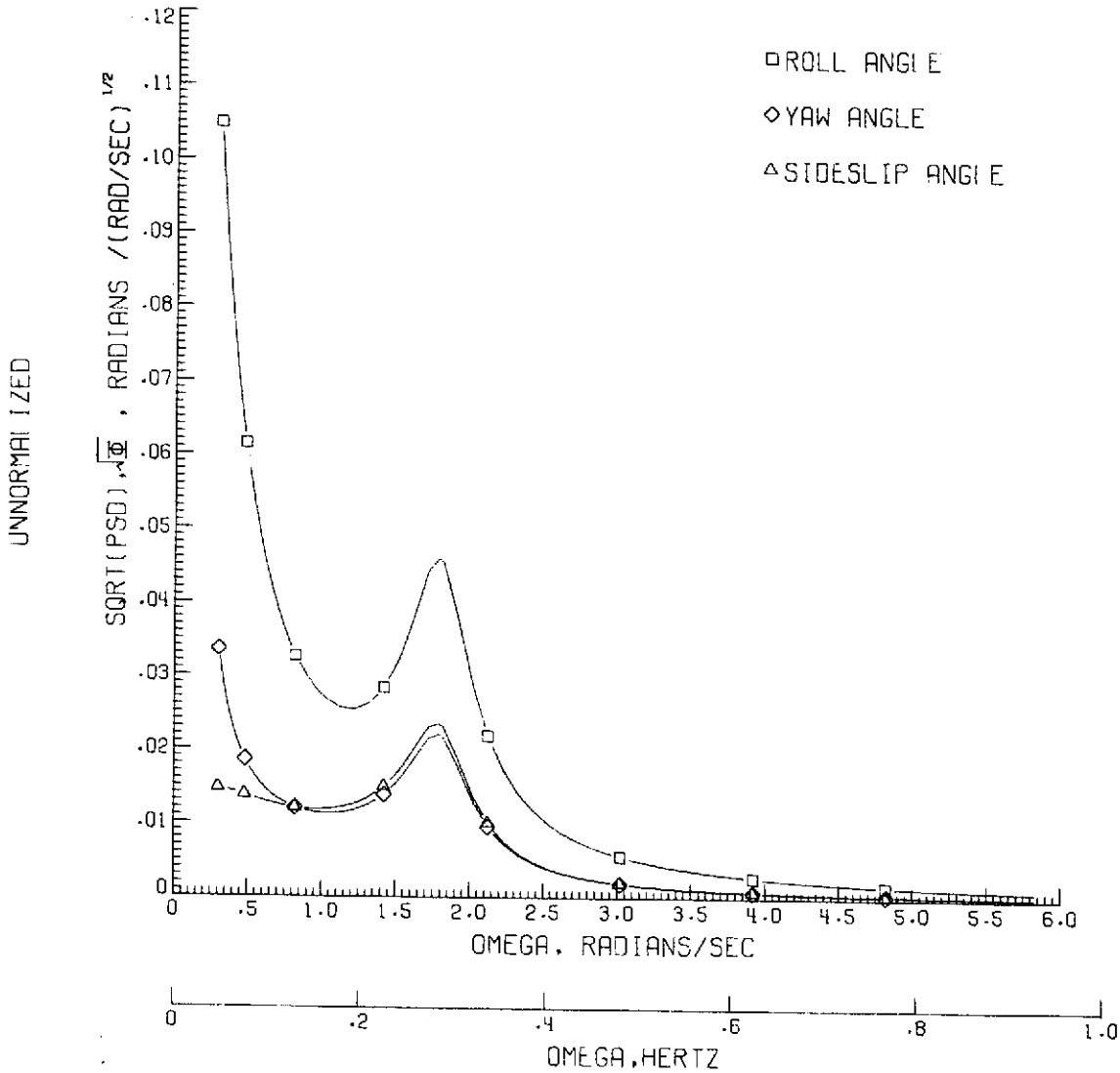

(e) Square root of the dimensional power spectral density response for each of the lateral displacements. The average gust intensity was 1.83 m/sec (6 ft/sec).

Figure 2.- Concluded.

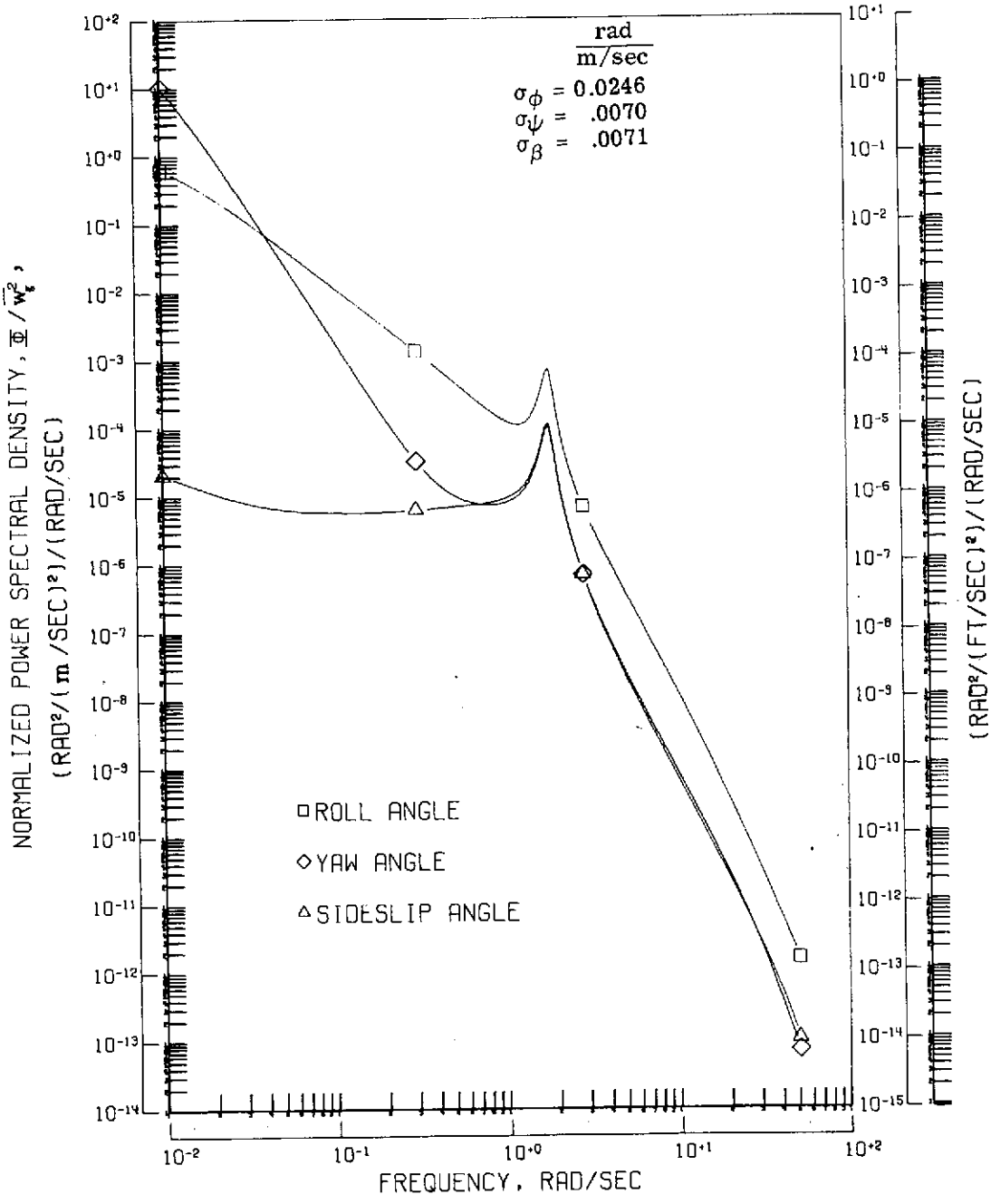

(a) Normalized total power spectral density response for each of the lateral displacements.

Figure 3.- Response of "conventional C" airplane to random gusts for an assumed scale length of 335.28 m (1100 ft).

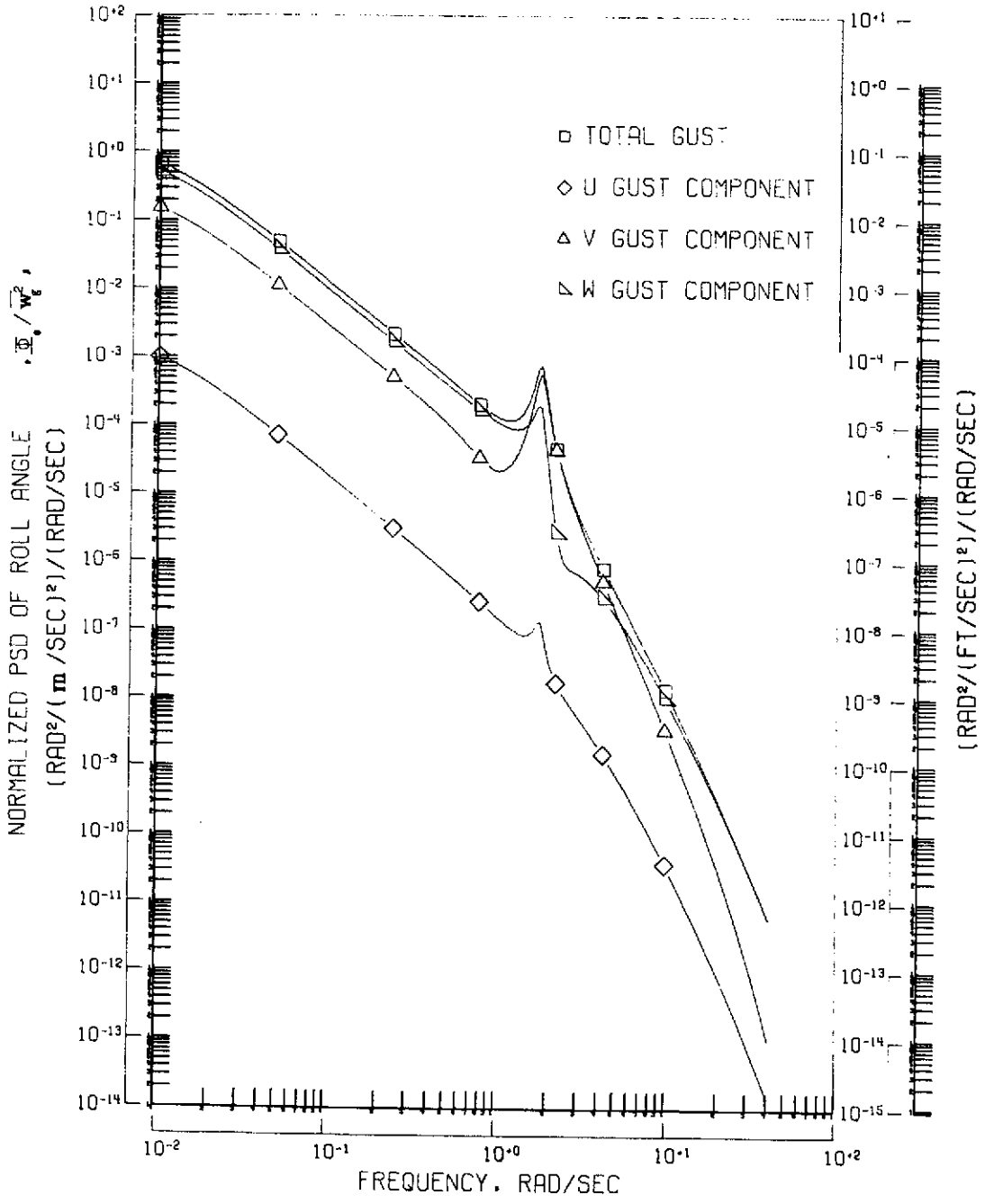

(b) Normalized total and individual component power spectral density response in roll for each of the gust components.

Figure 3.- Continued.

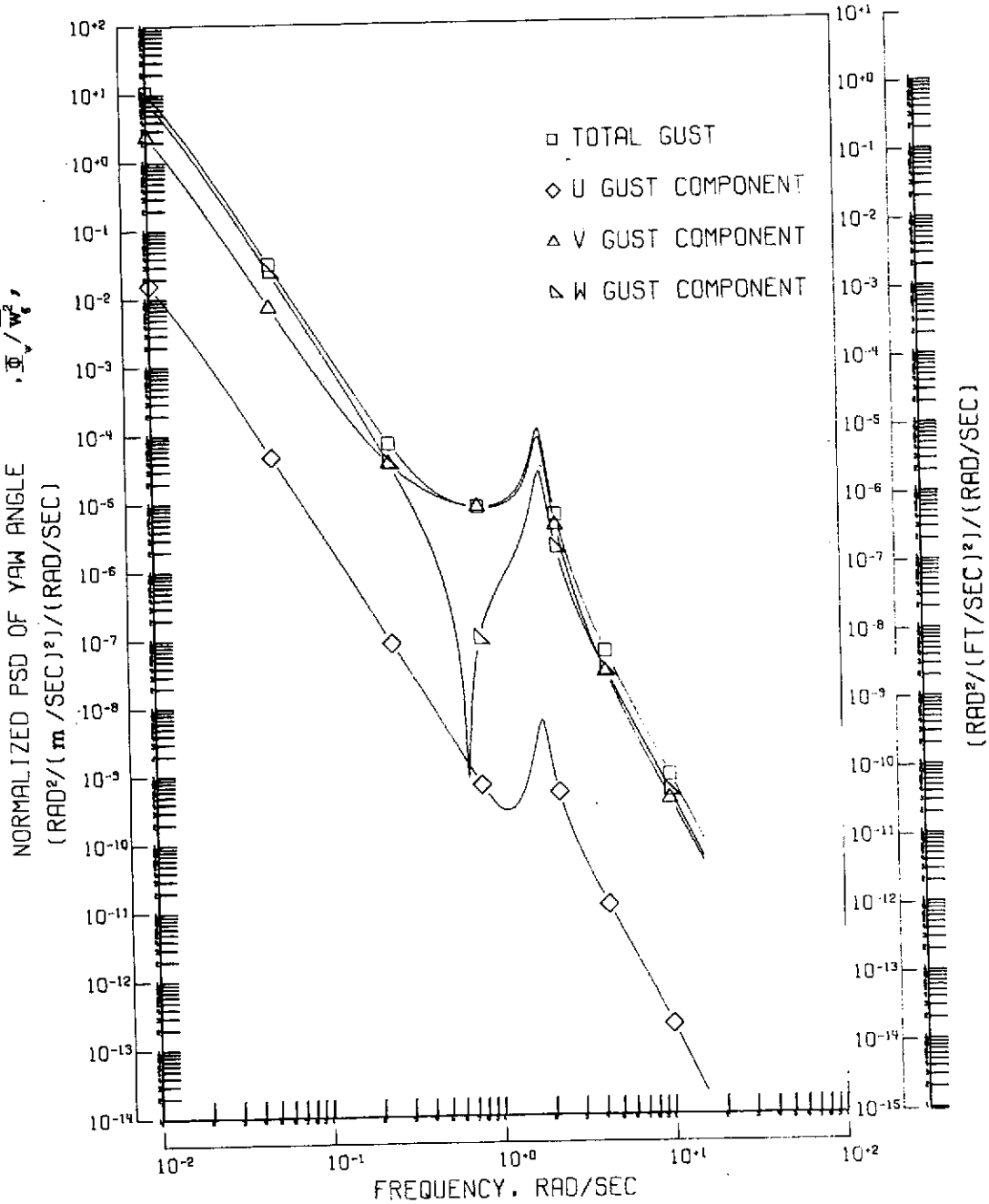

(c) Normalized total and individual component power spectral density response in yaw for each of the gust components.

Figure 3.- Continued.

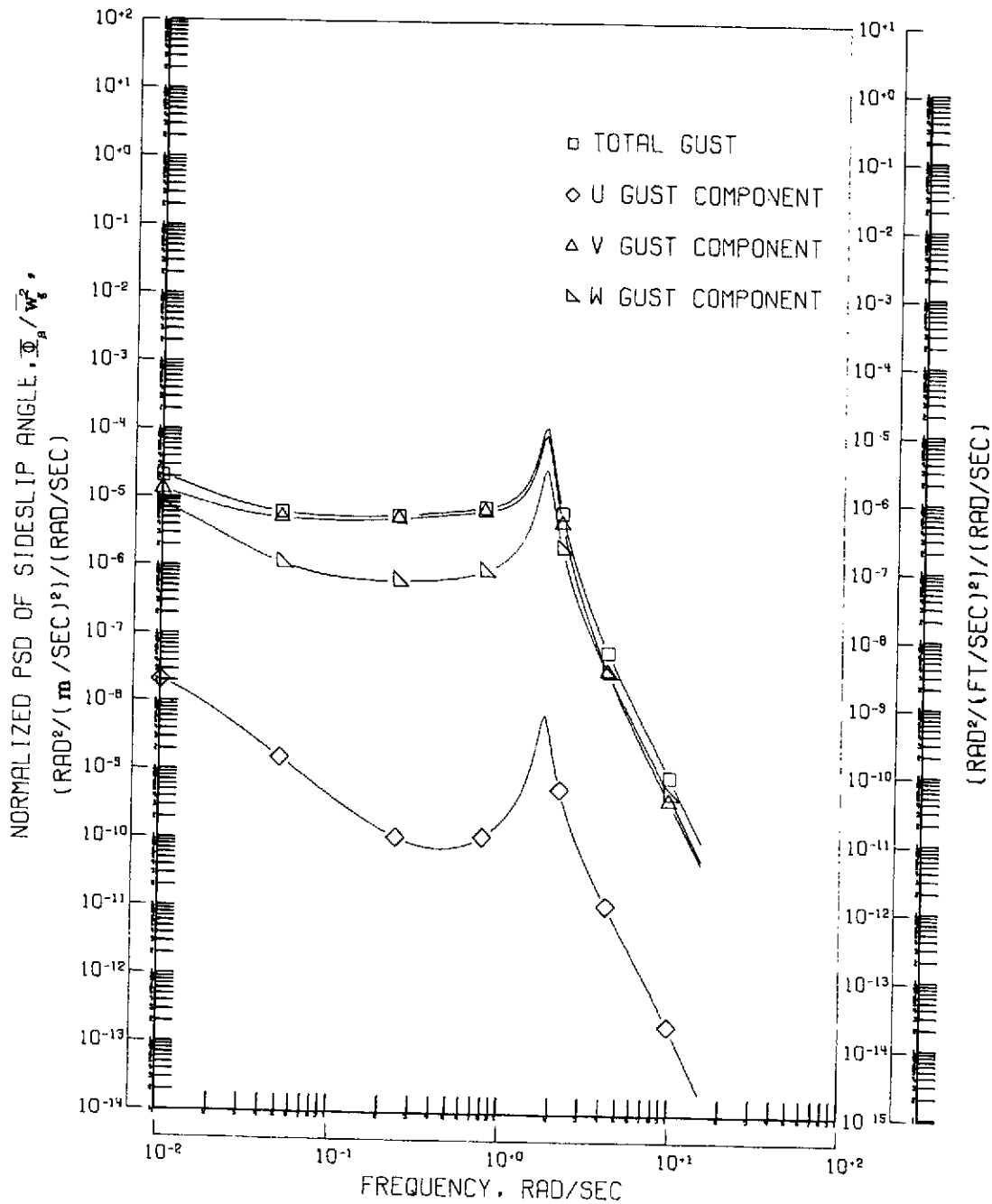

(d) Normalized total and individual component power spectral density response in sideslip for each of the gust components.

Figure 3.- Continued.

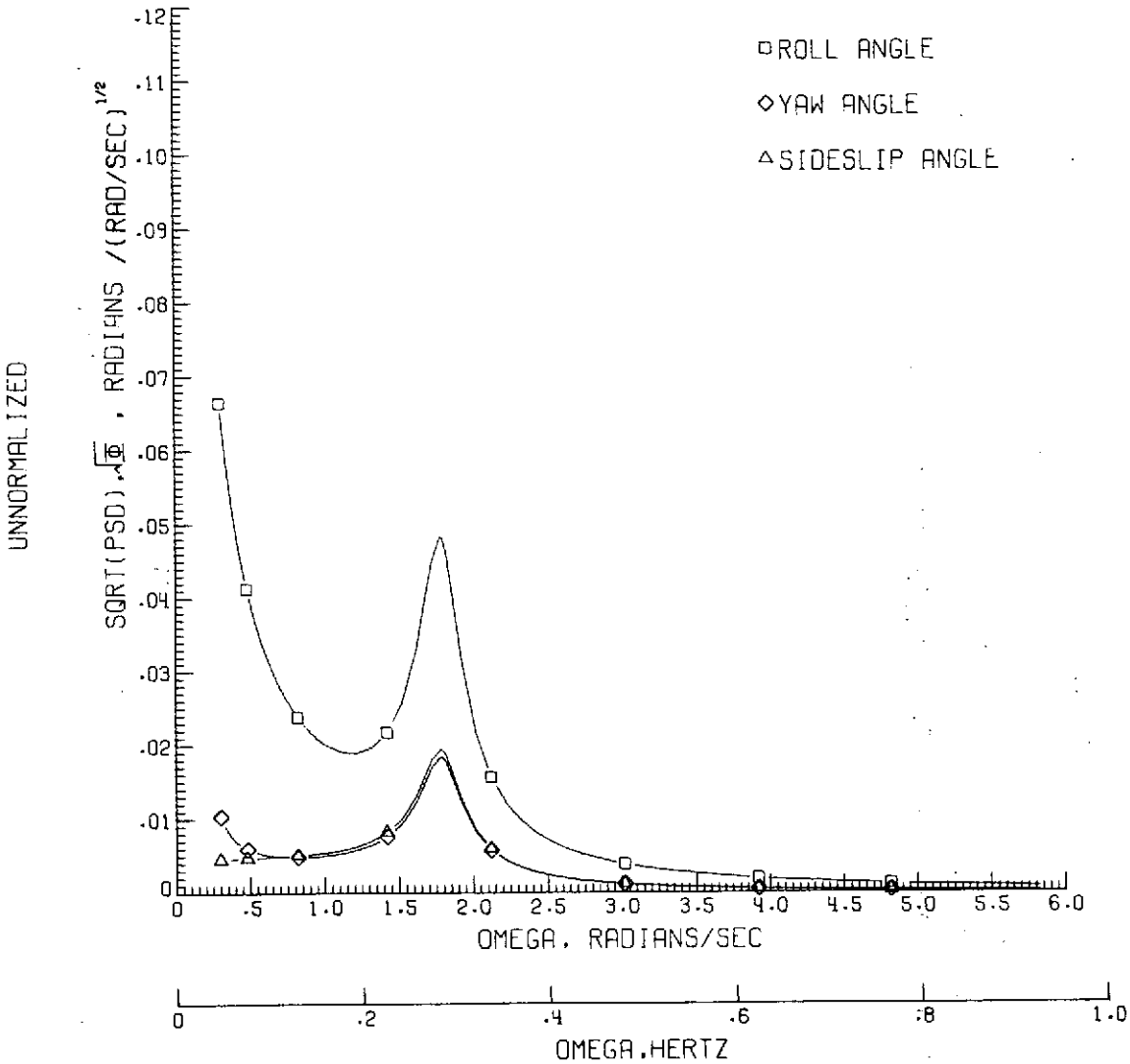

(e) Square root of the dimensional power spectral density response for each of the lateral displacements. The average gust intensity was 1.83 m/sec (6 ft/sec).

Figure 3.- Concluded.

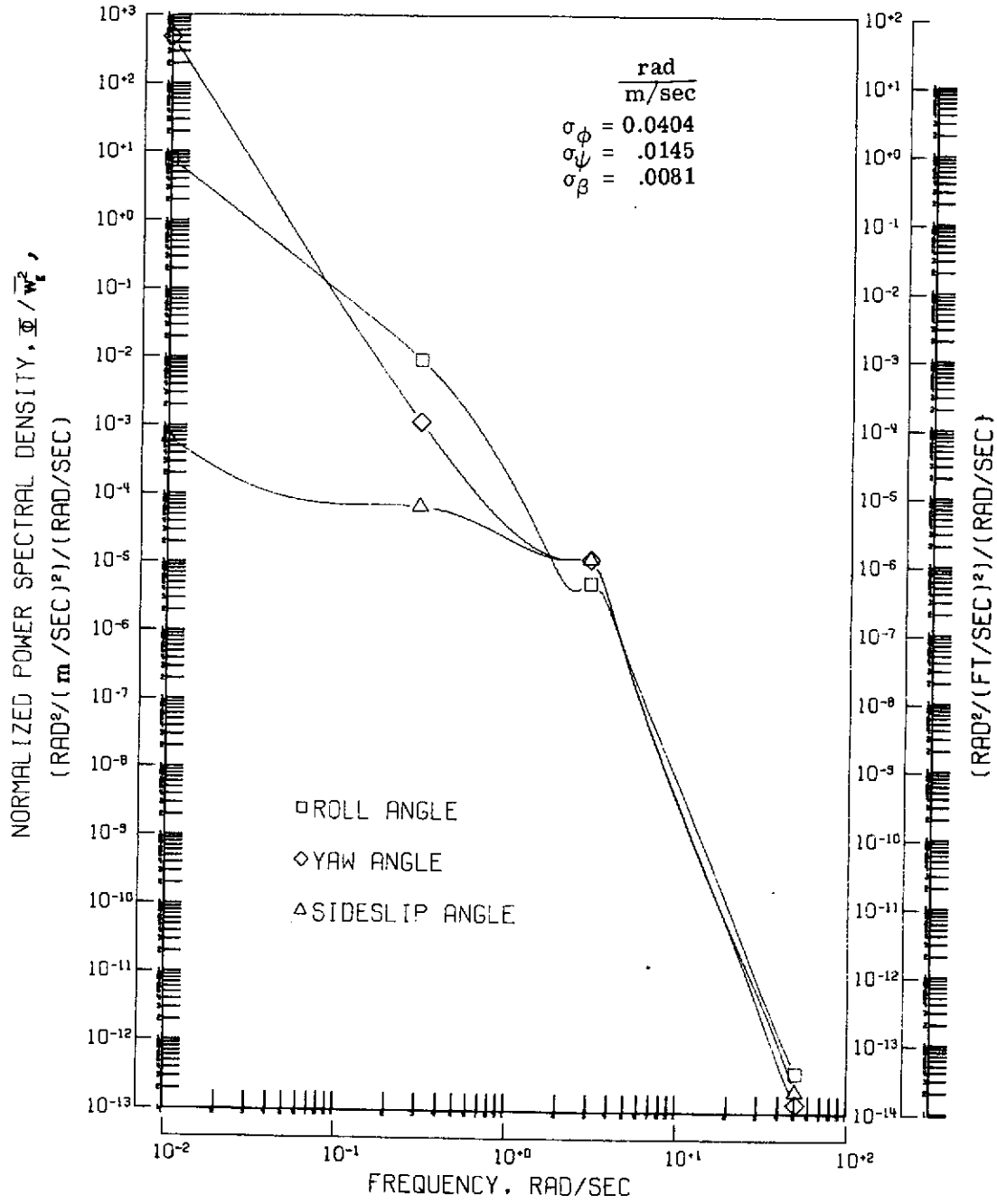

(a) Normalized total power spectral density response for each of the lateral displacements.

Figure 4.- Response of "large STOL A" airplane to random gusts for an assumed scale length of 335.28 m (1100 ft).

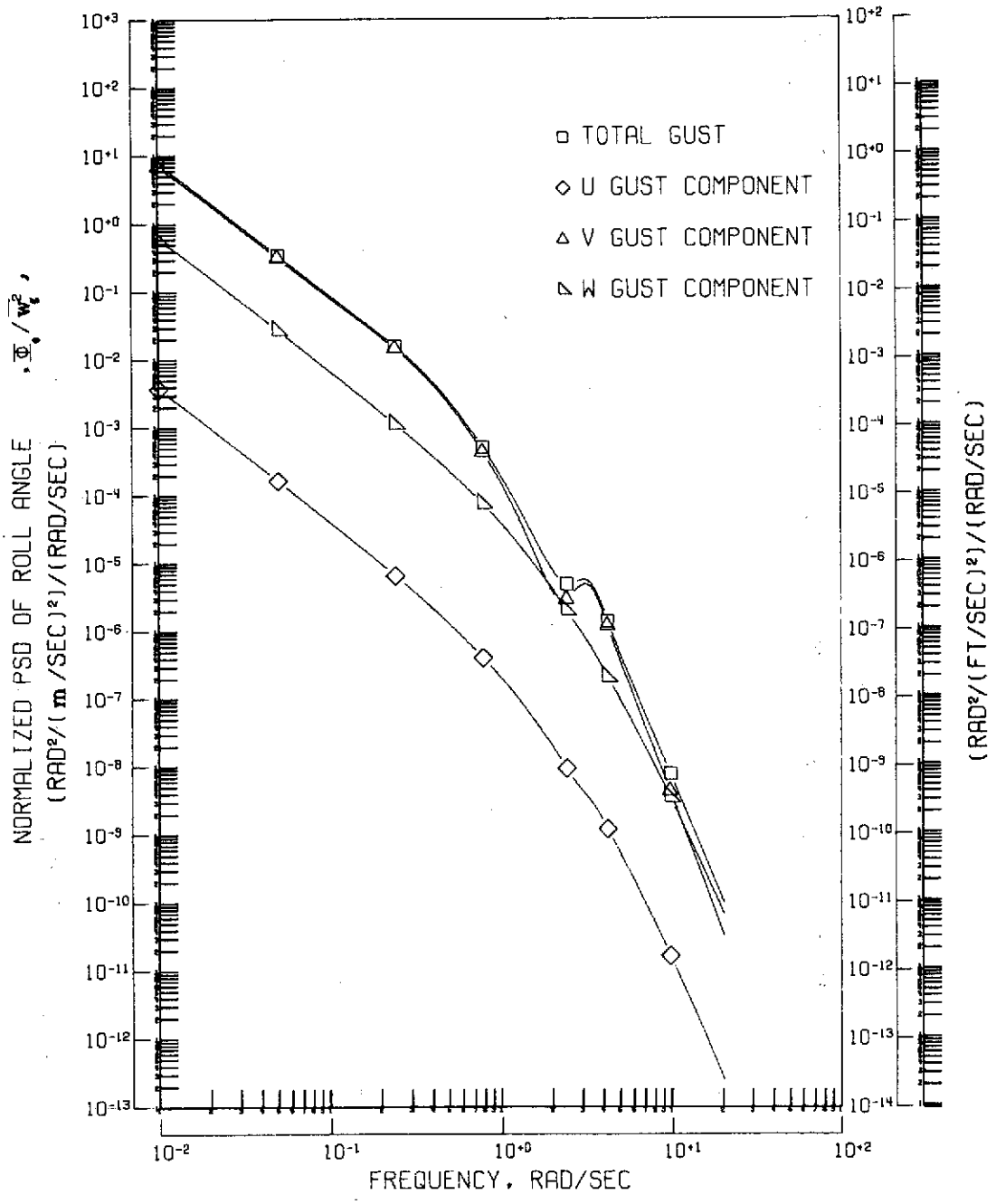

(b) Normalized total and individual component power spectral density response in roll for each of the gust components.

Figure 4.- Continued.

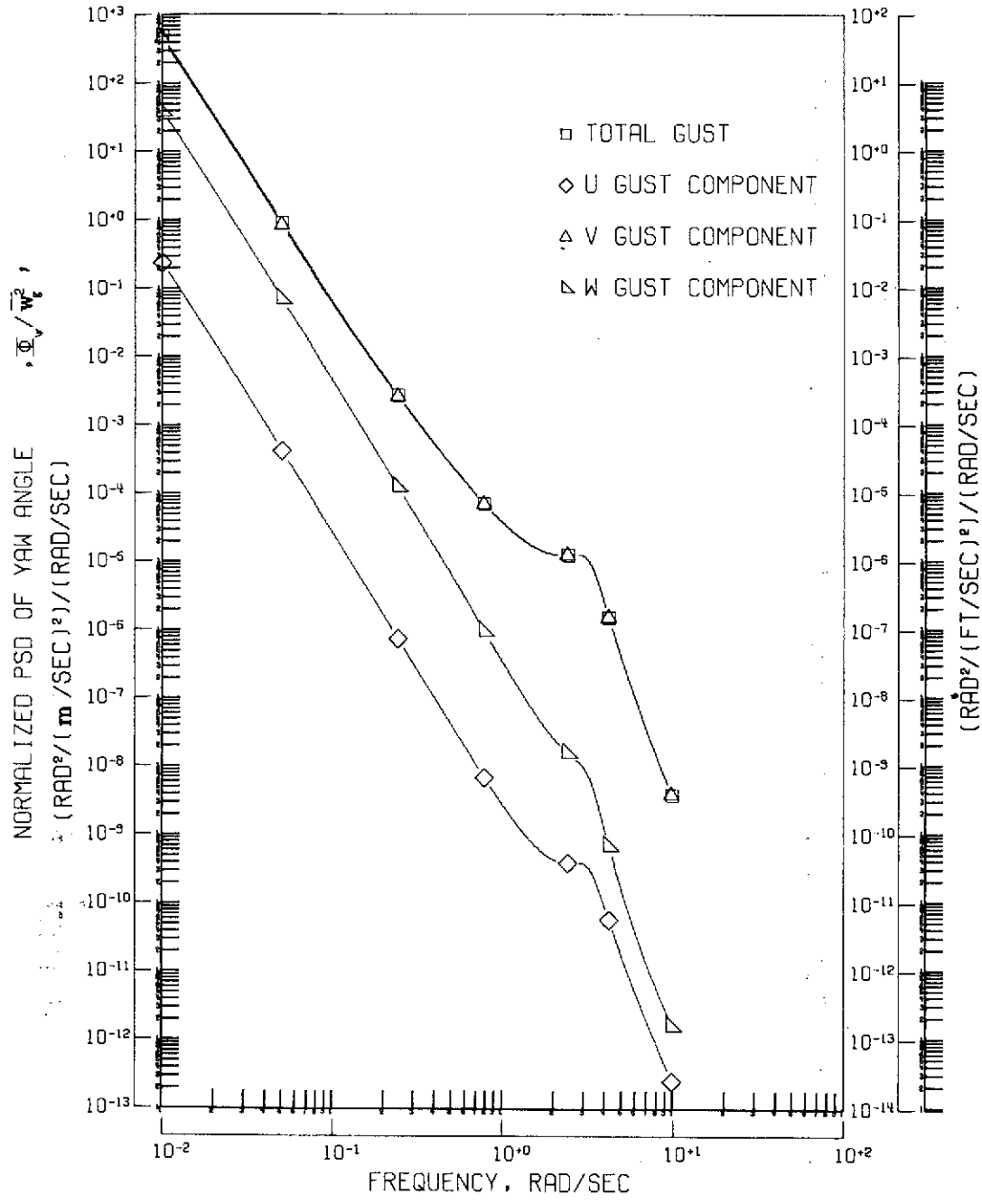

(c) Normalized total and individual component power spectral density response in yaw for each of the gust components.

Figure 4.- Continued.

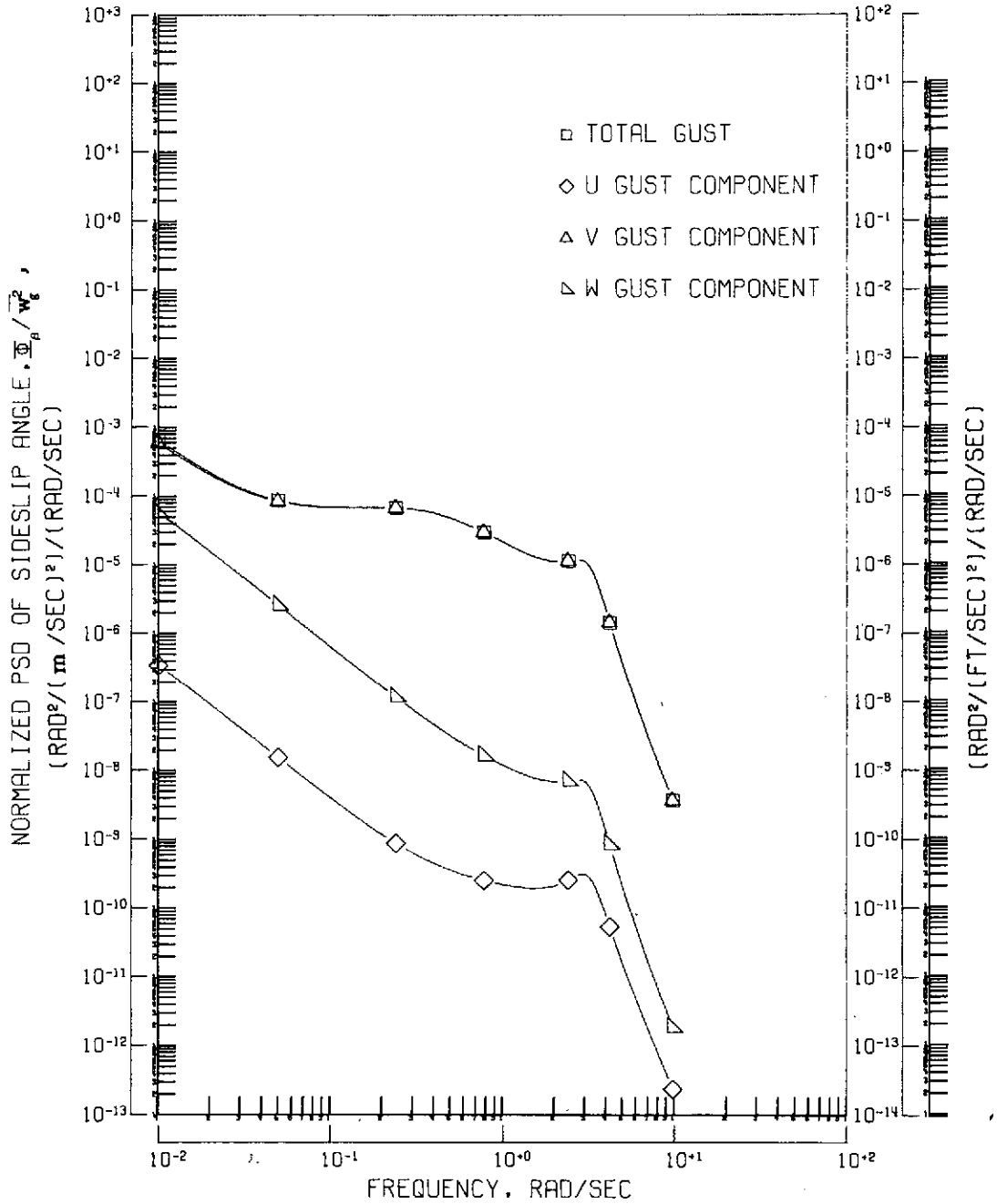

(d) Normalized total and individual component power spectral density response in sideslip for each of the gust components.

Figure 4.- Continued.

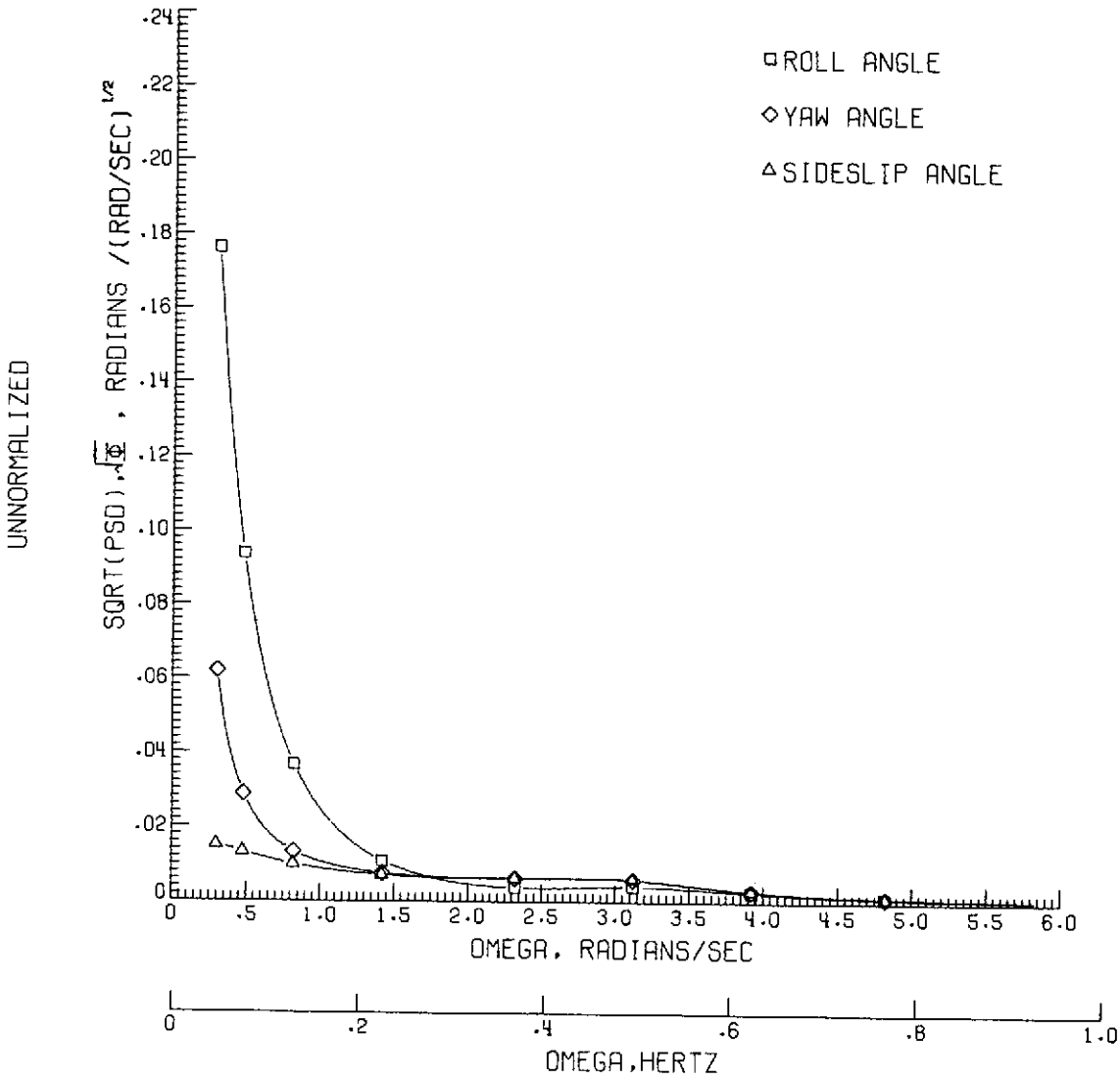

(e) Square root of the dimensional power spectral density response for each of the lateral displacements. The average gust intensity was 1.83 m/sec (6 ft/sec).

Figure 4.- Concluded.

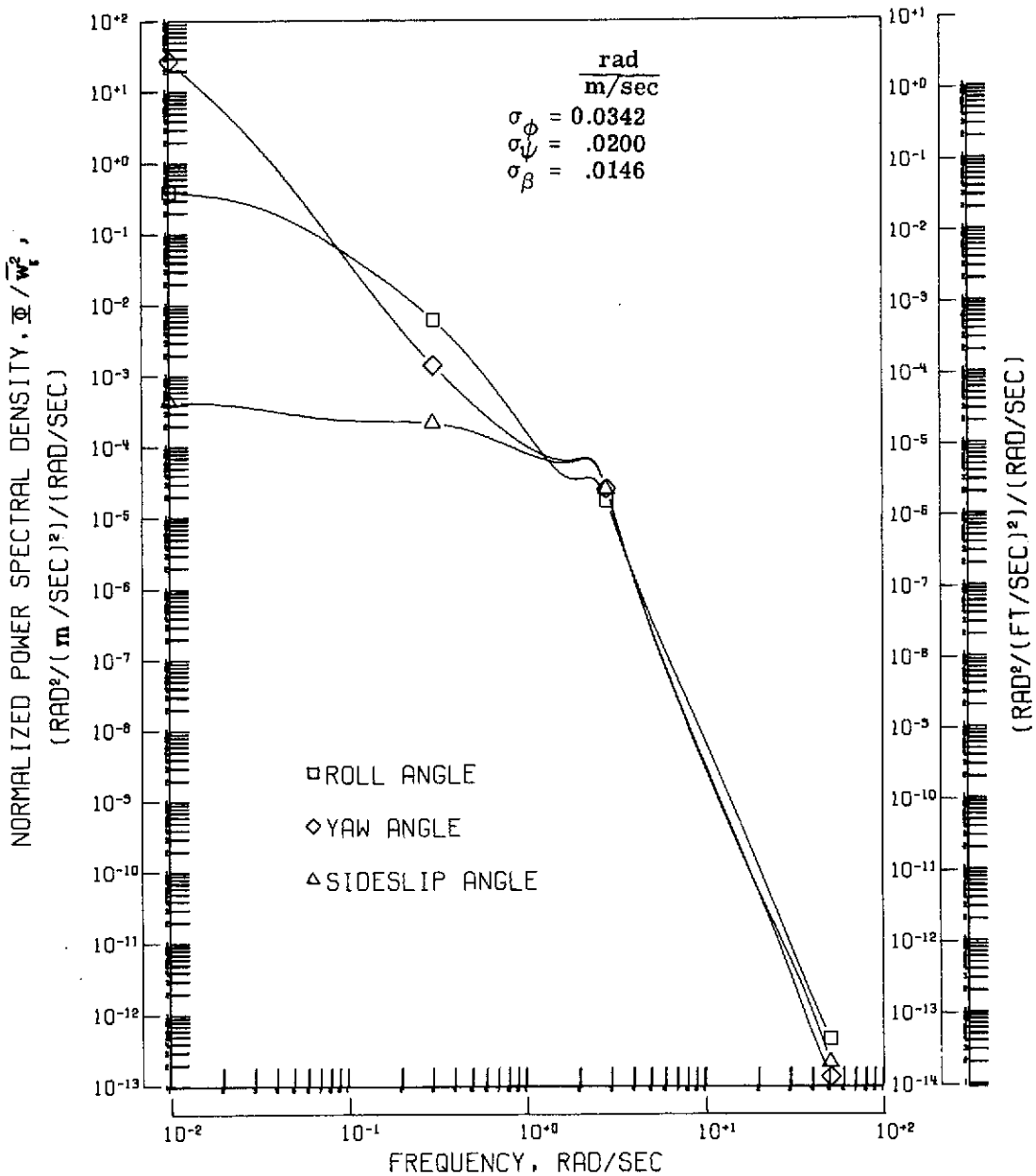

(a) Normalized total power spectral density response for each of the lateral displacements.

Figure 5.- Response of "large STOL B" airplane to random gusts for an assumed scale length of 335.28 m (1100 ft).

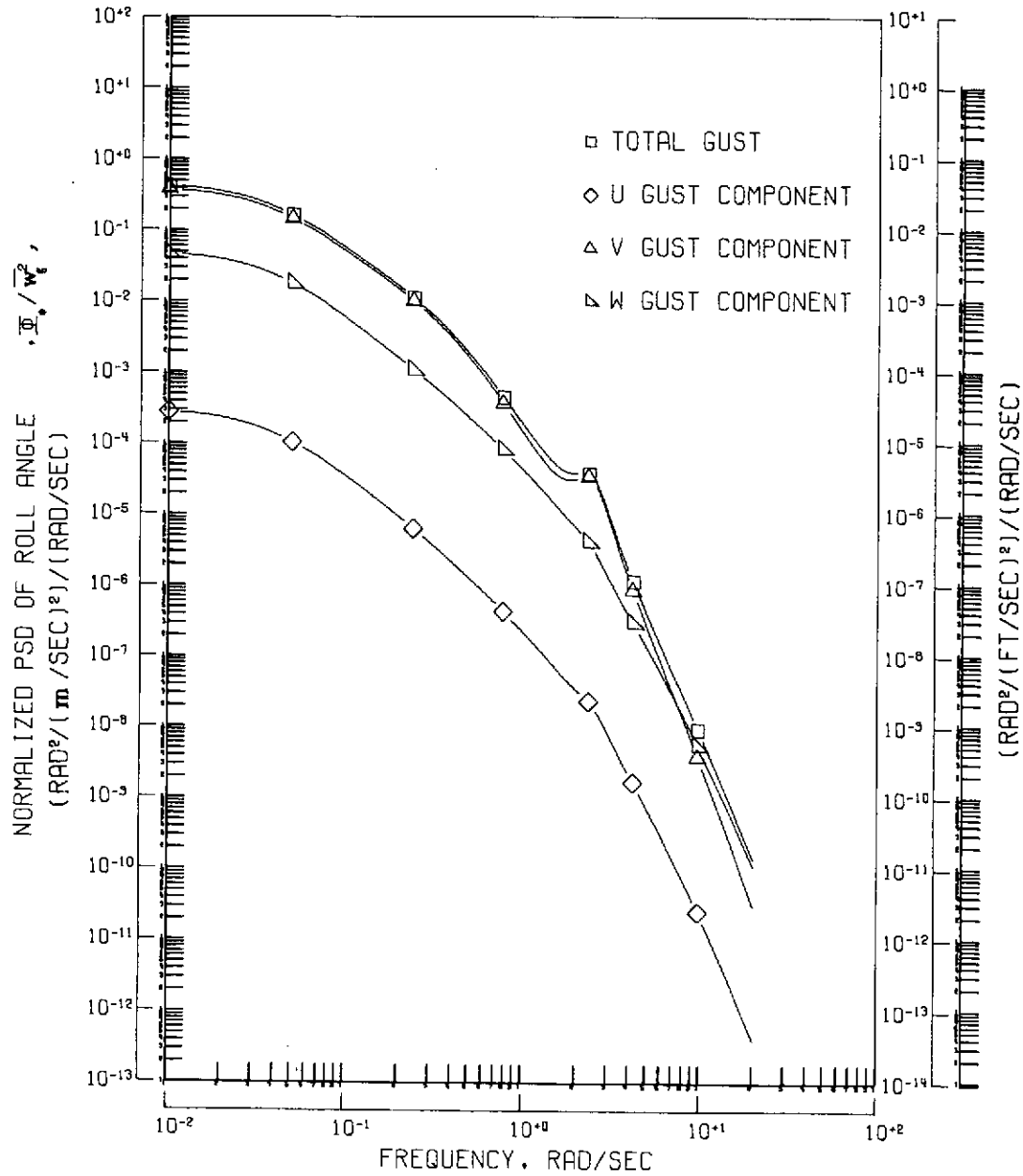

(b) Normalized total and individual component power spectral density response in roll for each of the gust components.

Figure 5.- Continued.

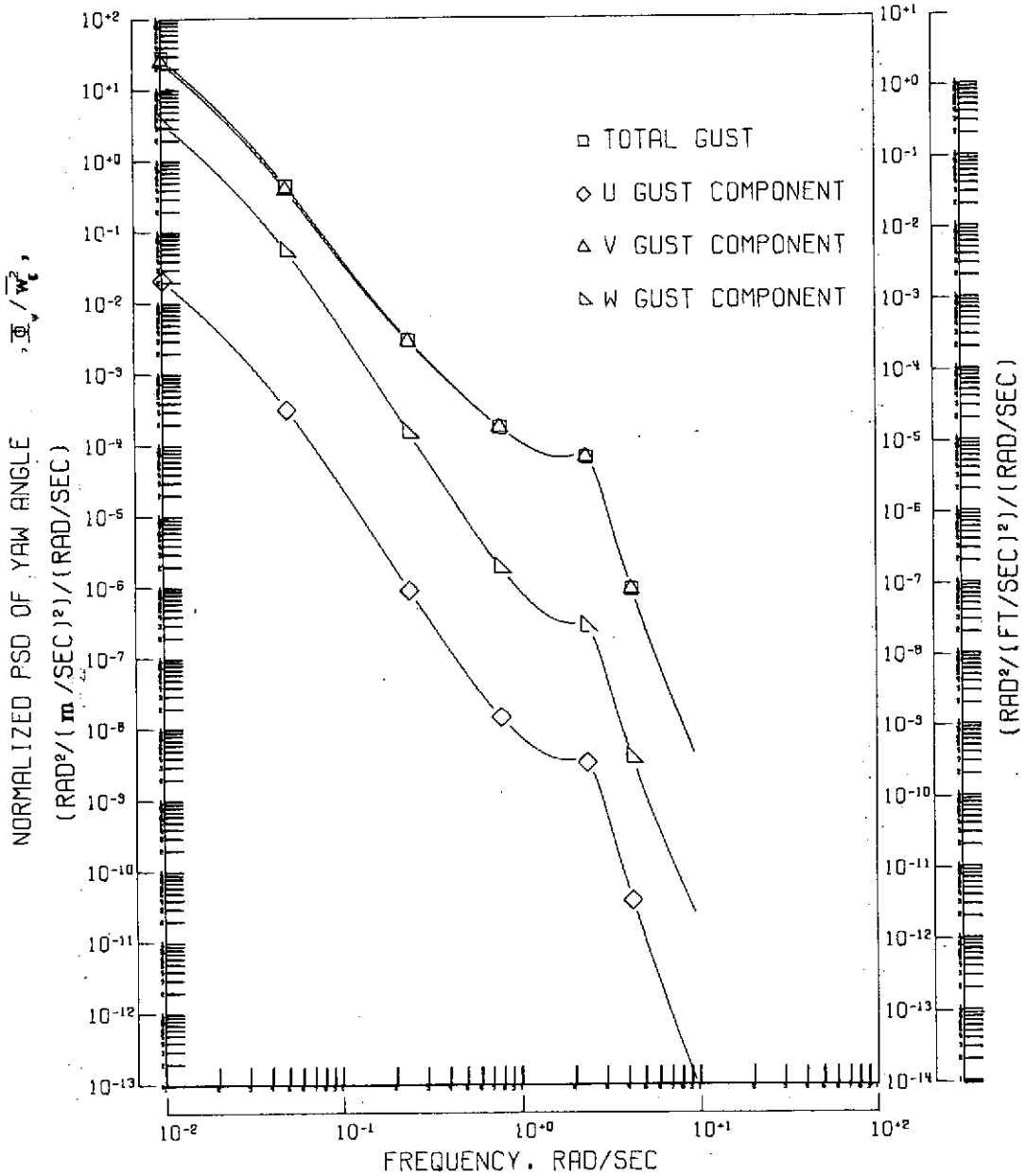

(c) Normalized total and individual component power spectral density response in yaw for each of the gust components.

Figure 5.- Continued.

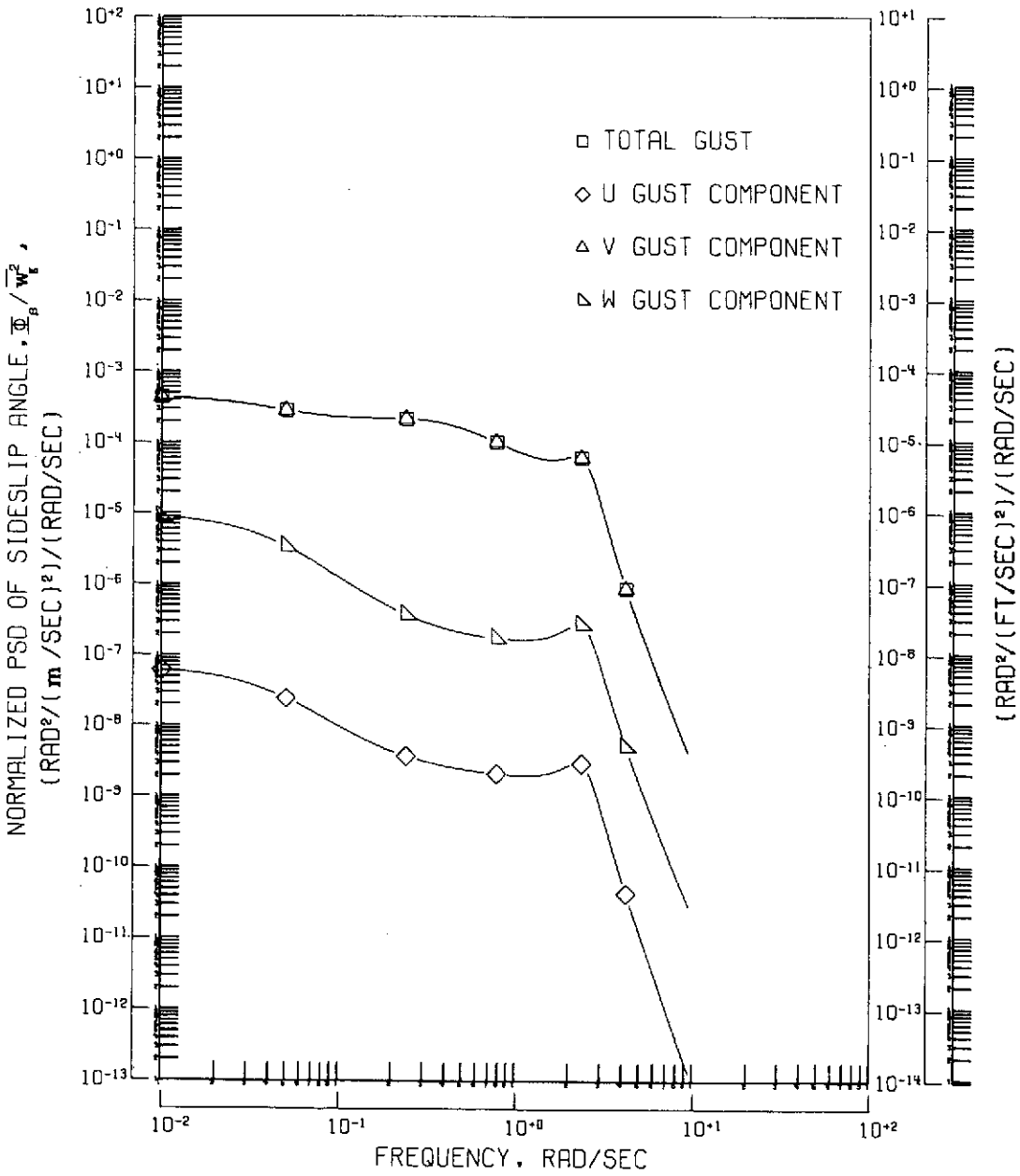

(d) Normalized total and individual component power spectral density response in sideslip for each of the gust components.

Figure 5.- Continued.

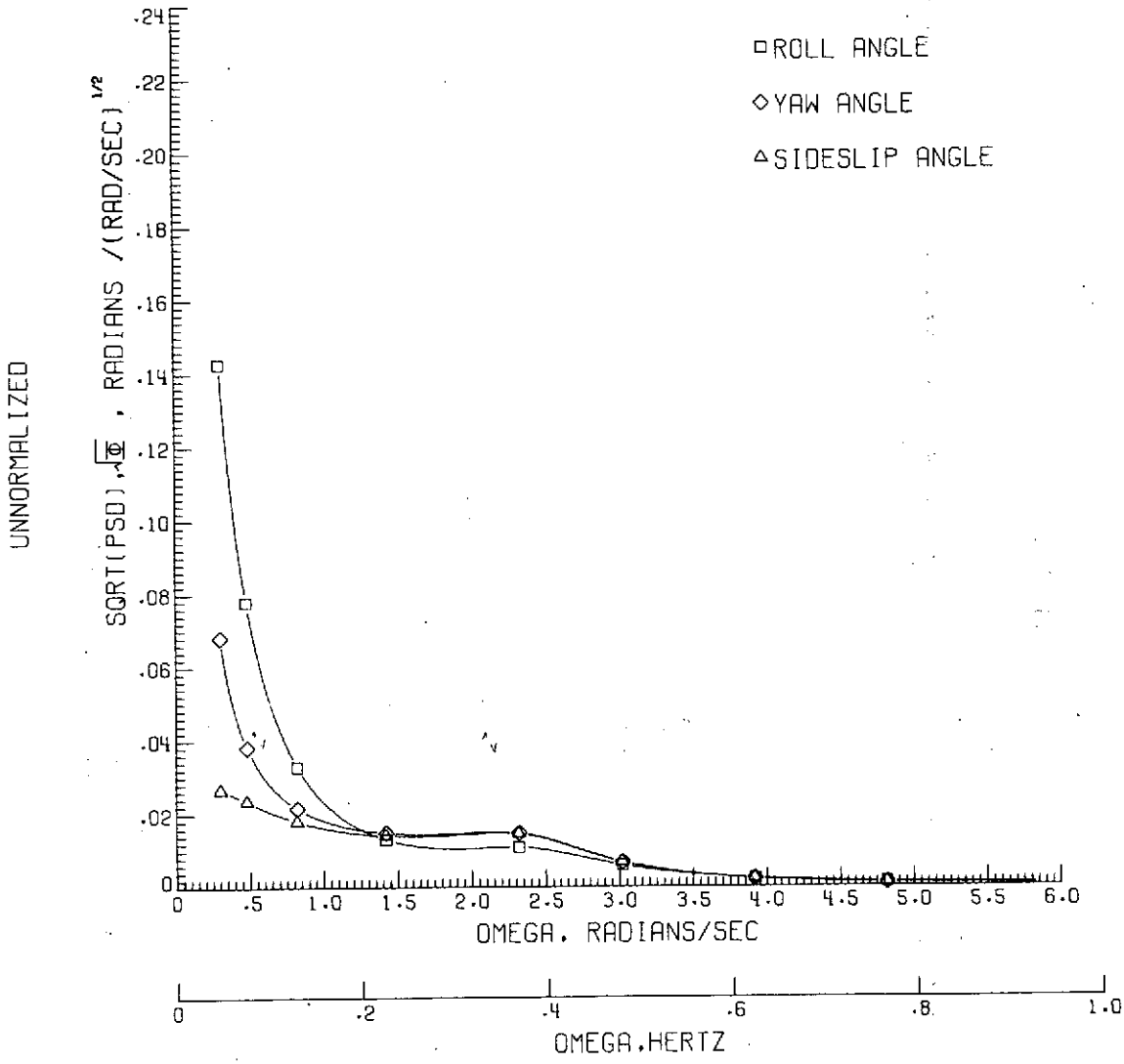

(e) Square root of the dimensional power spectral density response for each of the lateral displacements. The average gust intensity was 1.83 m/sec (6 ft/sec).

Figure 5.- Concluded.

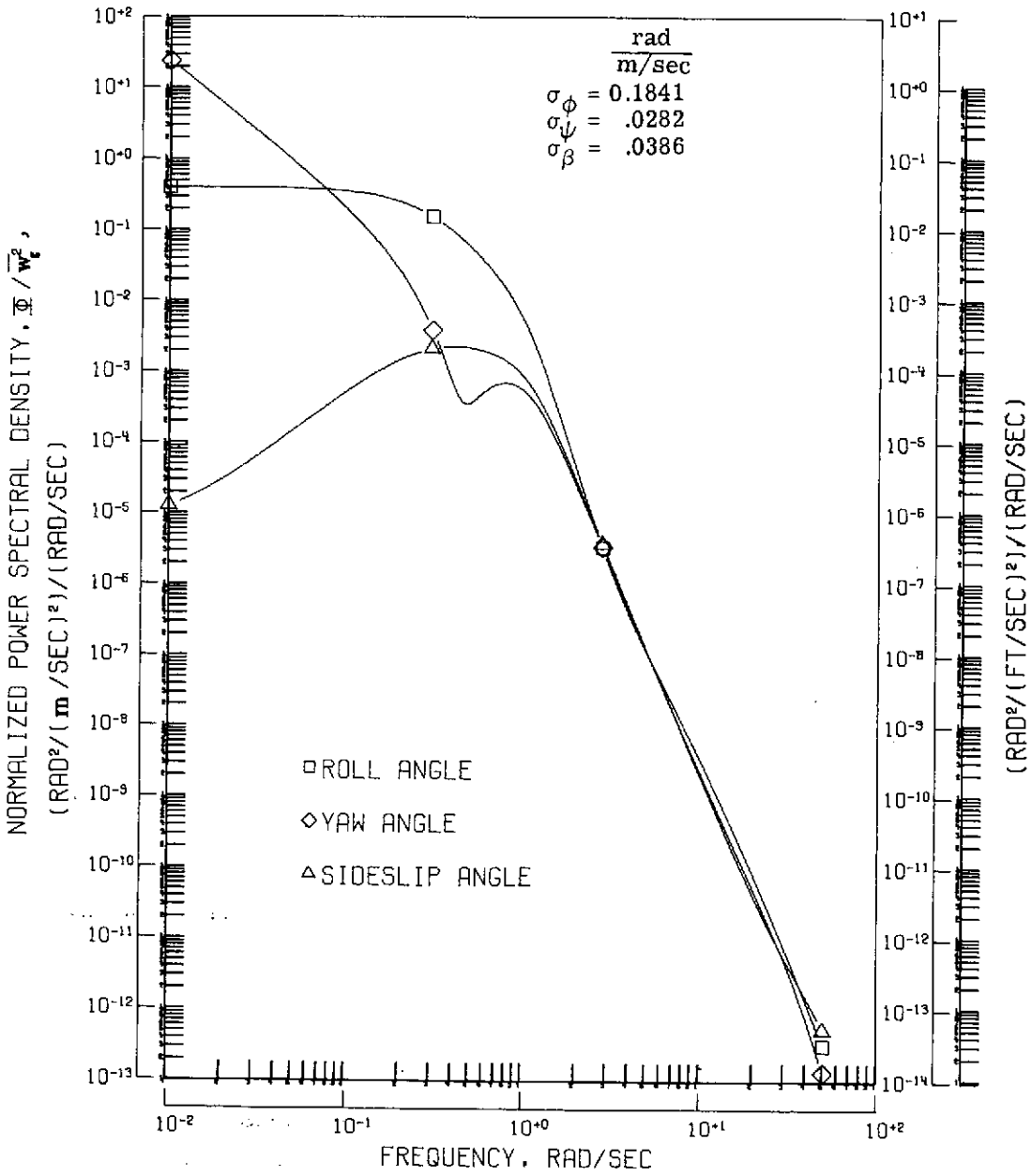

(a) Normalized total power spectral density response for each of the lateral displacements.

Figure 6.- Response of "large STOL C" airplane to random gusts for an assumed scale length of 335.28 m (1100 ft).

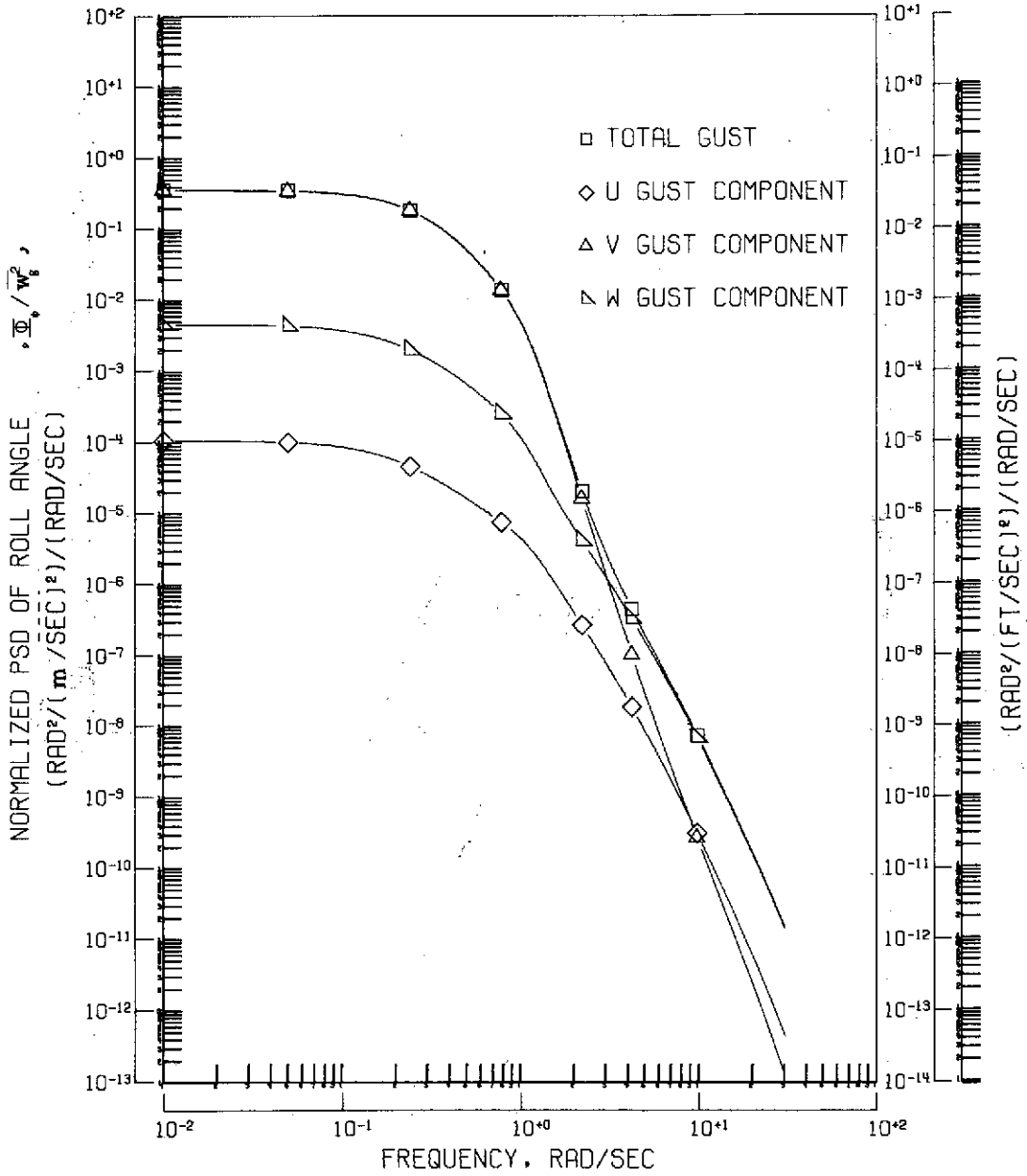

(b) Normalized total and individual component power spectral density response in roll for each of the gust components.

Figure 6.- Continued.

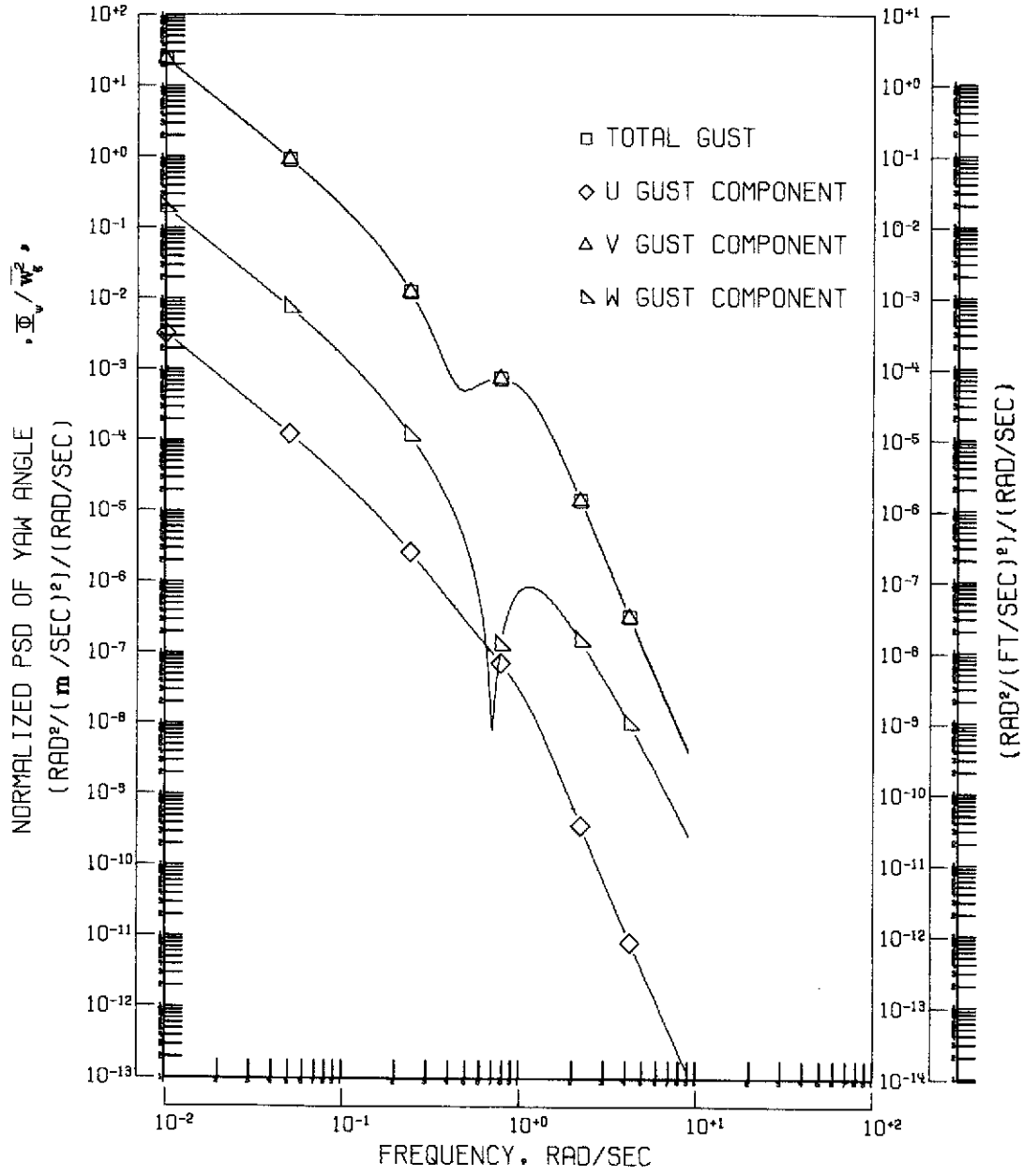

(c) Normalized total and individual component power spectral density response in yaw for each of the gust components.

Figure 6.- Continued.

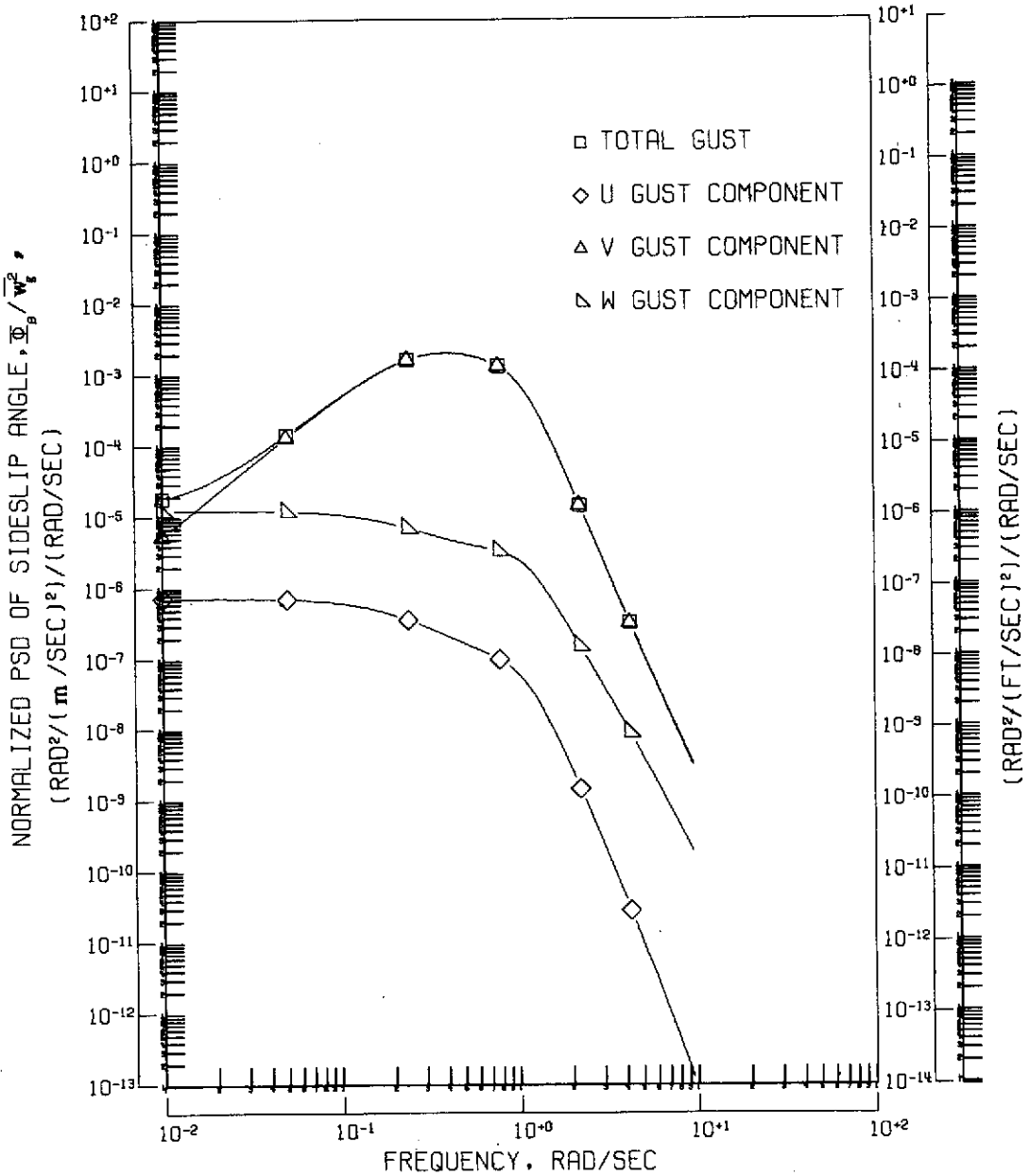

(d) Normalized total and individual component power spectral density response in sideslip for each of the gust components.

Figure 6.- Continued.

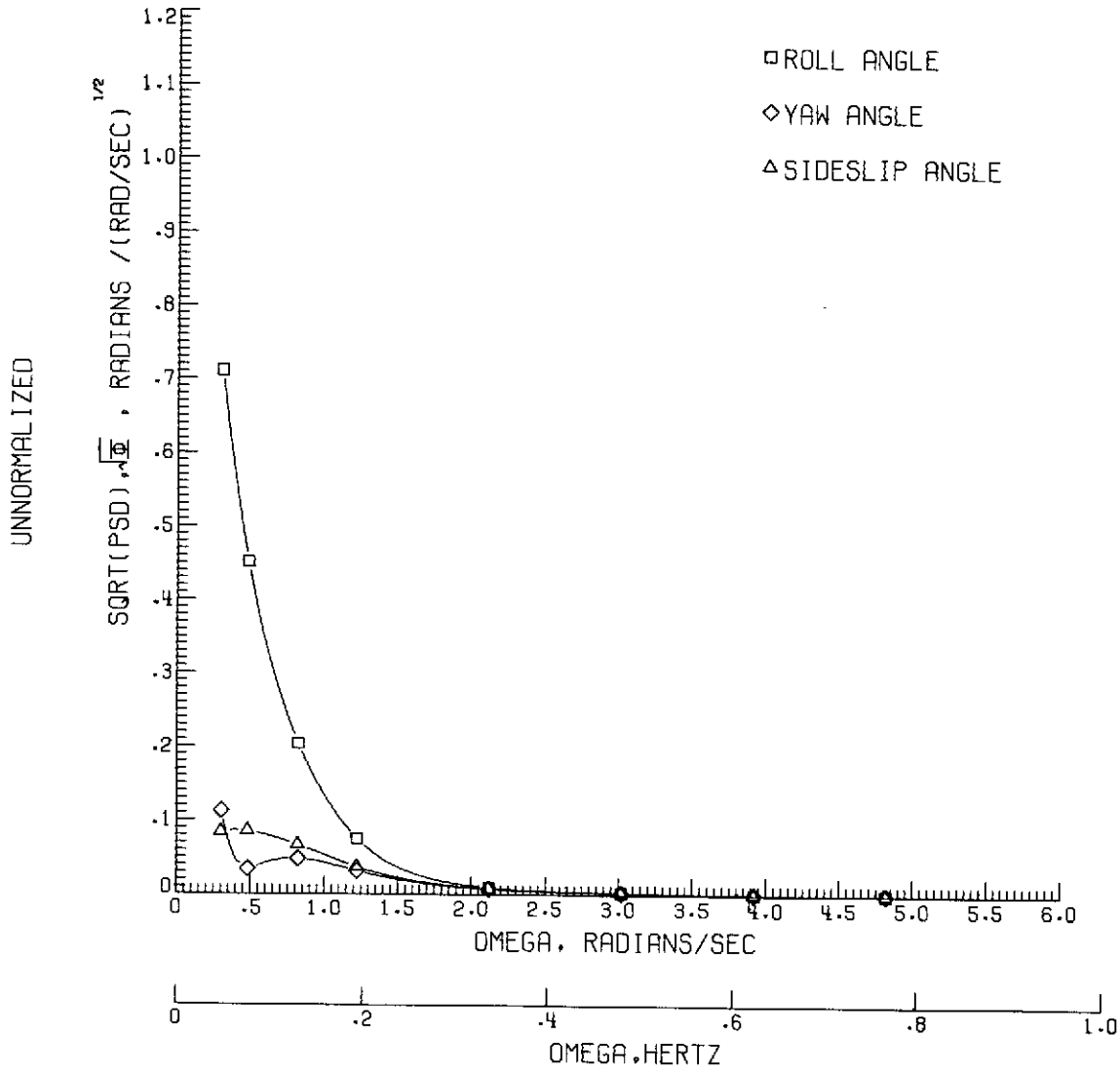

(e) Square root of the dimensional power spectral density response for each of the lateral displacements. The average gust intensity was 1.83 m/sec (6 ft/sec).

Figure 6.- Concluded.

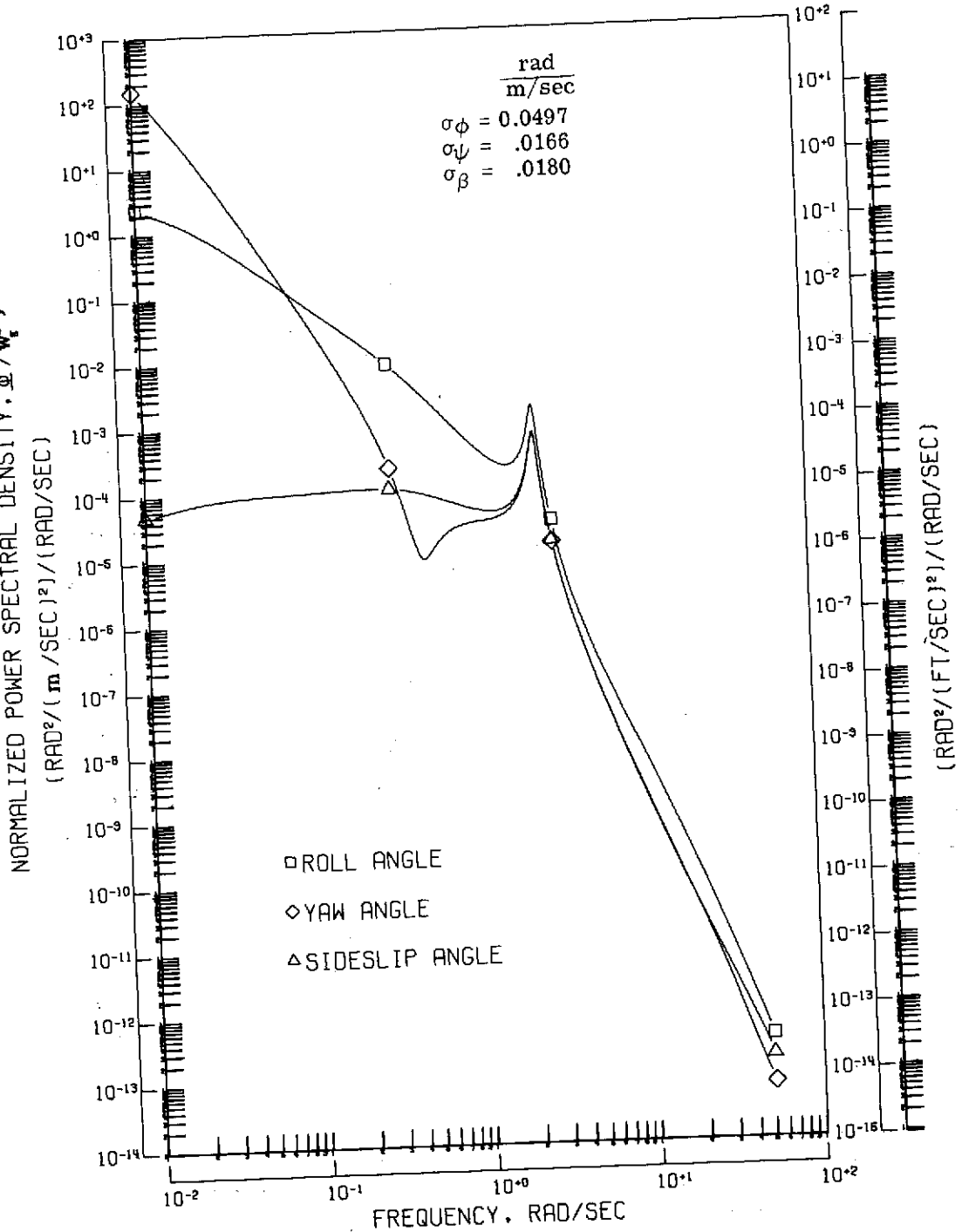

(a) Normalized total power spectral density response for each of the lateral displacements.

Figure 7.- Response of "large STOL D" airplane to random gusts for an assumed scale length of 335.28 m (1100 ft).

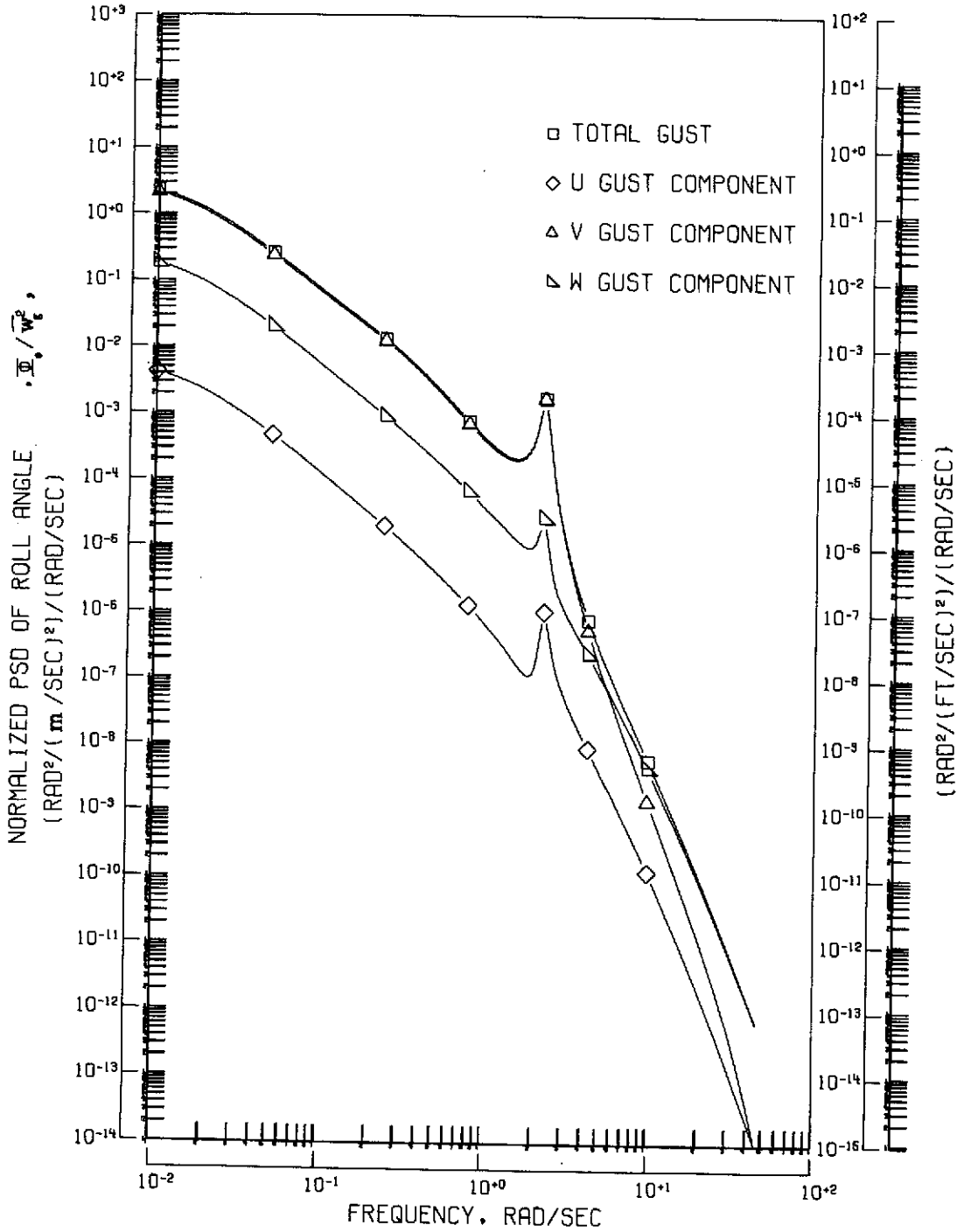

(b) Normalized total and individual component power spectral density response in roll for each of the gust components.

Figure 7.- Continued.

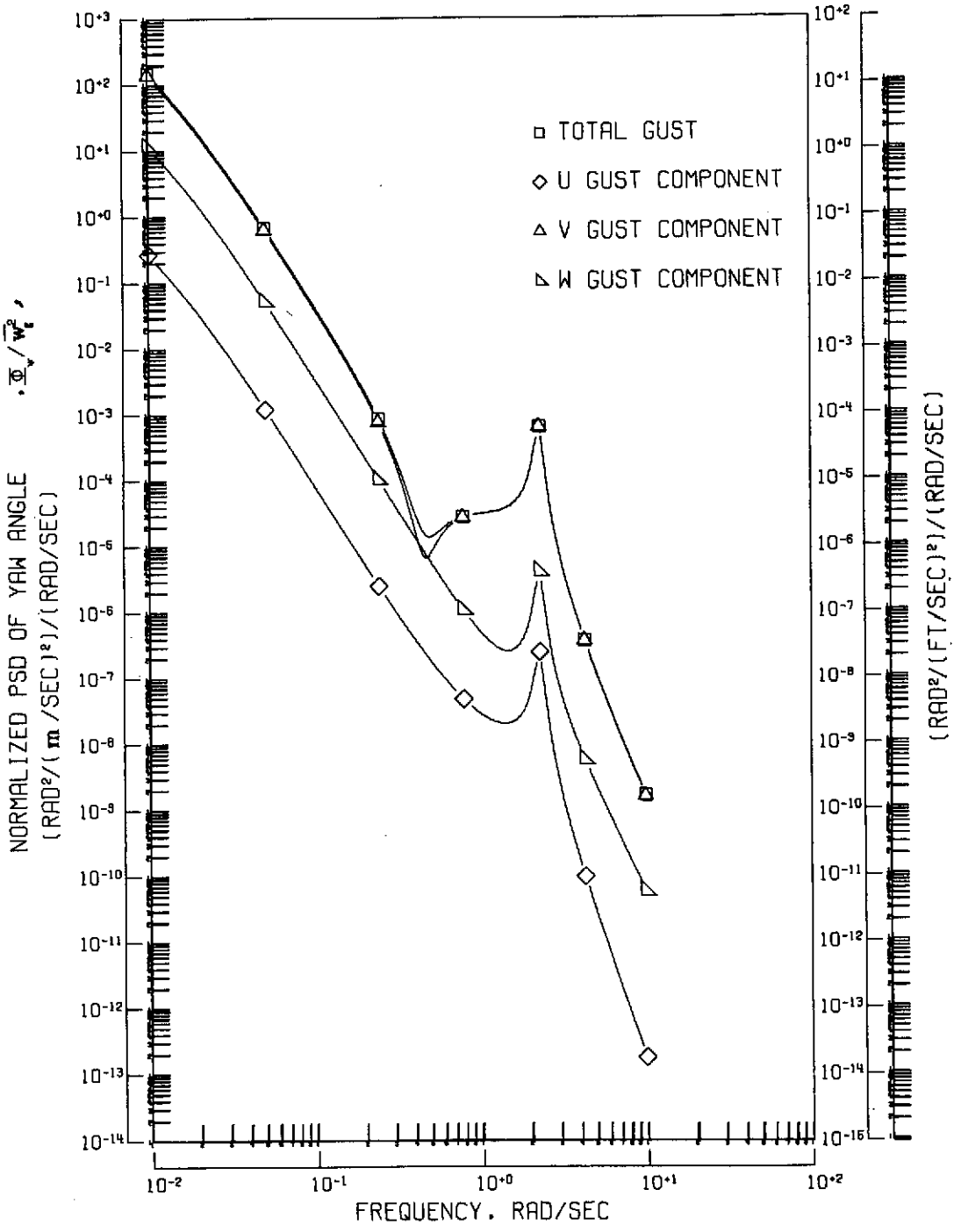

(c) Normalized total and individual component power spectral density response in yaw for each of the gust components.

Figure 7.- Continued.

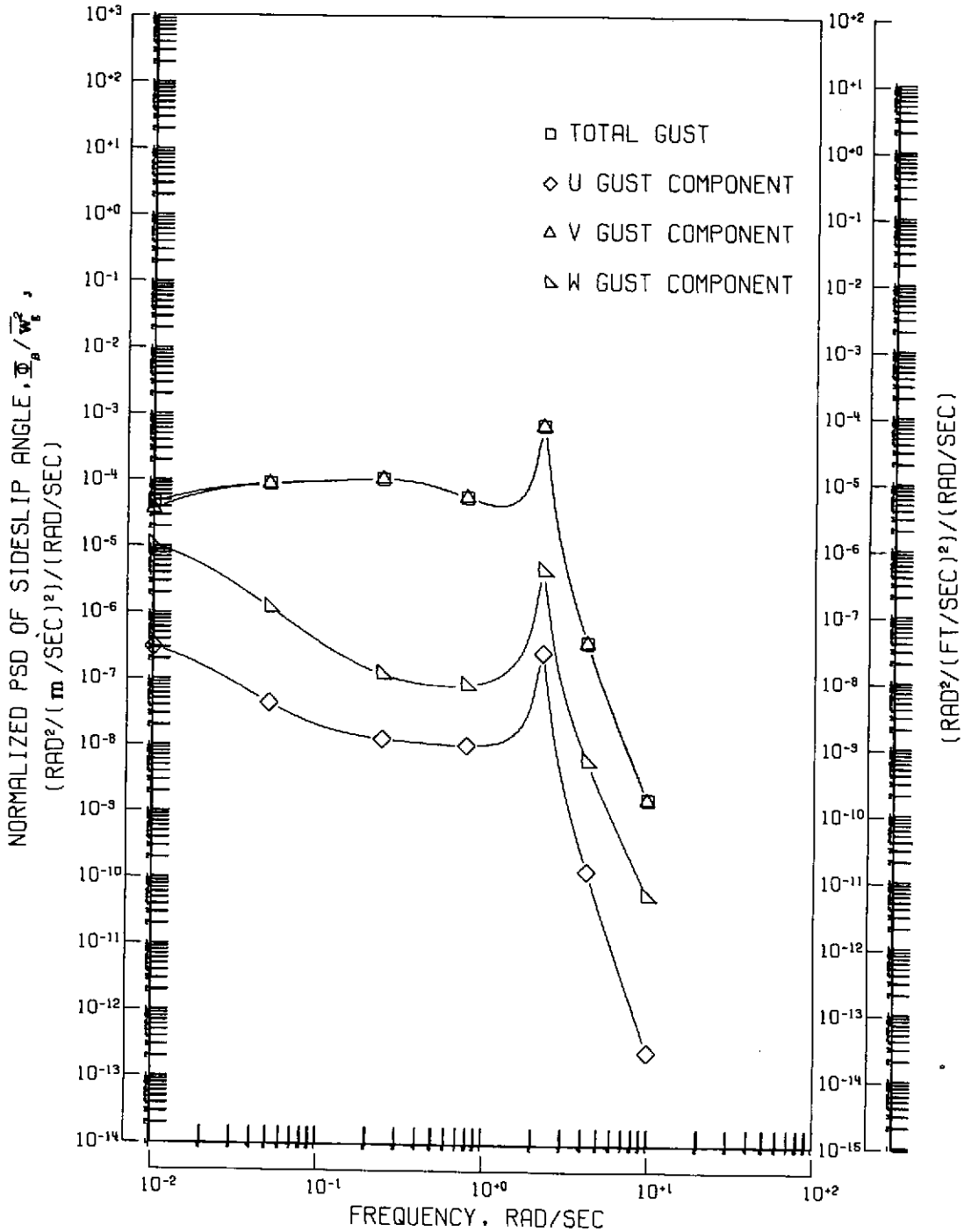

(d) Normalized total and individual component power spectral density response in sideslip for each of the gust components.

Figure 7.- Continued.

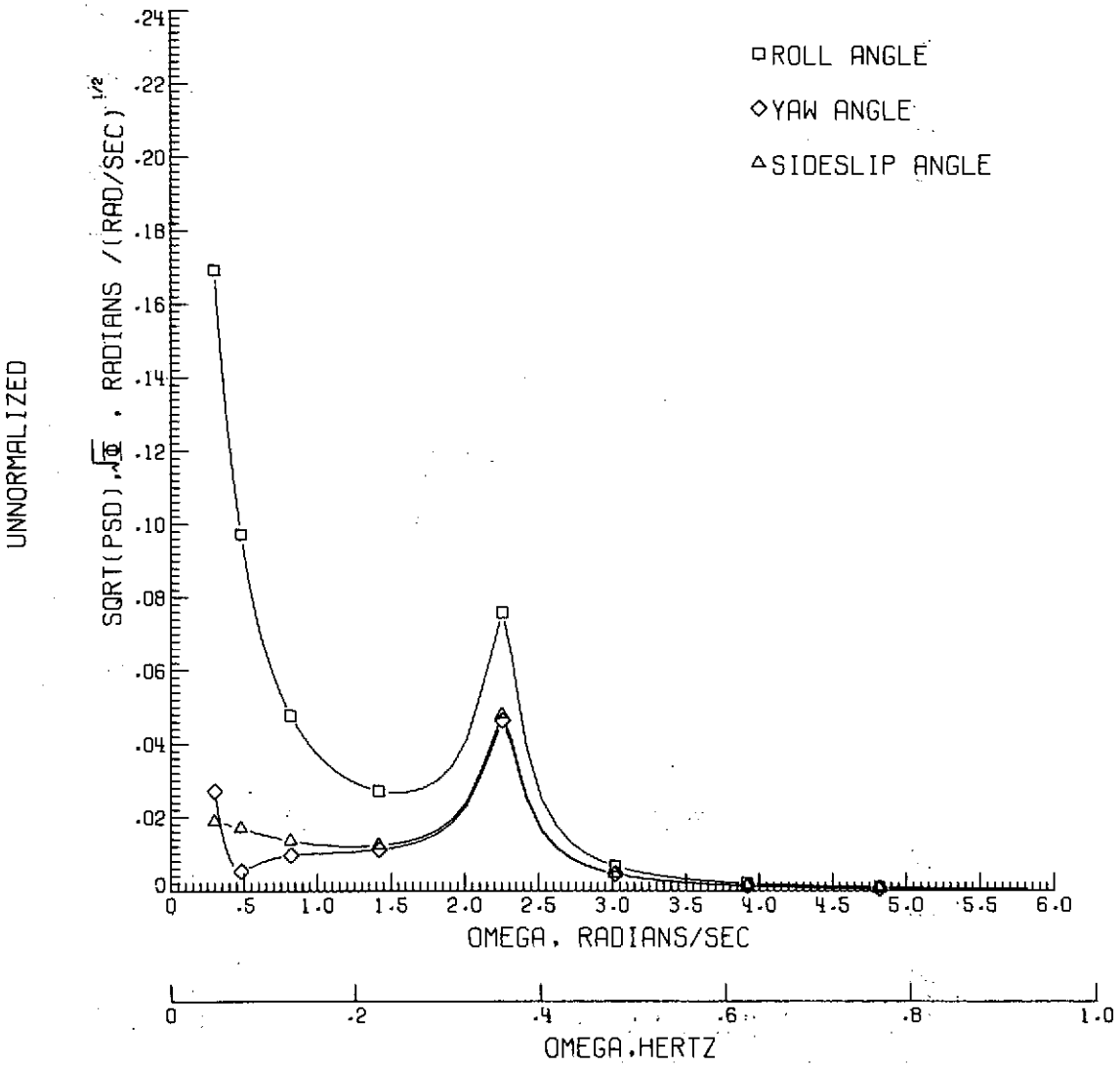

(e) Square root of the dimensional power spectral density response for each of the lateral displacements. The average gust intensity was 1.83 m/sec (6 ft/sec).

Figure 7.- Concluded.

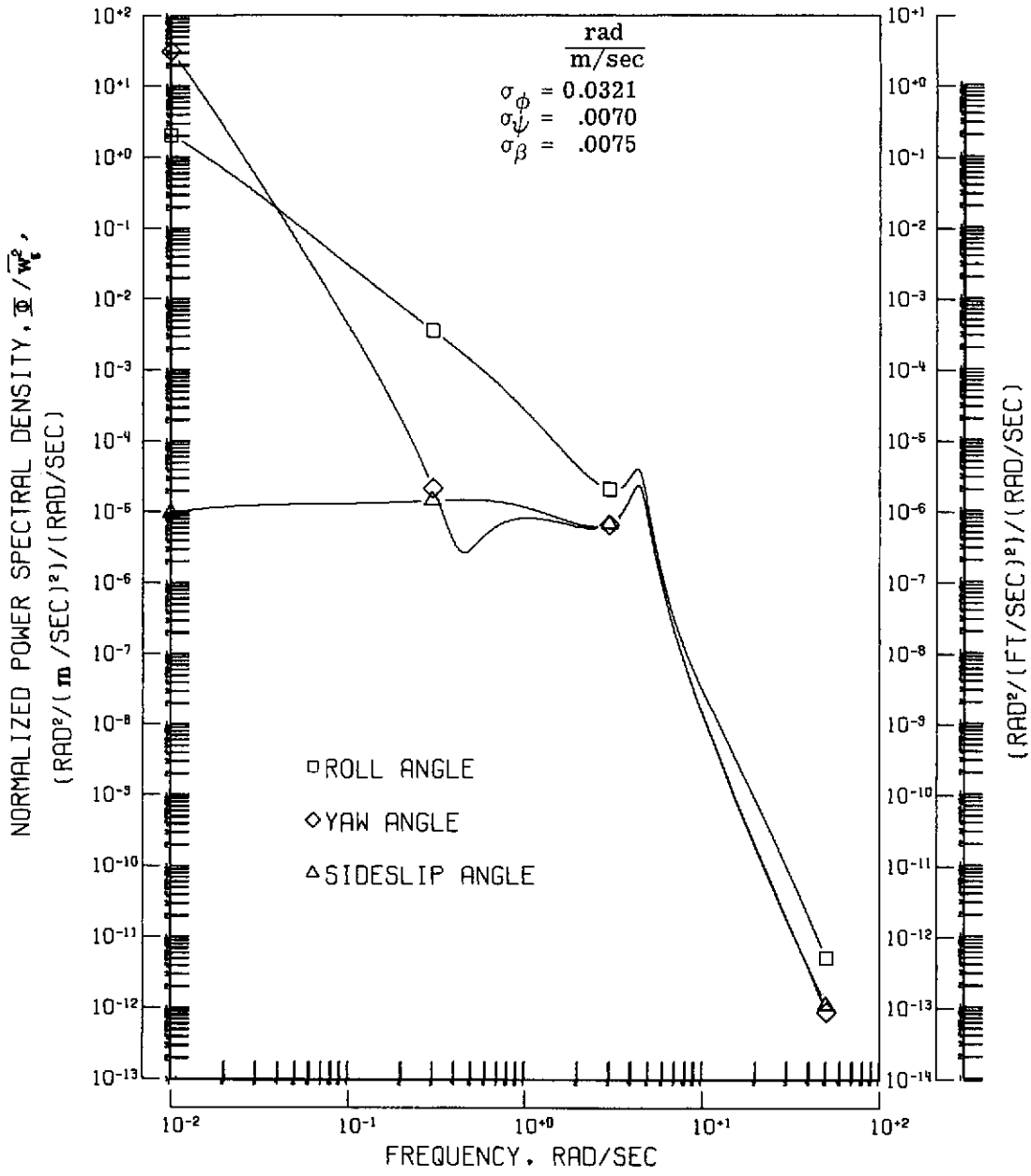

(a) Normalized total power spectral density response for each of the lateral displacements.

Figure 8.- Response of "large STOL E" airplane to random gusts for an assumed scale length of 335.28 m (1100 ft).

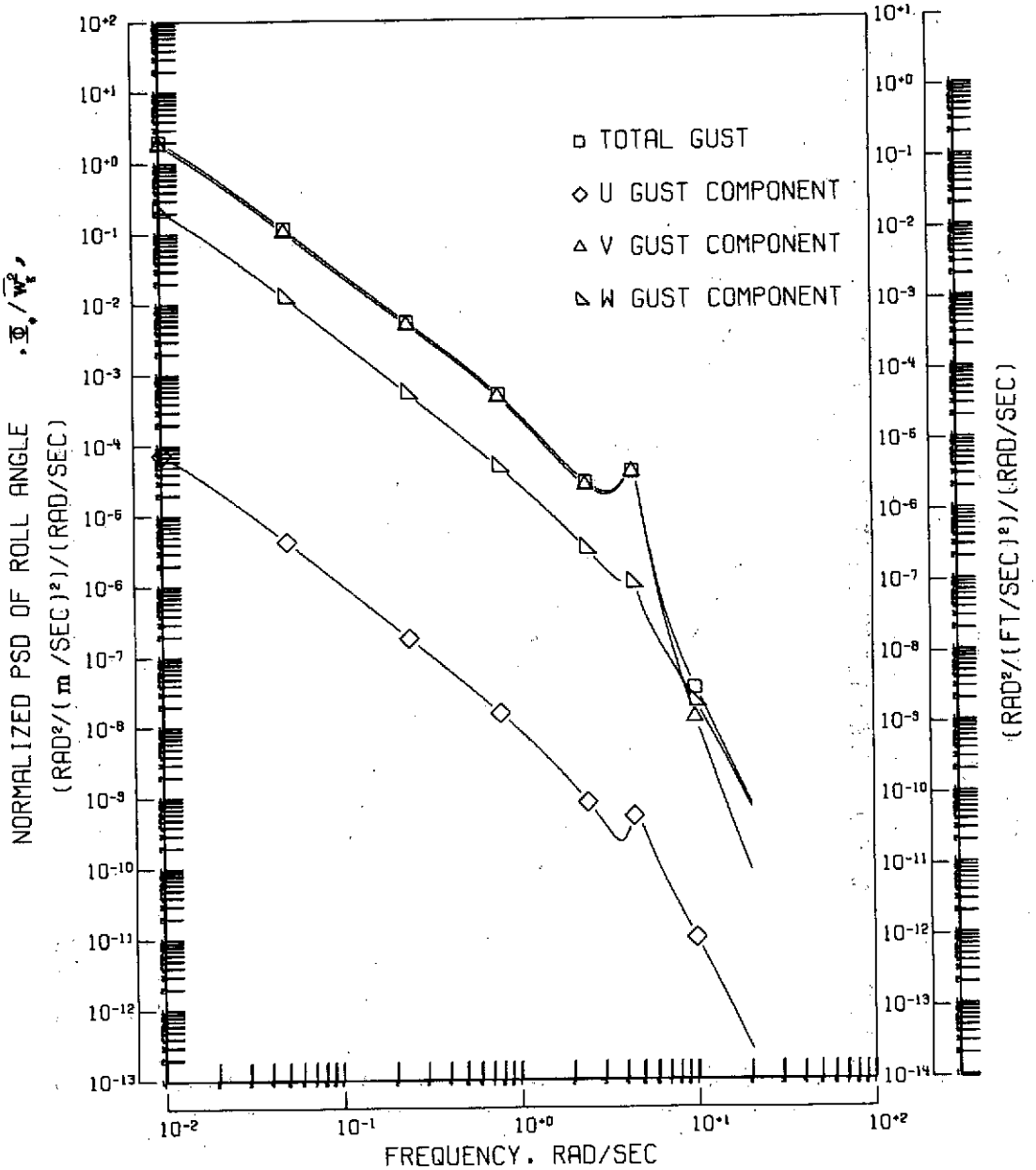

(b) Normalized total and individual component power spectral density response in roll for each of the gust components.

Figure 8.- Continued.

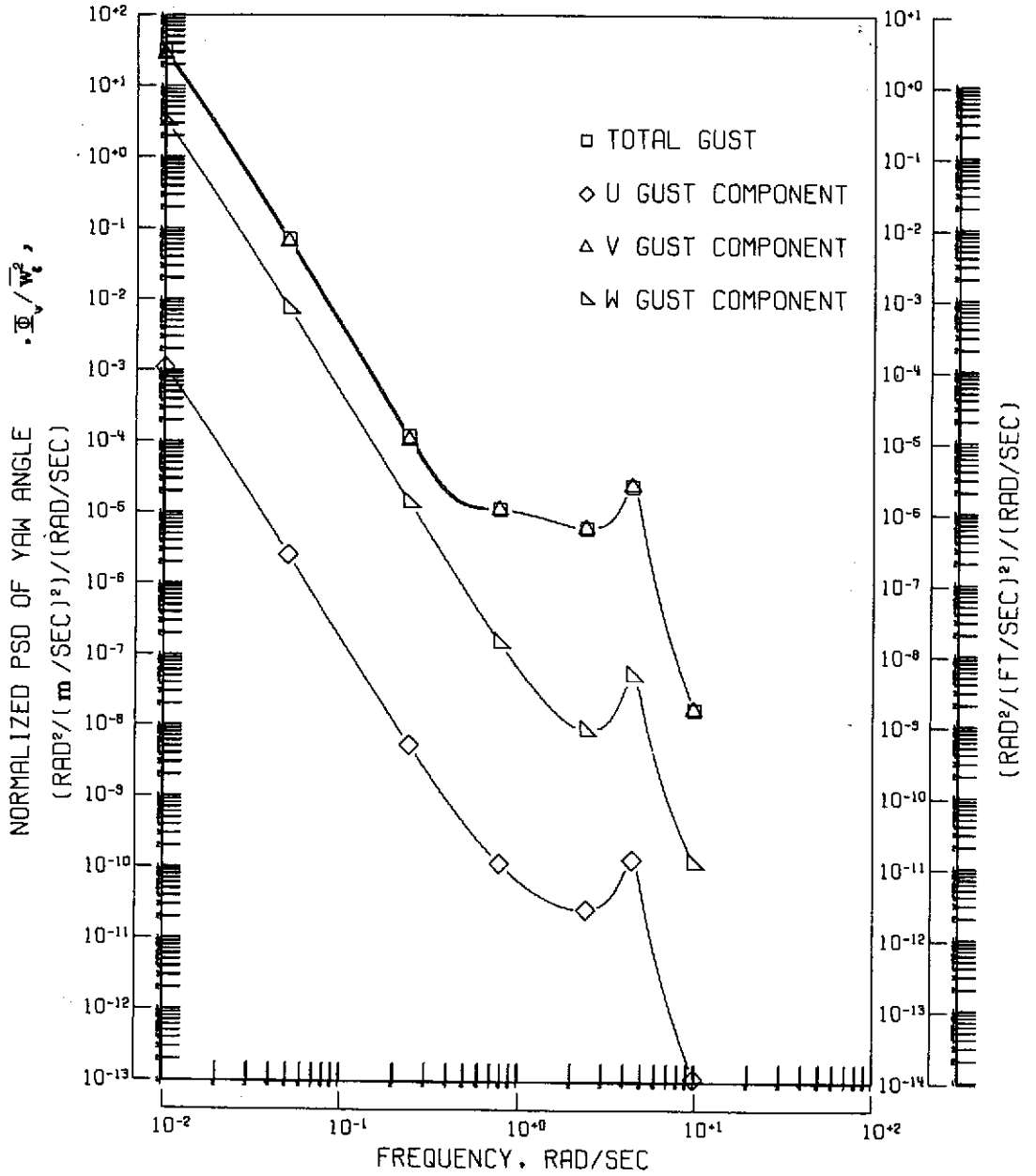

(c) Normalized total and individual component power spectral density response in yaw for each of the gust components.

Figure 8.- Continued.

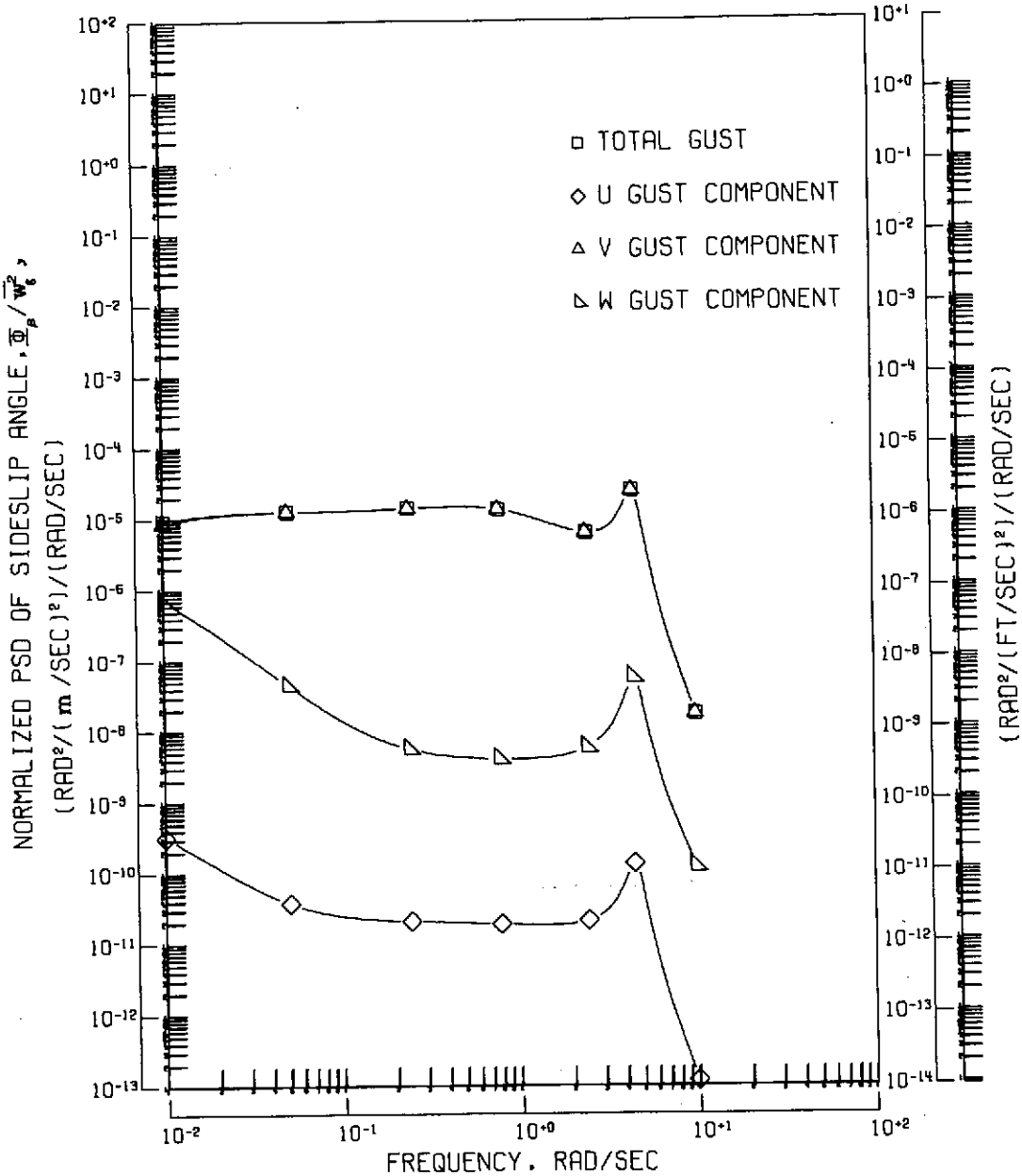

(d) Normalized total and individual component power spectral density response in sideslip for each of the gust components.

Figure 8.- Continued.

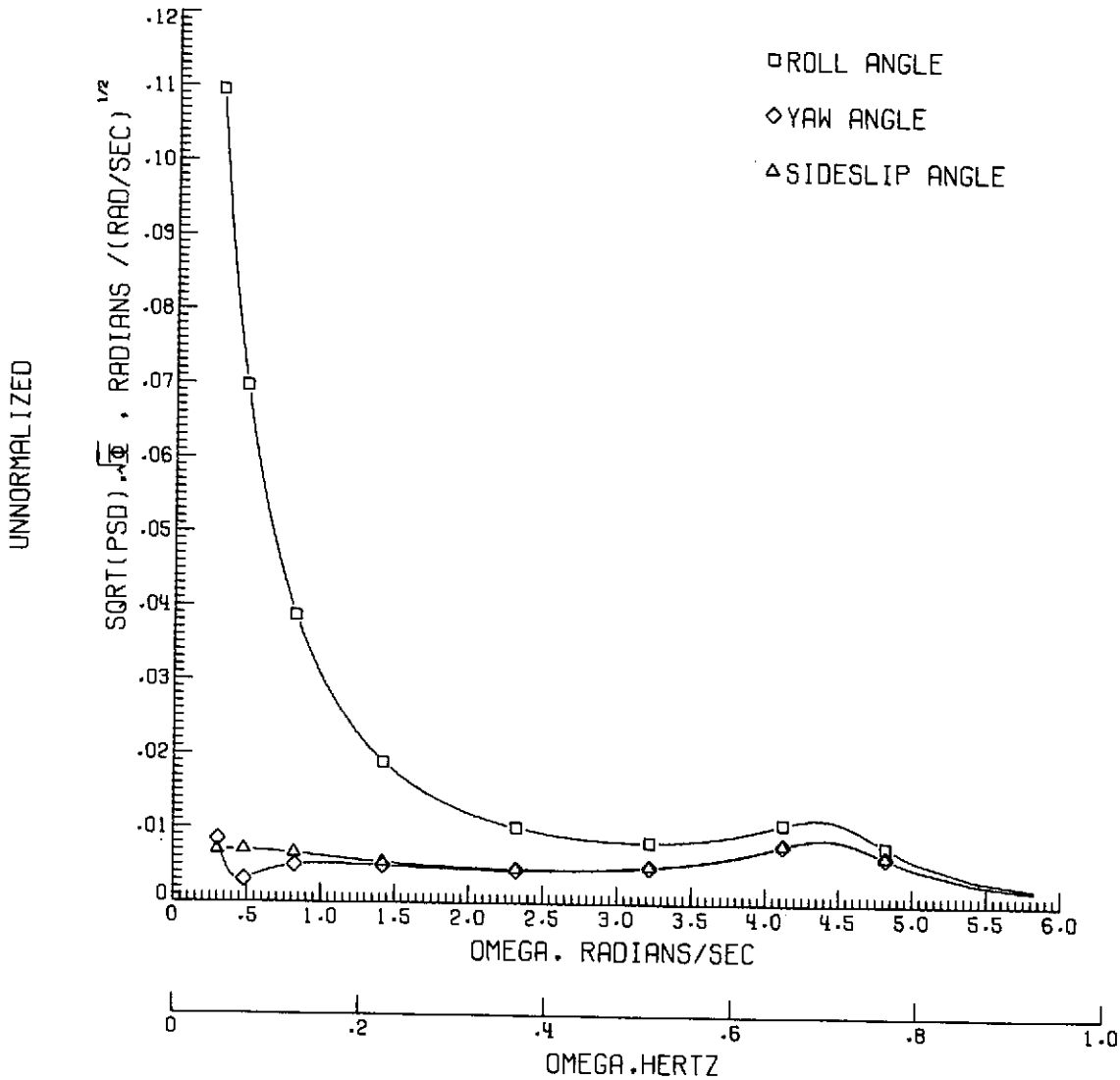

(e) Square root of the dimensional power spectral density response for each of the lateral displacements. The average gust intensity was 1.83 m/sec (6 ft/sec).

Figure 8.- Concluded.

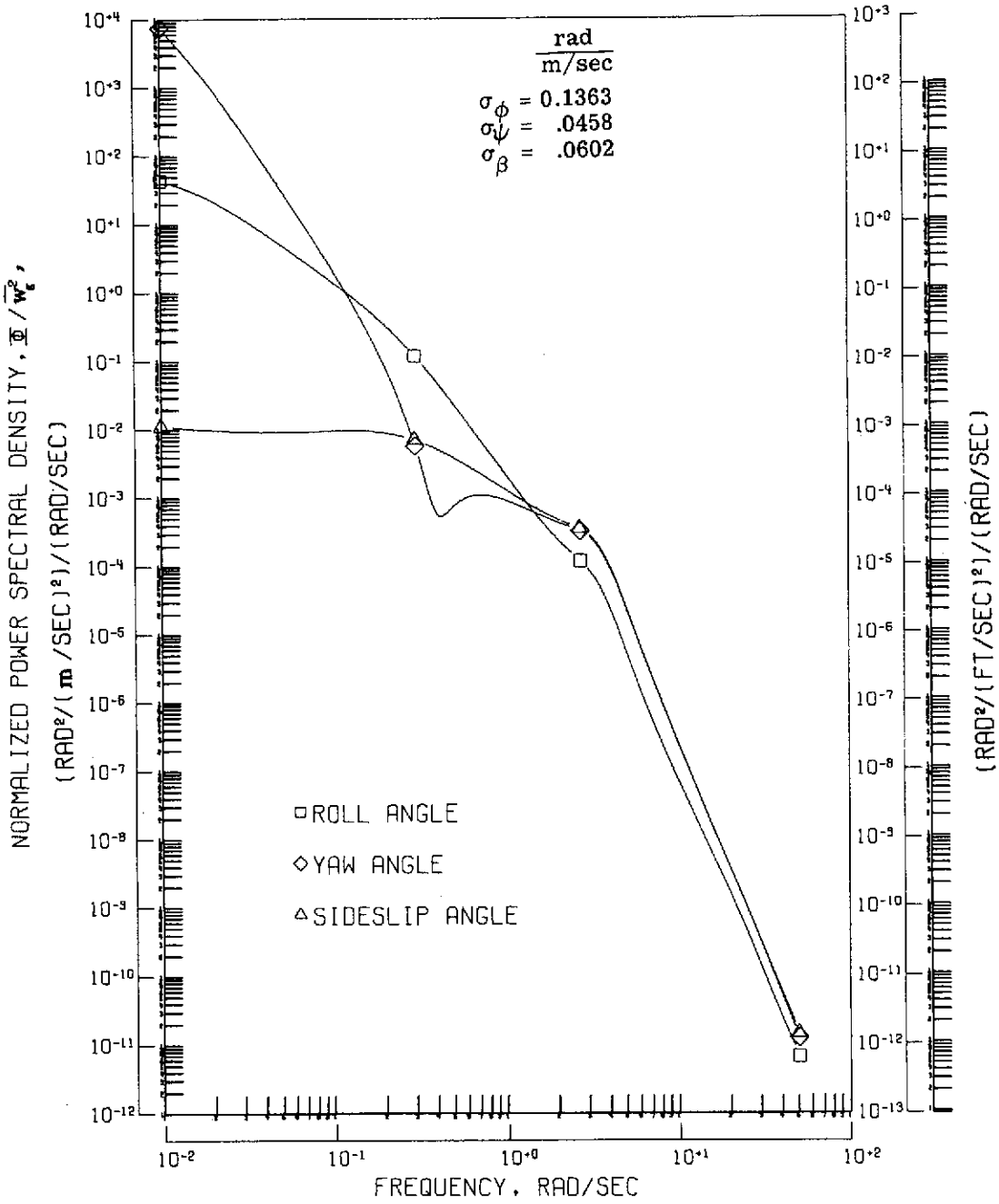

(a) Normalized total power spectral density response for each of the lateral displacements.

Figure 9.- Response of "small STOL A" airplane to random gusts for an assumed scale length of 335.28 m (1100 ft).

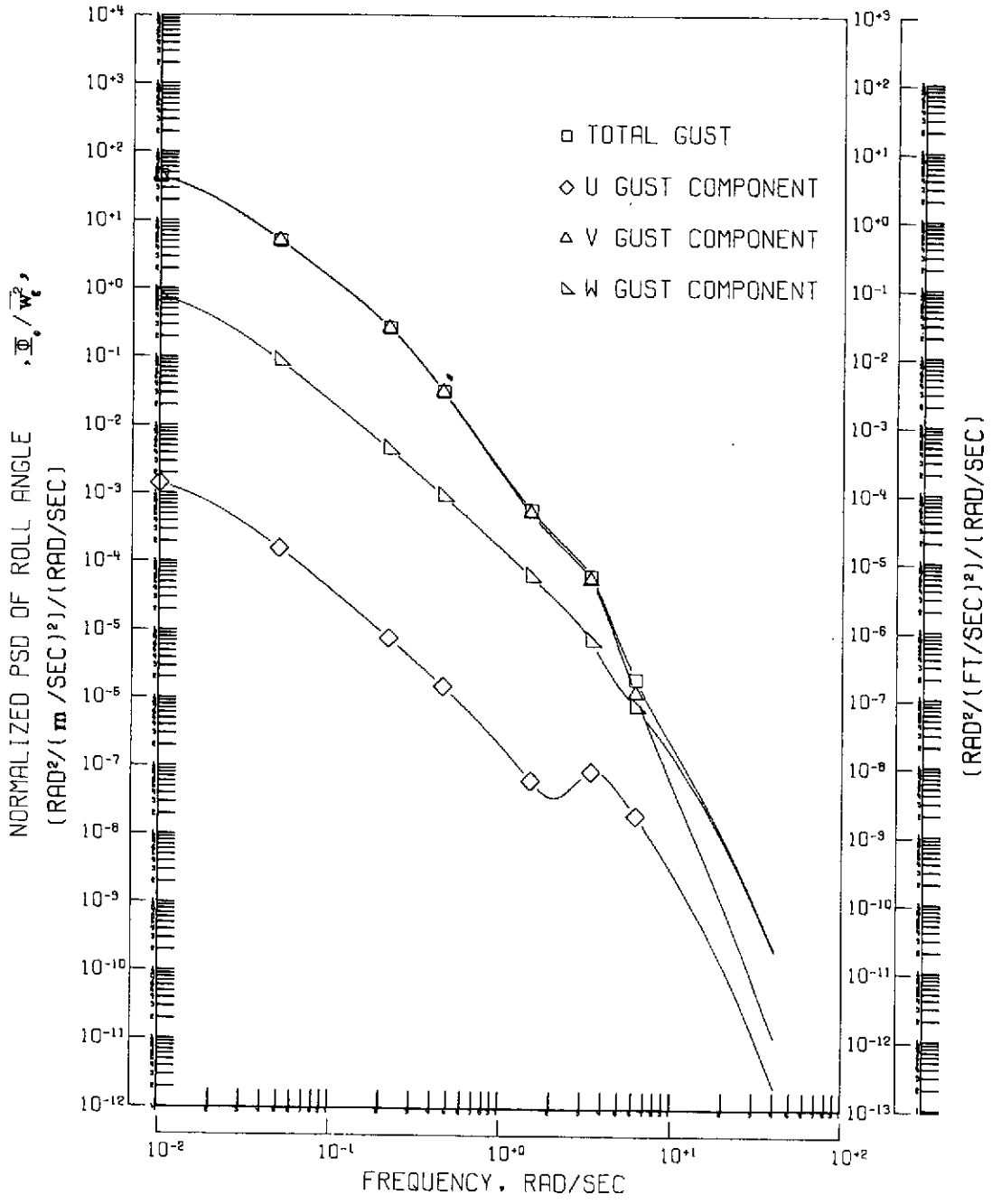

(b) Normalized total and individual component power spectral density response in roll for each of the gust components.

Figure 9.- Continued.

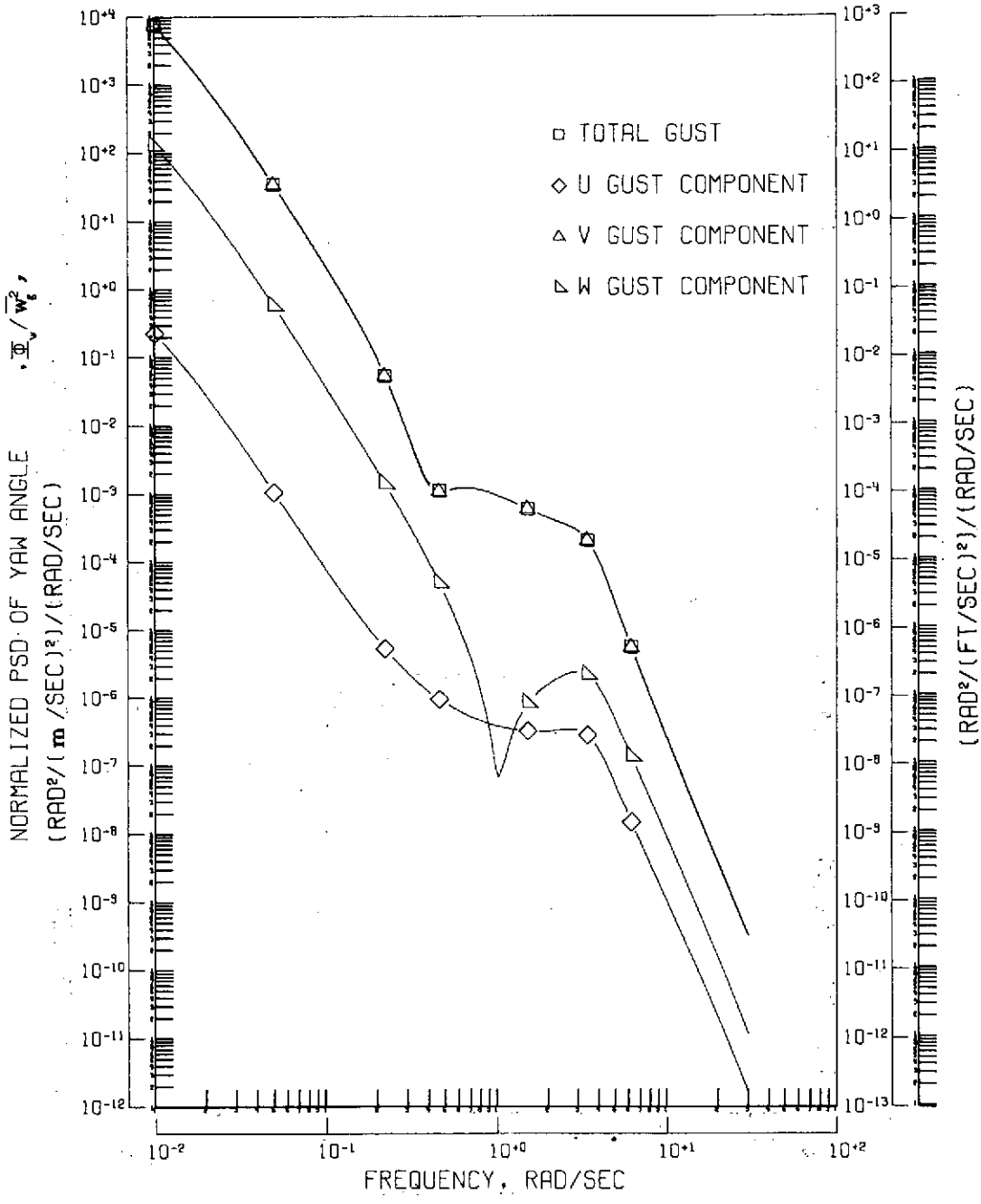

(c) Normalized total and individual component power spectral density response in yaw for each of the gust components.

Figure 9.- Continued.

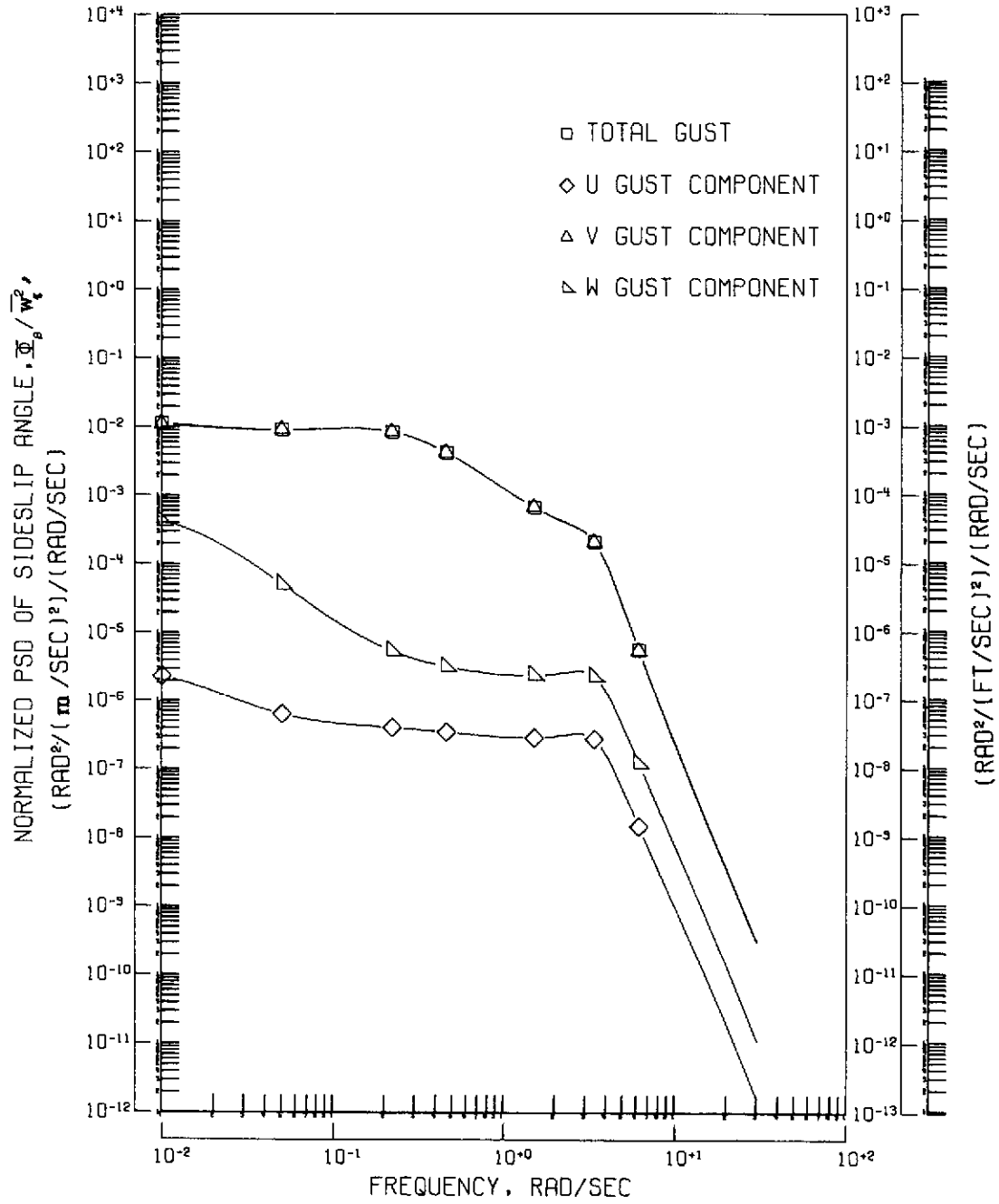

(d) Normalized total and individual component power spectral density response in sideslip for each of the gust components.

Figure 9.- Continued.

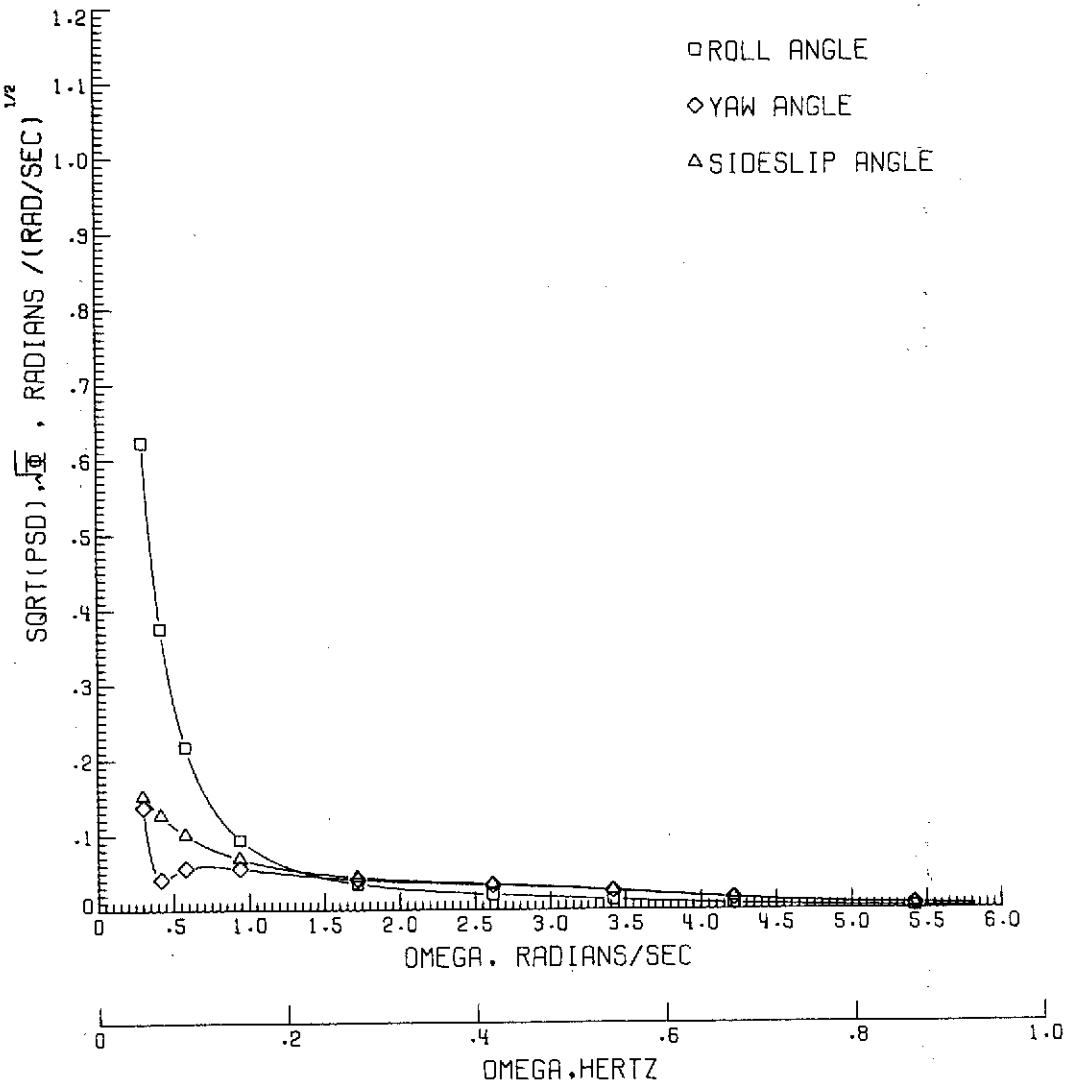

(e) Square root of the dimensional power spectral density response for each of the lateral displacements. The average gust intensity was 1.83 m/sec (6 ft/sec).

Figure 9.- Concluded.

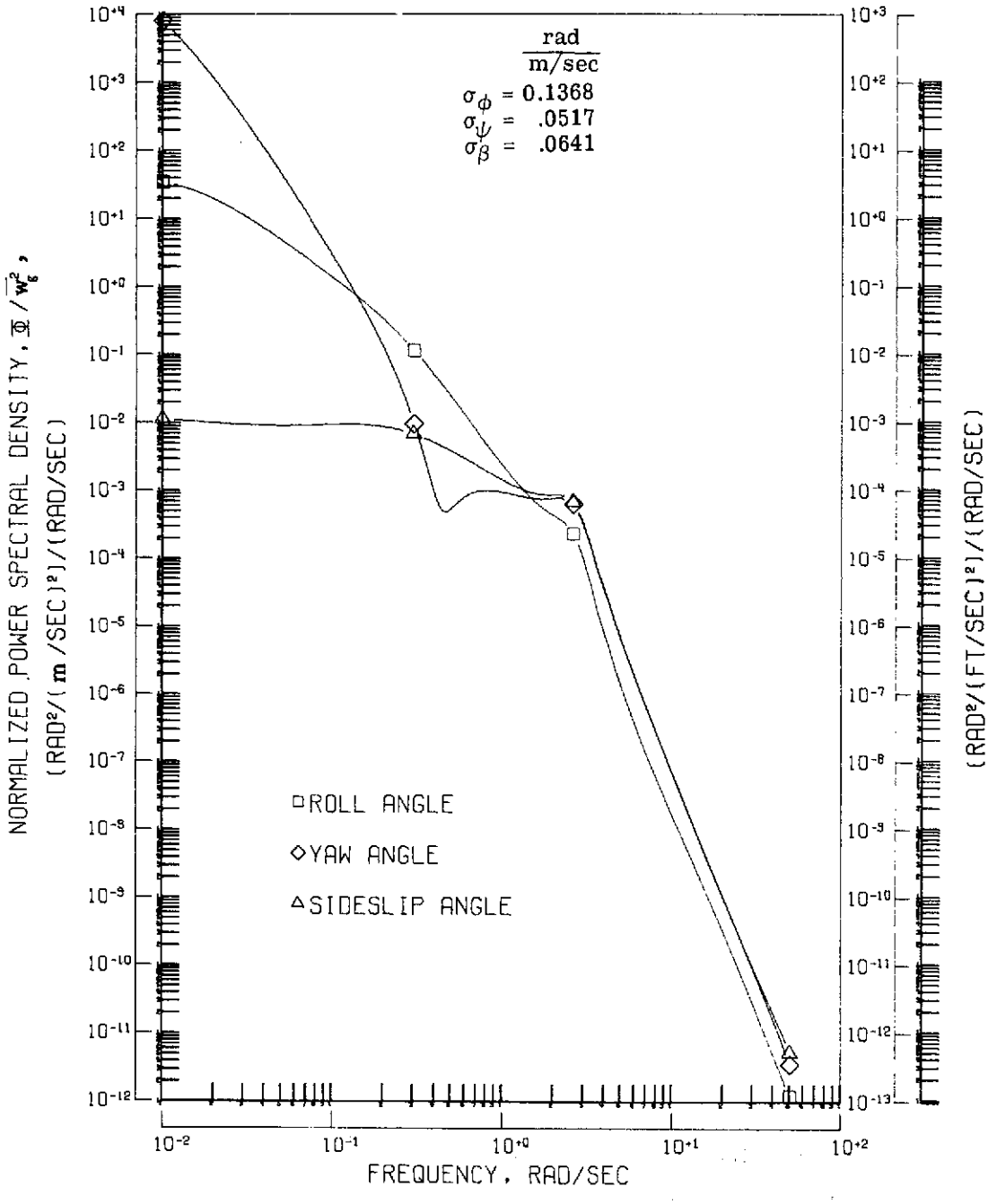

(a) Normalized total power spectral density response for each of the lateral displacements.

Figure 10.- Response of "small STOL B" airplane to random gusts for an assumed scale length of 335.28 m (1100 ft).

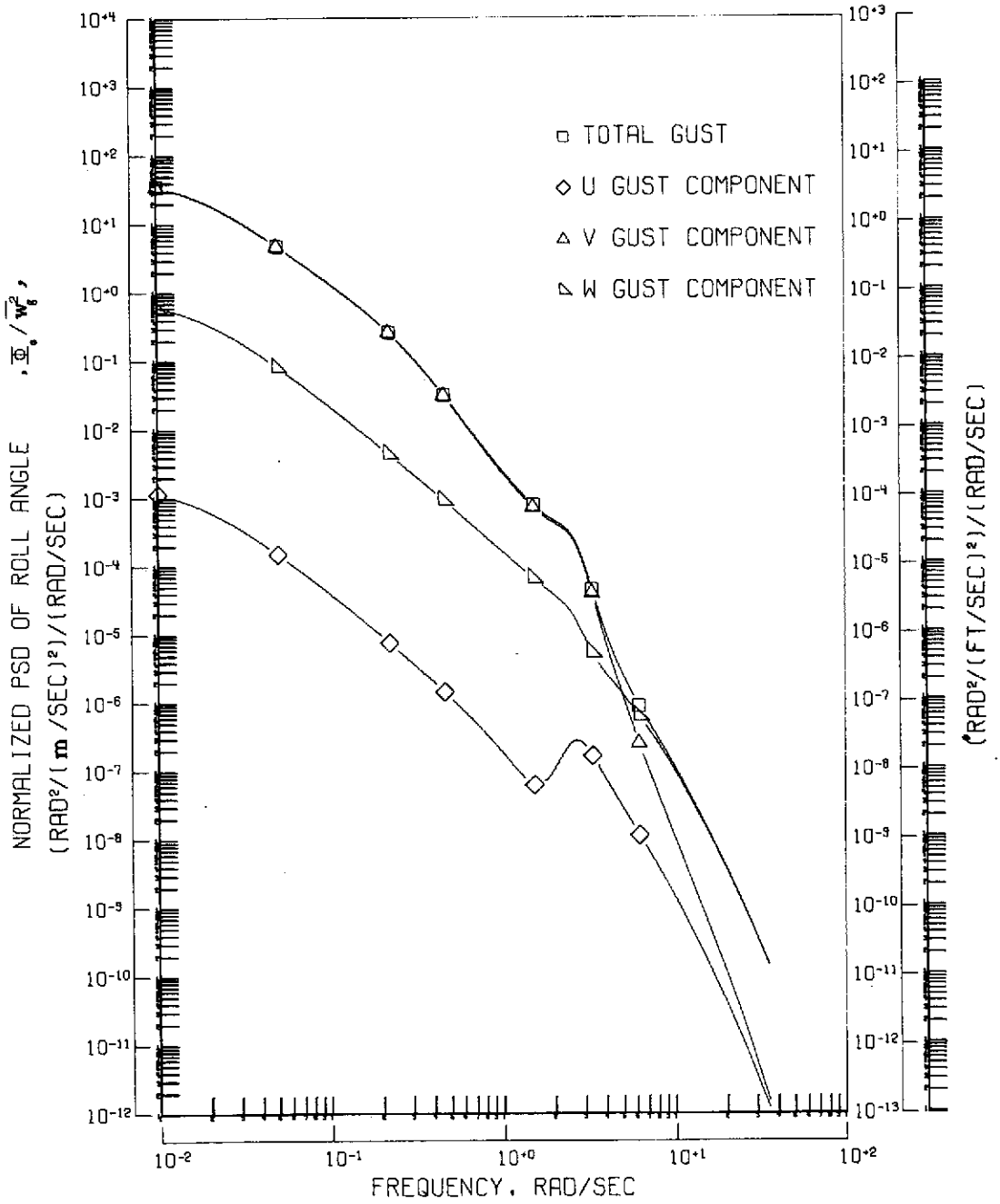

(b) Normalized total and individual component power spectral density response in roll for each of the gust components.

Figure 10.- Continued.

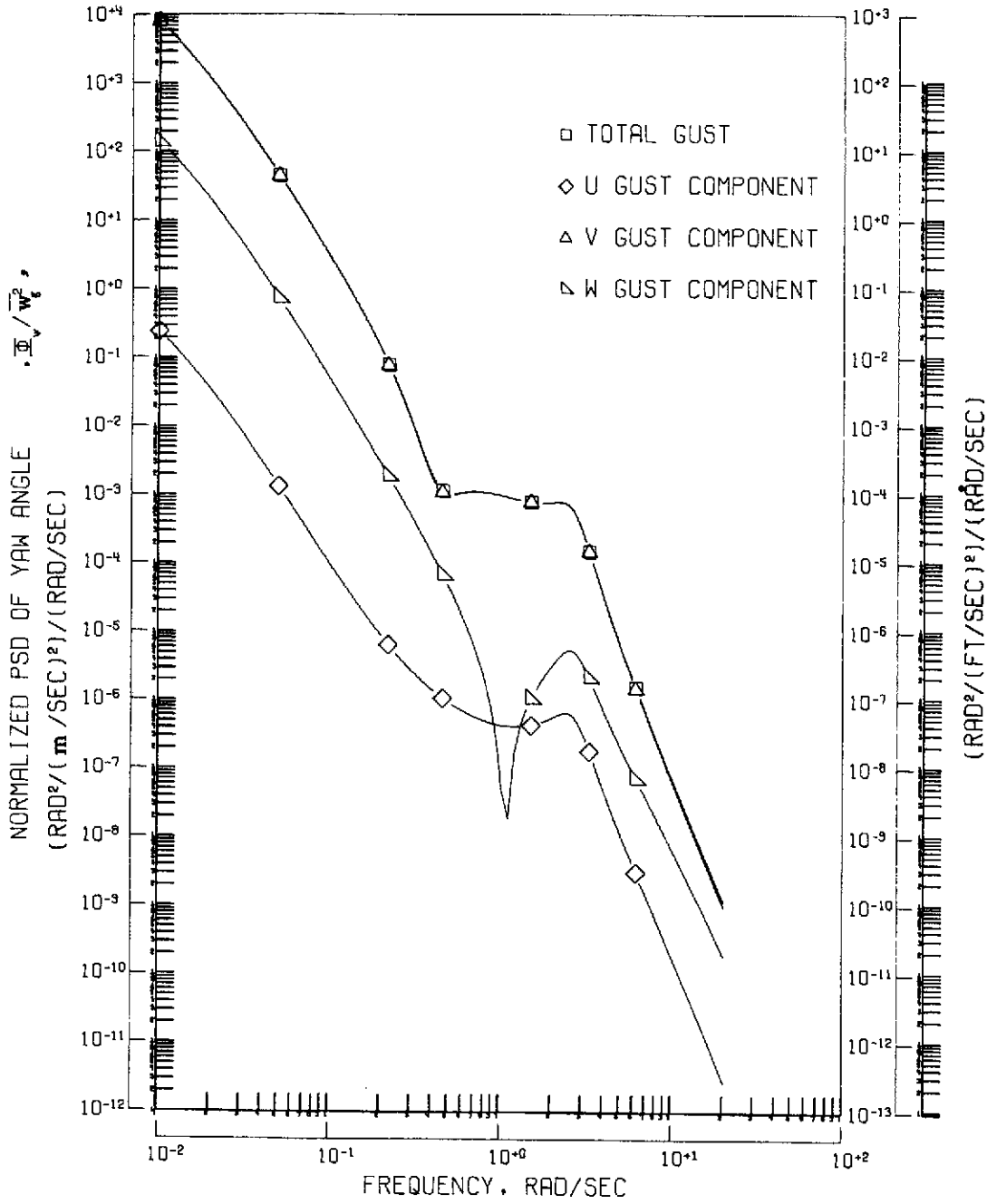

(c) Normalized total and individual component power spectral density response in yaw for each of the gust components.

Figure 10.- Continued.

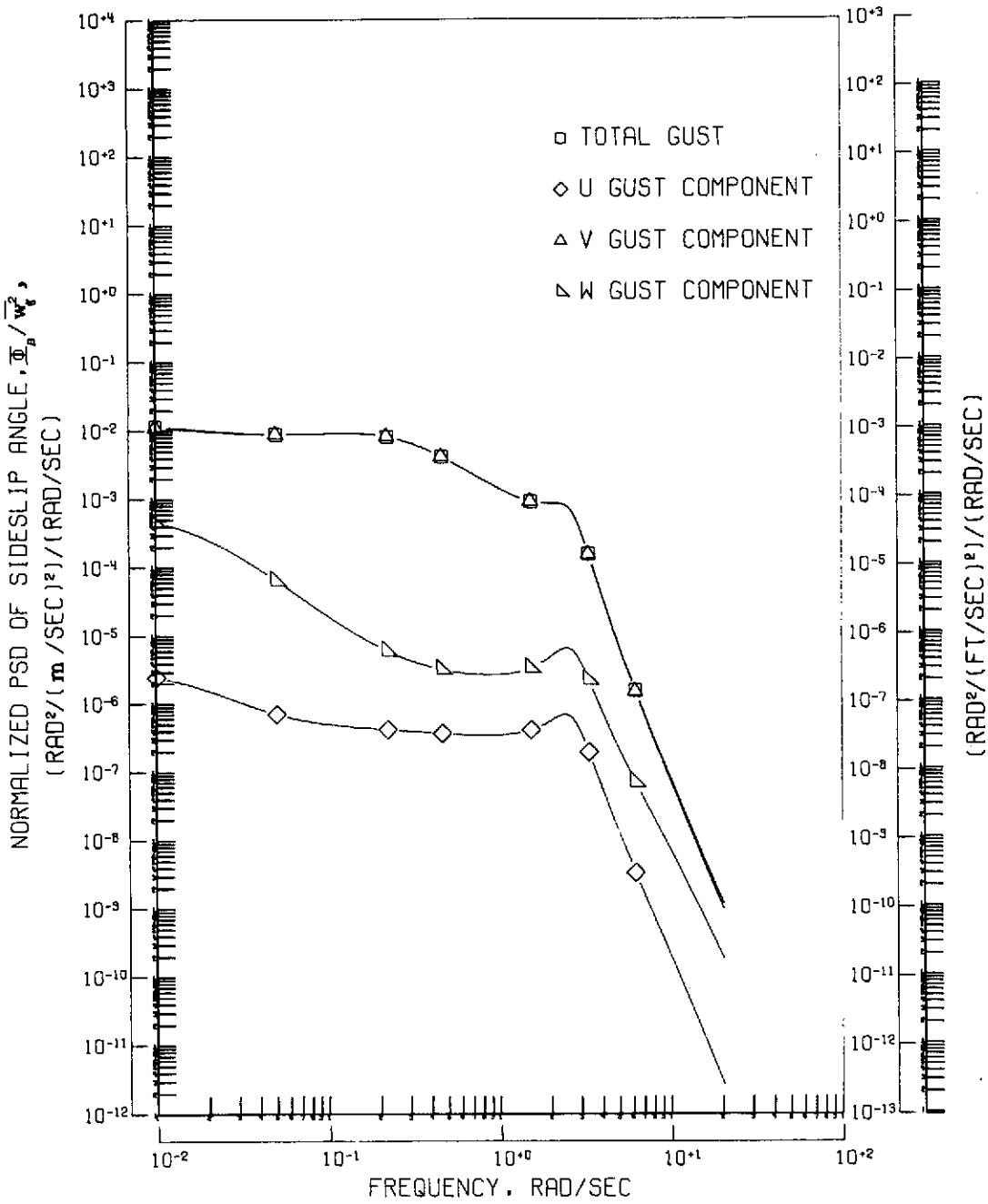

(d) Normalized total and individual component power spectral density response in sideslip for each of the gust components.

Figure 10.- Continued.

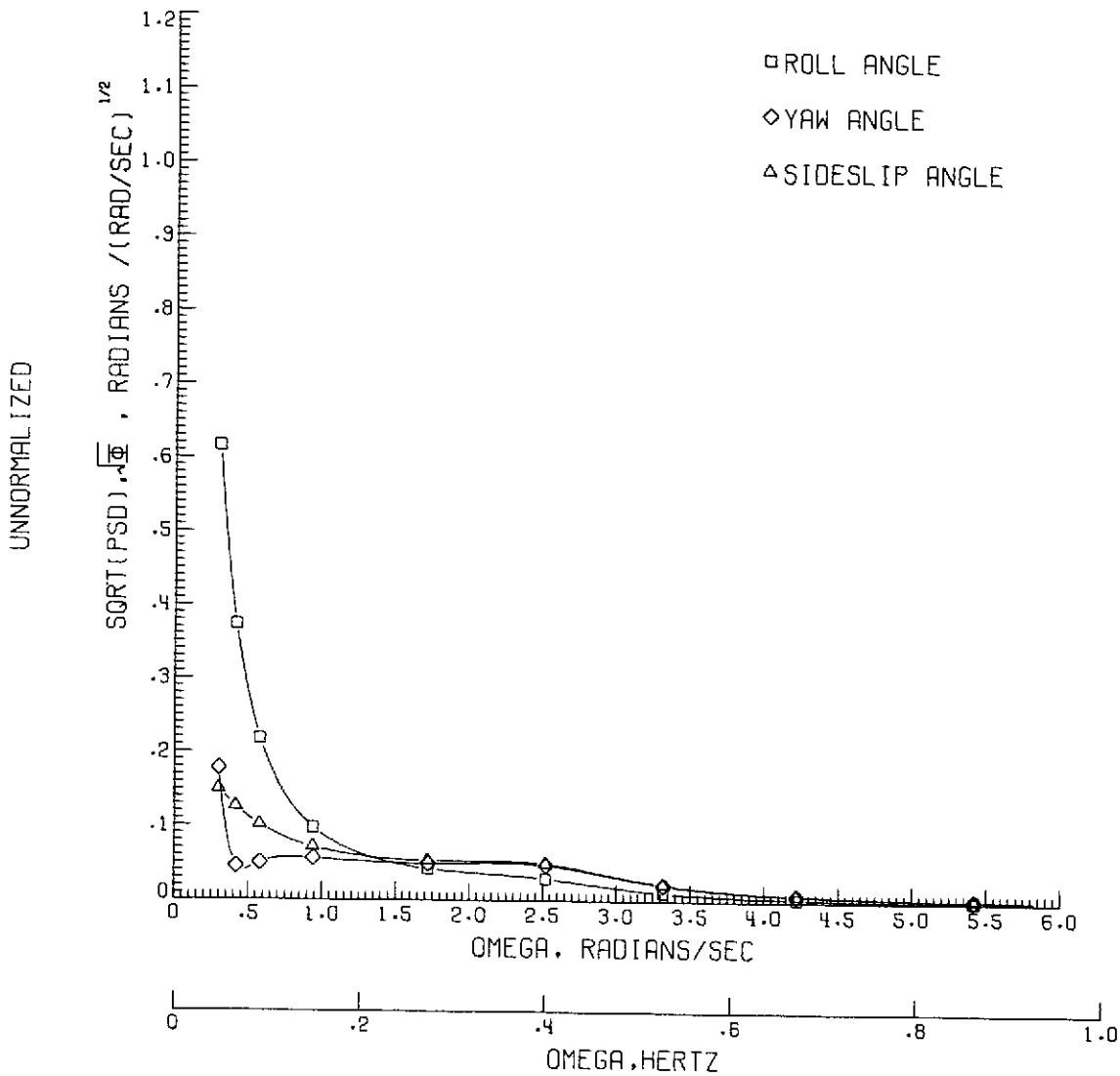

(e) Square root of the dimensional power spectral density response for each of the lateral displacements. The average gust intensity was 1.83 m/sec (6 ft/sec).

Figure 10.- Concluded.

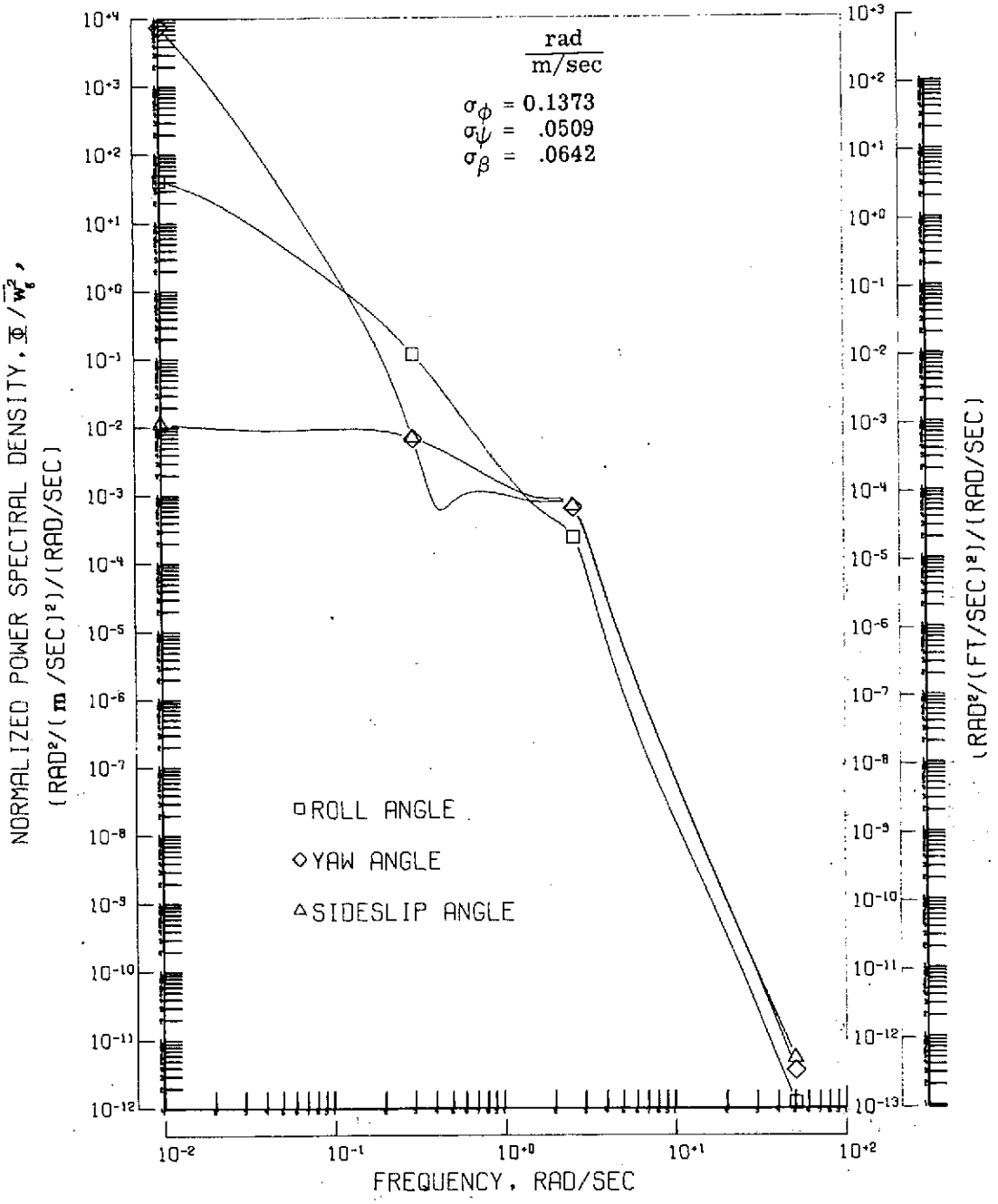

(a) Normalized total power spectral density response for each of the lateral displacements.

Figure 11.- Response of "small STOL C" airplane to random gusts for an assumed scale length of 335.28 m (1100 ft).

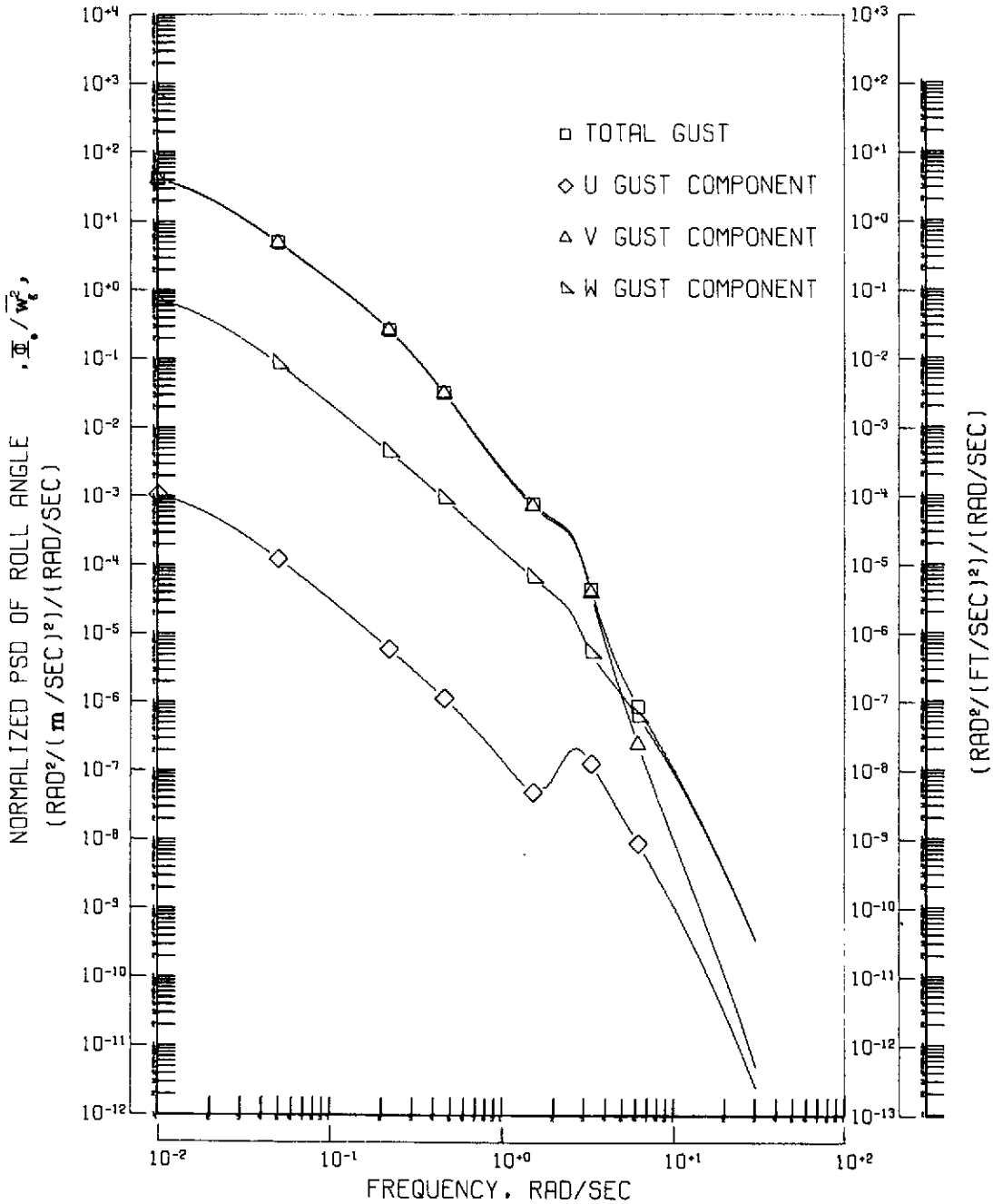

(b) Normalized total and individual component power spectral density response in roll for each of the gust components.

Figure 11.- Continued.

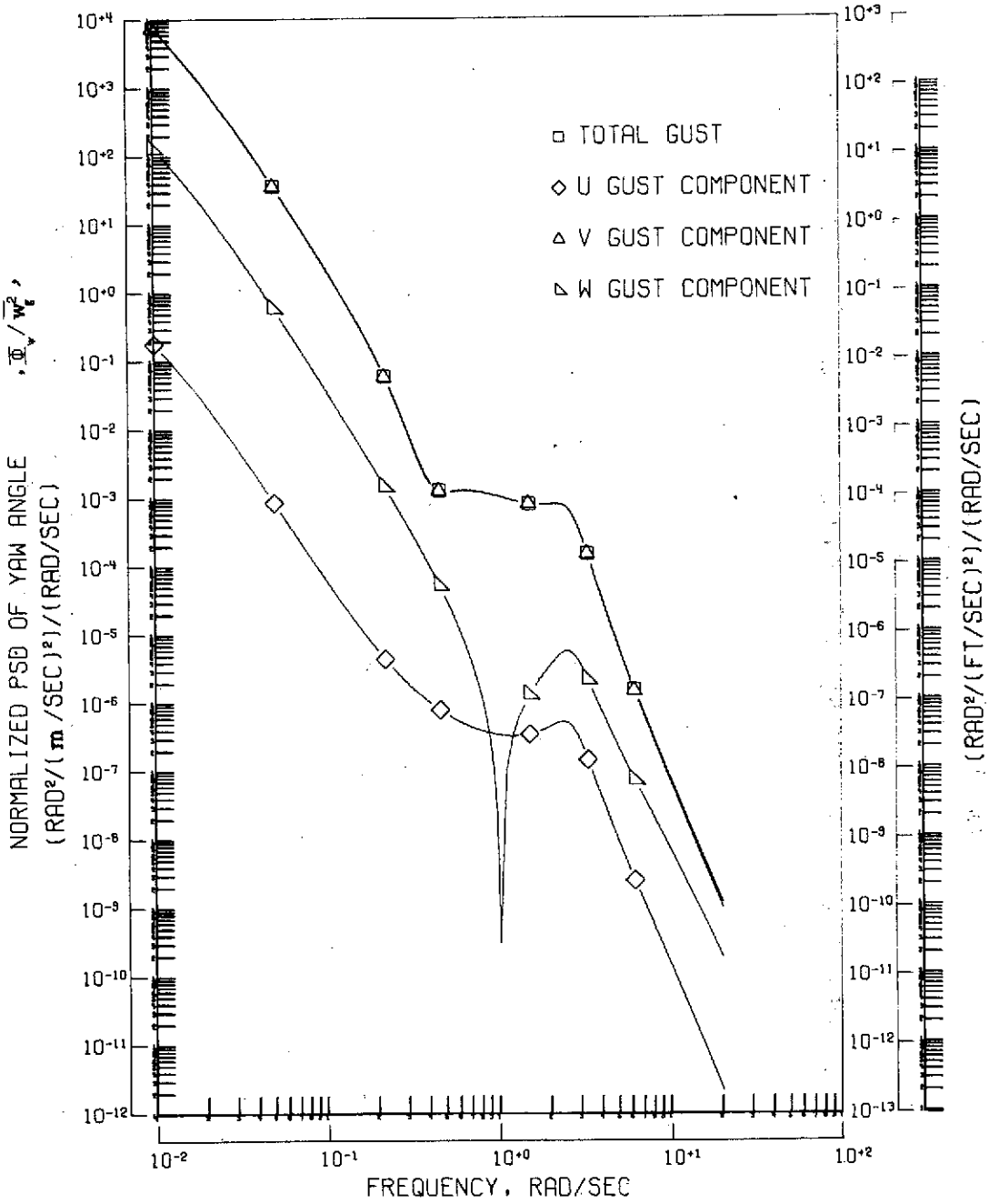

(c) Normalized total and individual component power spectral density response in yaw for each of the gust components.

Figure 11.- Continued.

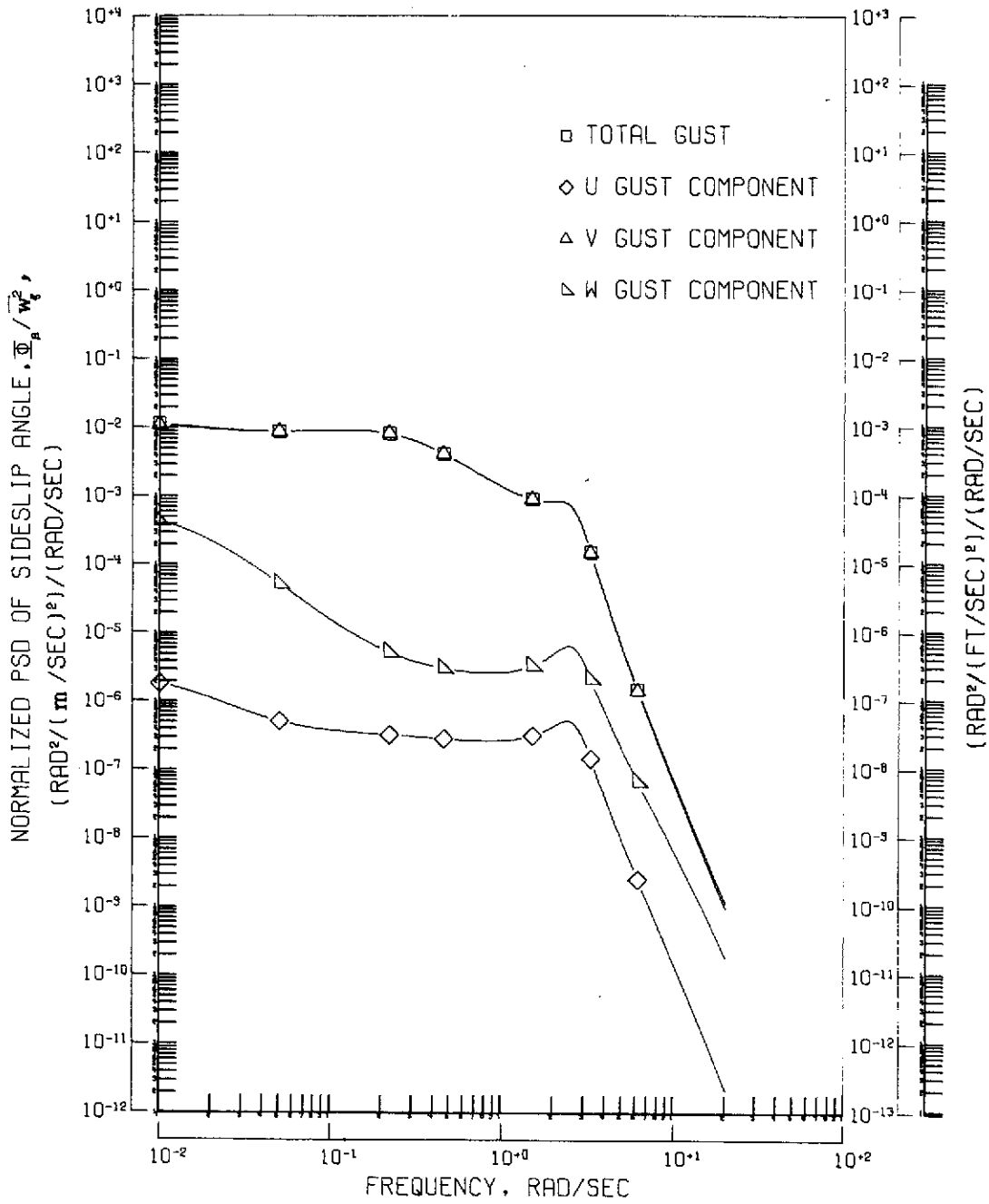

(d) Normalized total and individual component power spectral density response in sideslip for each of the gust components.

Figure 11.- Continued.

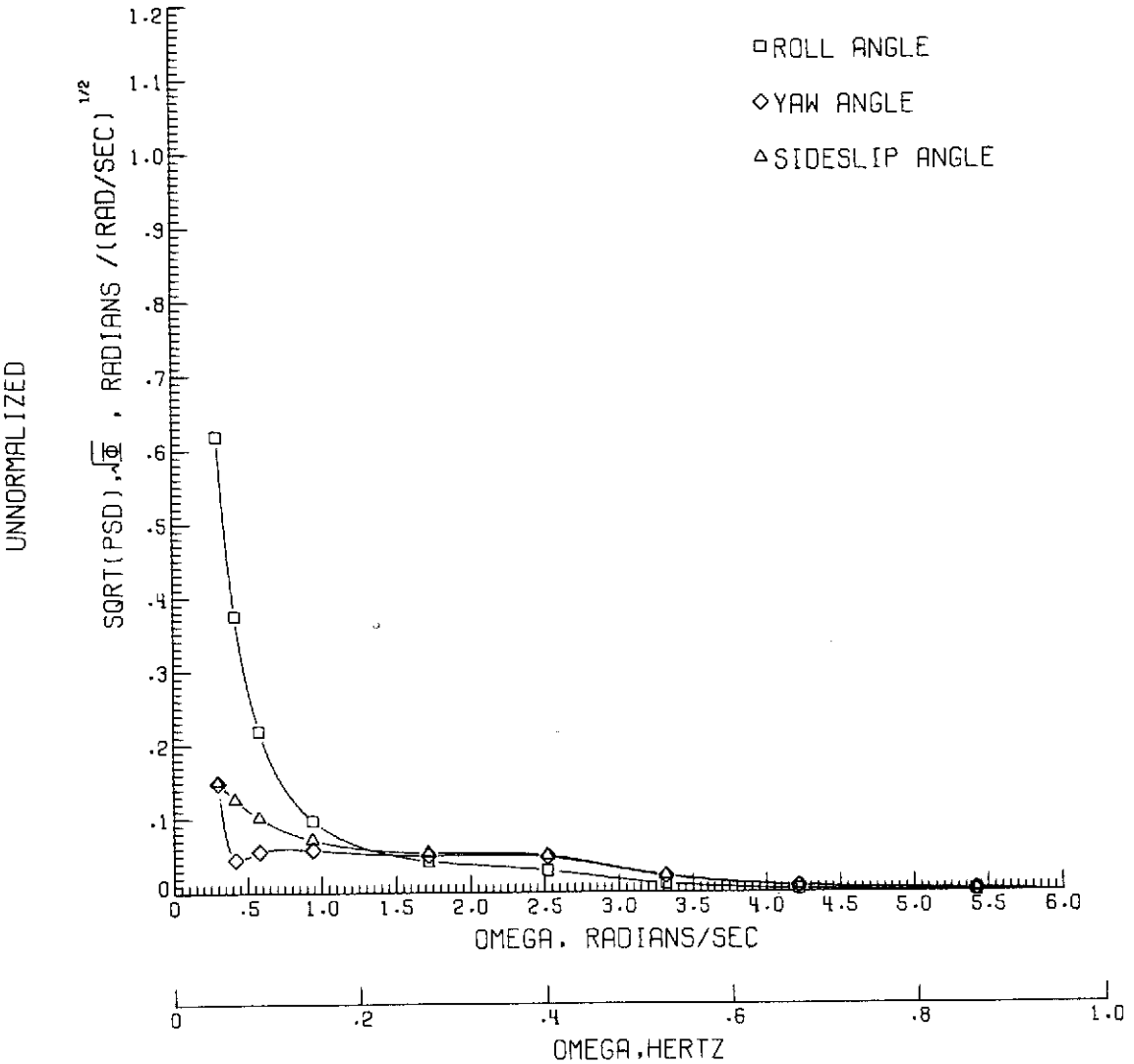

(e) Square root of the dimensional power spectral density response for each of the lateral displacements. The average gust intensity was 1.83 m/sec (6 ft/sec).

Figure 11.- Concluded.

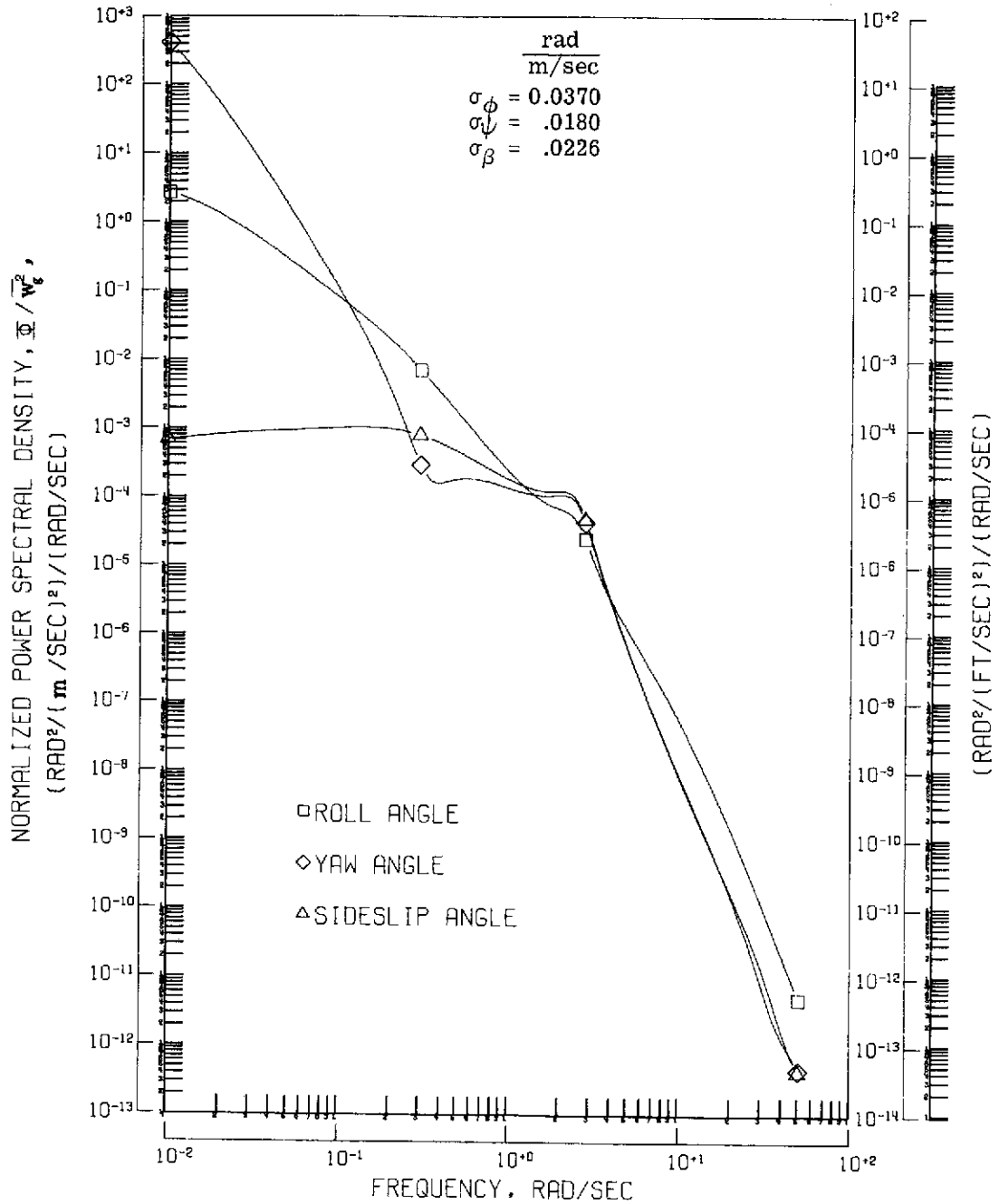

(a) Normalized total power spectral density response for each of the lateral displacements.

Figure 12.- Response of "small STOL D" airplane to random gusts for an assumed scale length of 335.28 m (1100 ft).

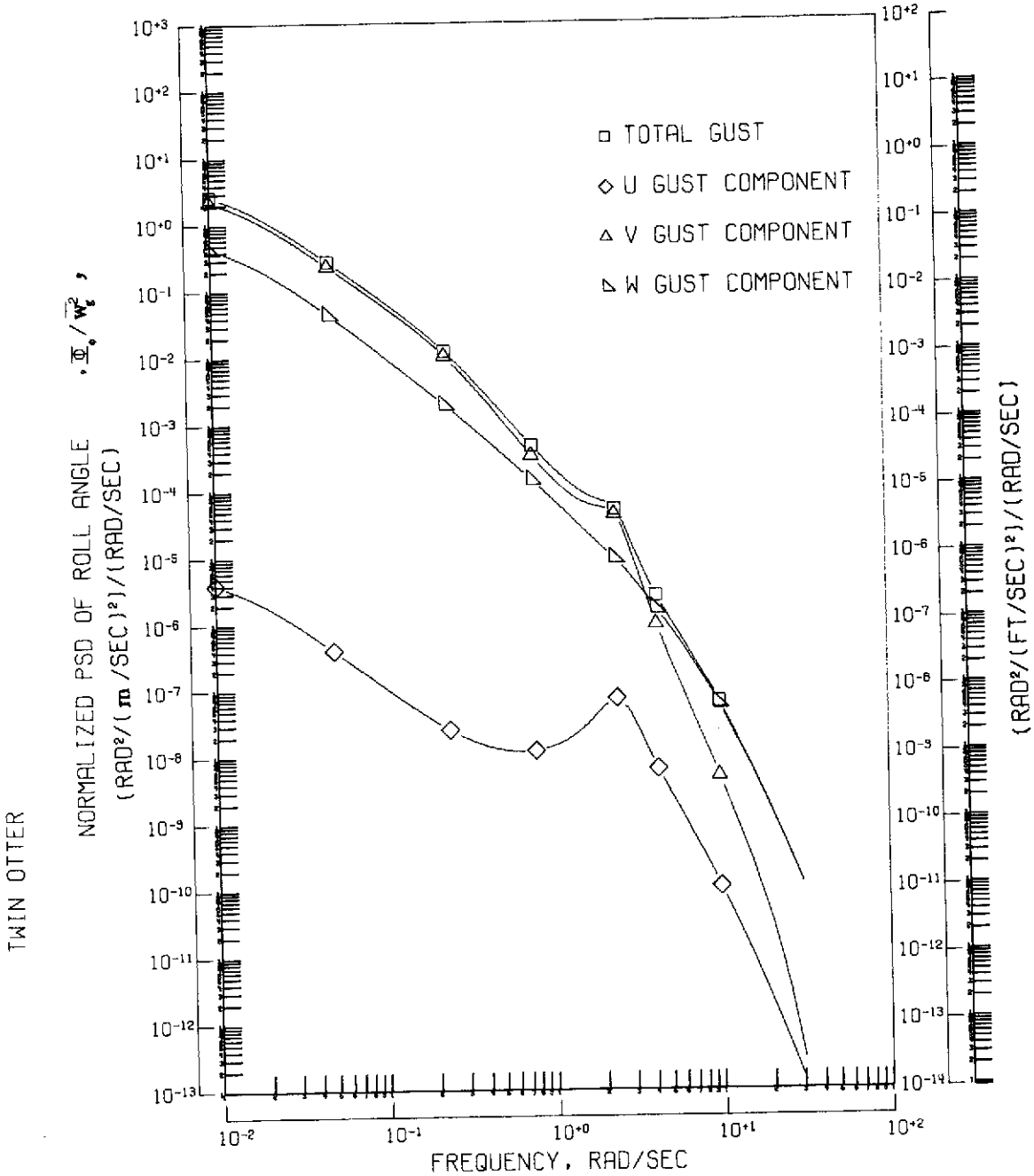

(b) Normalized total and individual component power spectral density response in roll for each of the gust components.

Figure 12.- Continued.

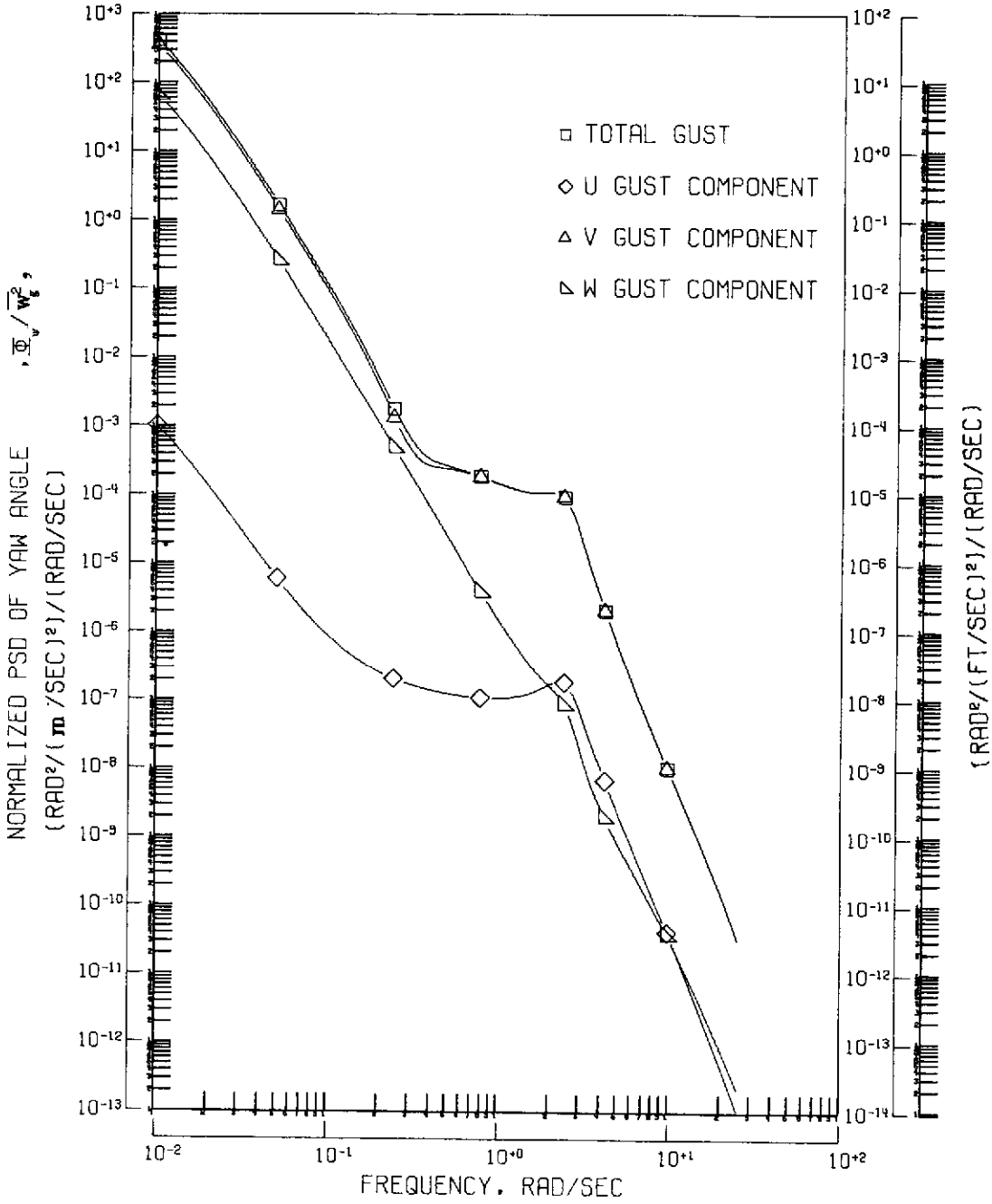

(c) Normalized total and individual component power spectral density response in yaw for each of the gust components.

Figure 12.- Continued.

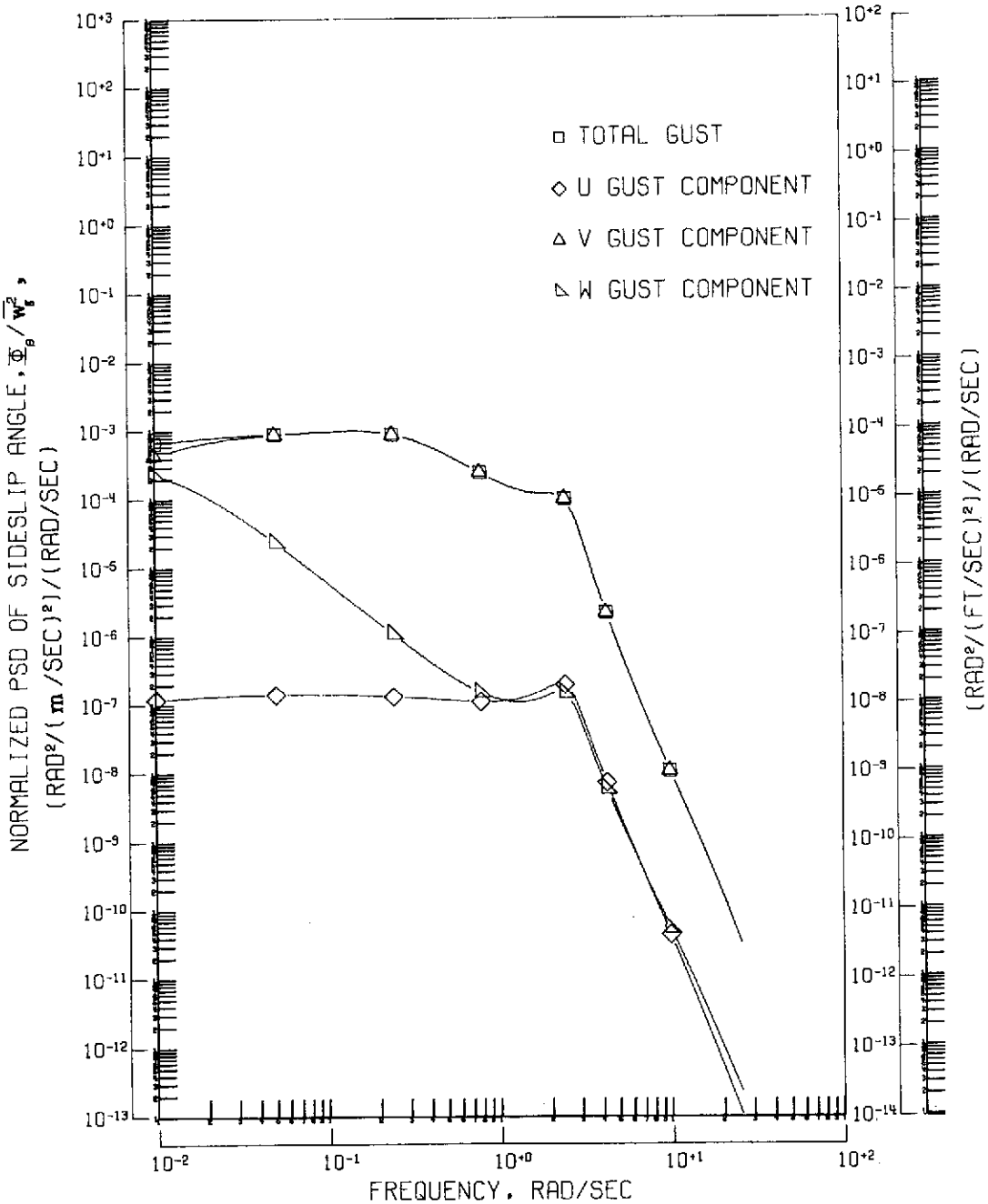

(d) Normalized total and individual component power spectral density response in sideslip for each of the gust components.

Figure 12.- Continued.

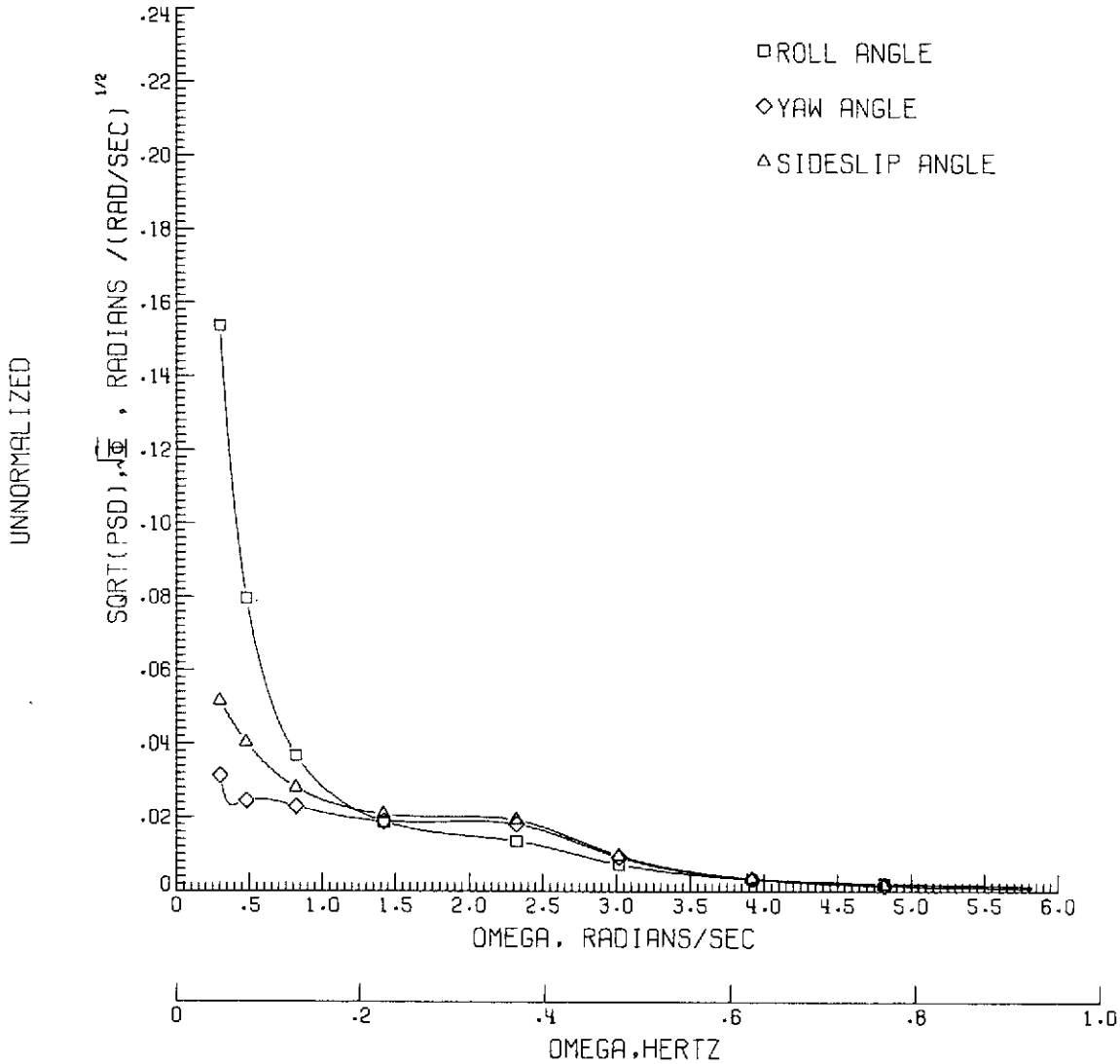

(e) Square root of the dimensional power spectral density response for each of the lateral displacements. The average gust intensity was 1.83 m/sec (6 ft/sec).

Figure 12.- Concluded.

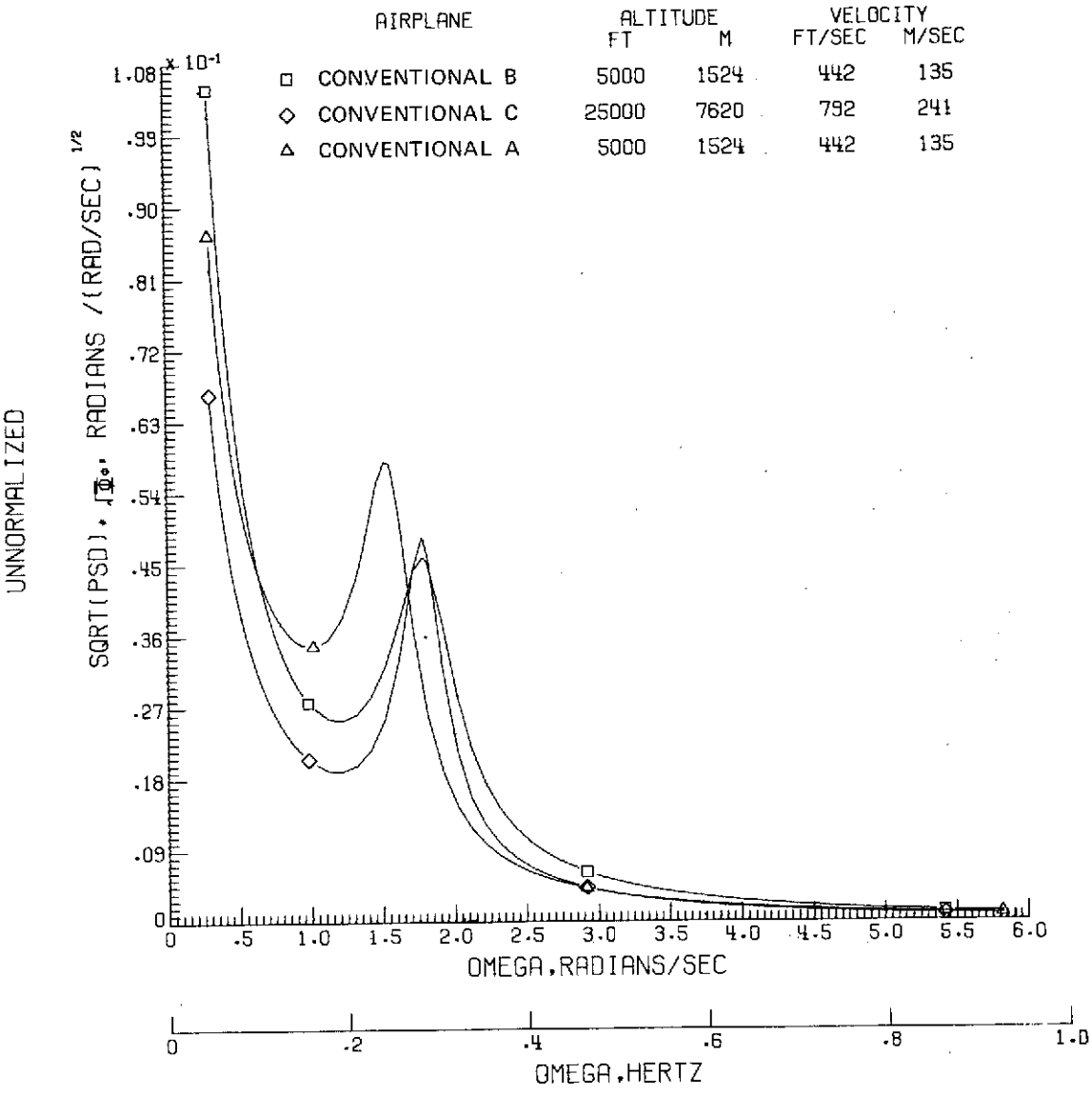

(a) Square root of roll angle power spectral density.

Figure 13.- Comparison of the square root of the power spectral density for "conventional A, B, and C" airplanes. $\left(\sqrt{\overline{w_g^2}} = 1.83 \text{ m/sec } (6 \text{ ft/sec}) \right.$ and $\left. L = 335.28 \text{ m } (1100 \text{ ft}).\right)$

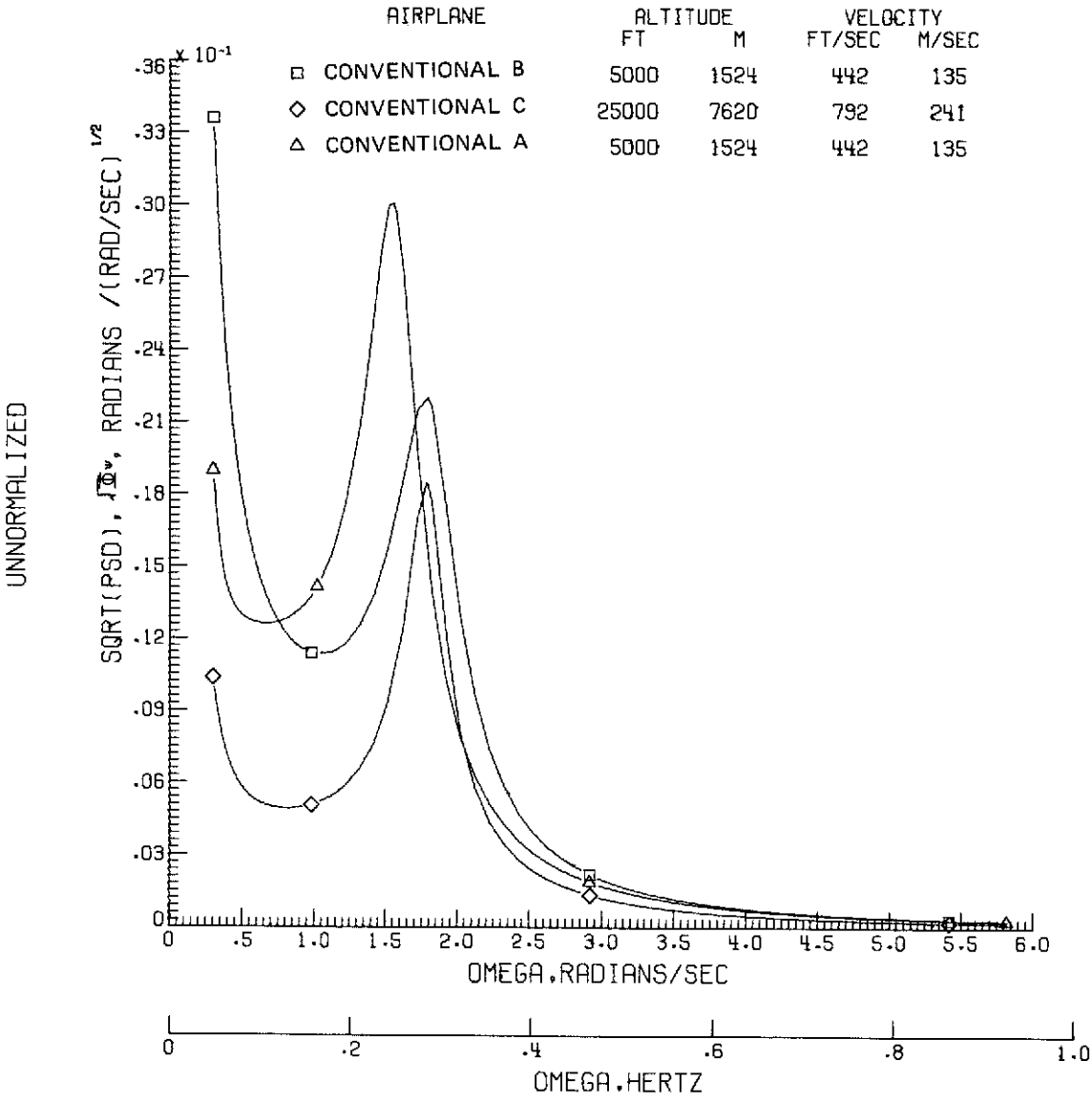

(b) Square root of yaw angle power spectral density.

Figure 13.- Continued.

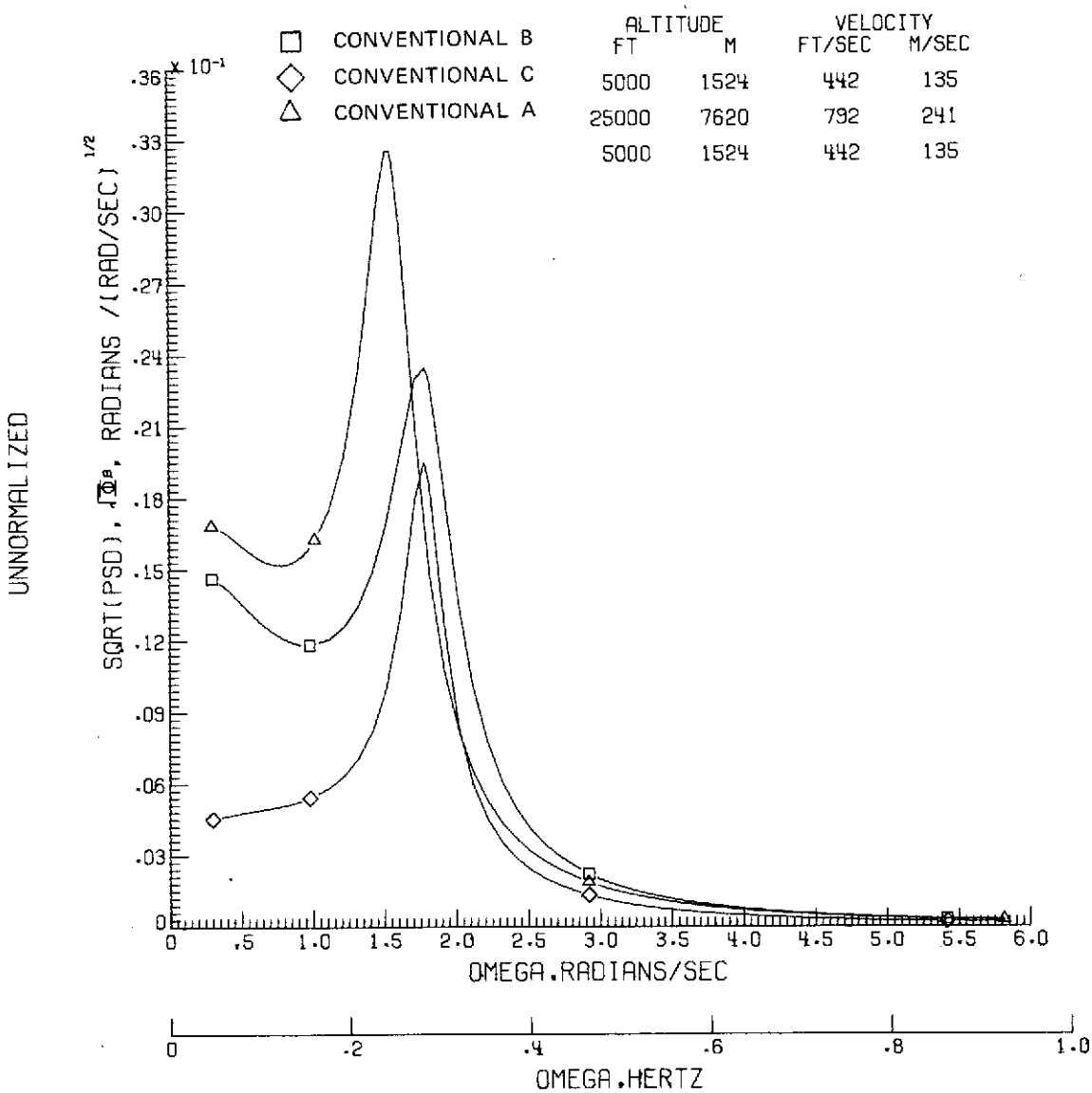

(c) Square root of sideslip angle power spectral density.

Figure 13.- Concluded.

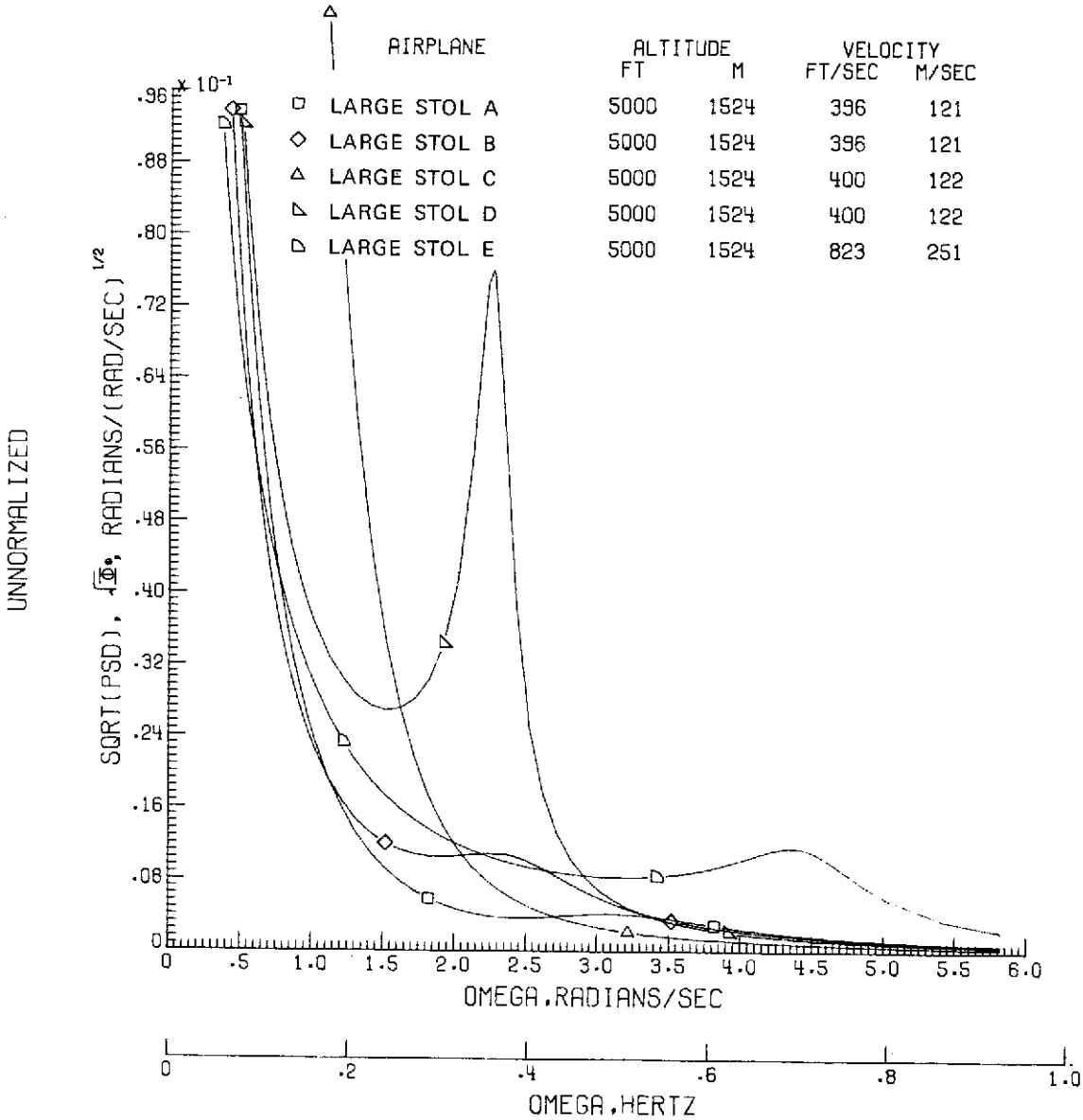

(a) Square root of roll angle power spectral density.

Figure 14.- Comparison of the square root of the power spectral density for "large STOL A, B, C, D, and E" airplanes. ($\sqrt{\overline{w_g^2}}$ = 1.83 m/sec (6 ft/sec) and L = 335.28 m (1100 ft).)

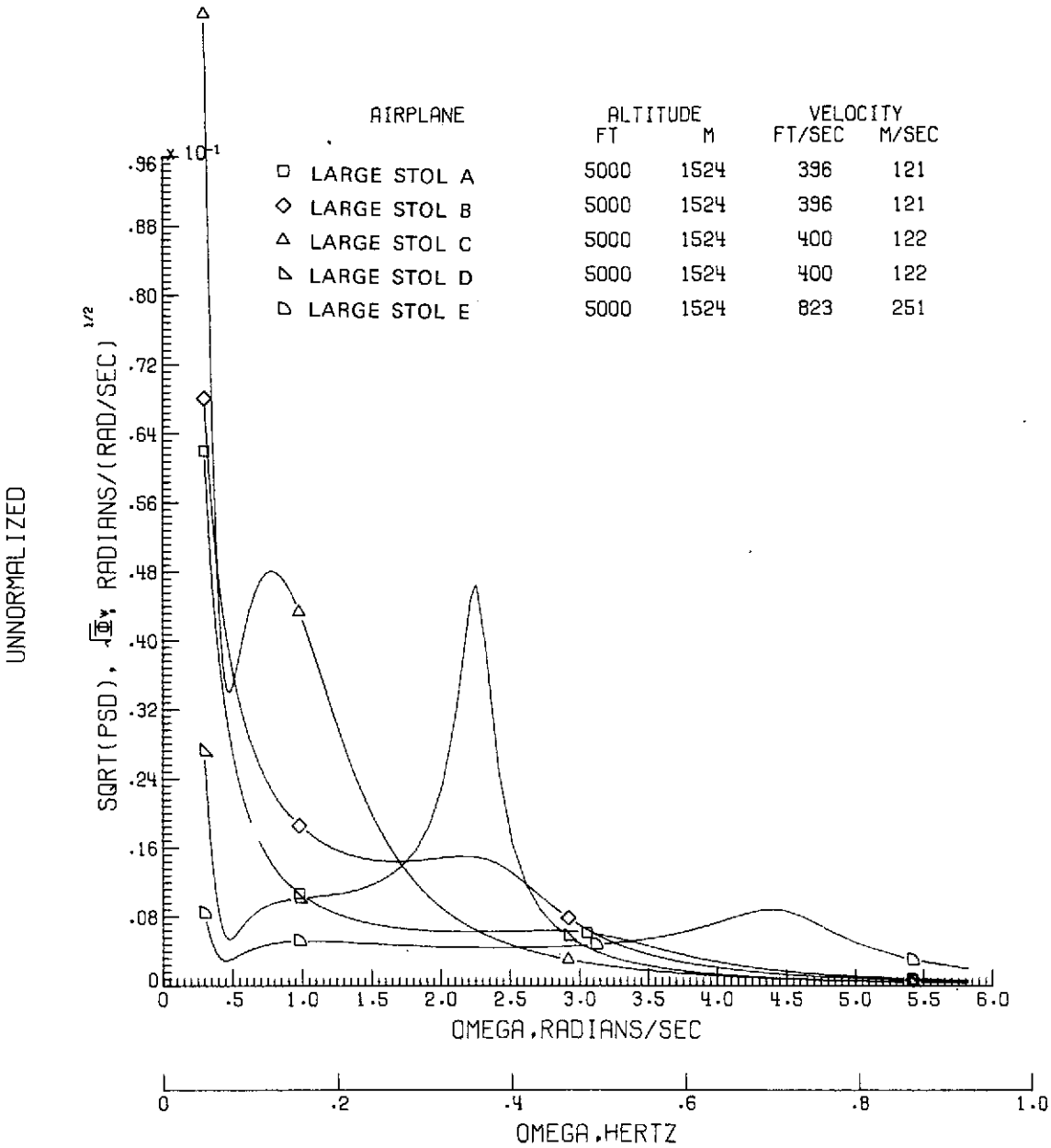

(b) Square root of yaw angle power spectral density.

Figure 14.- Continued.

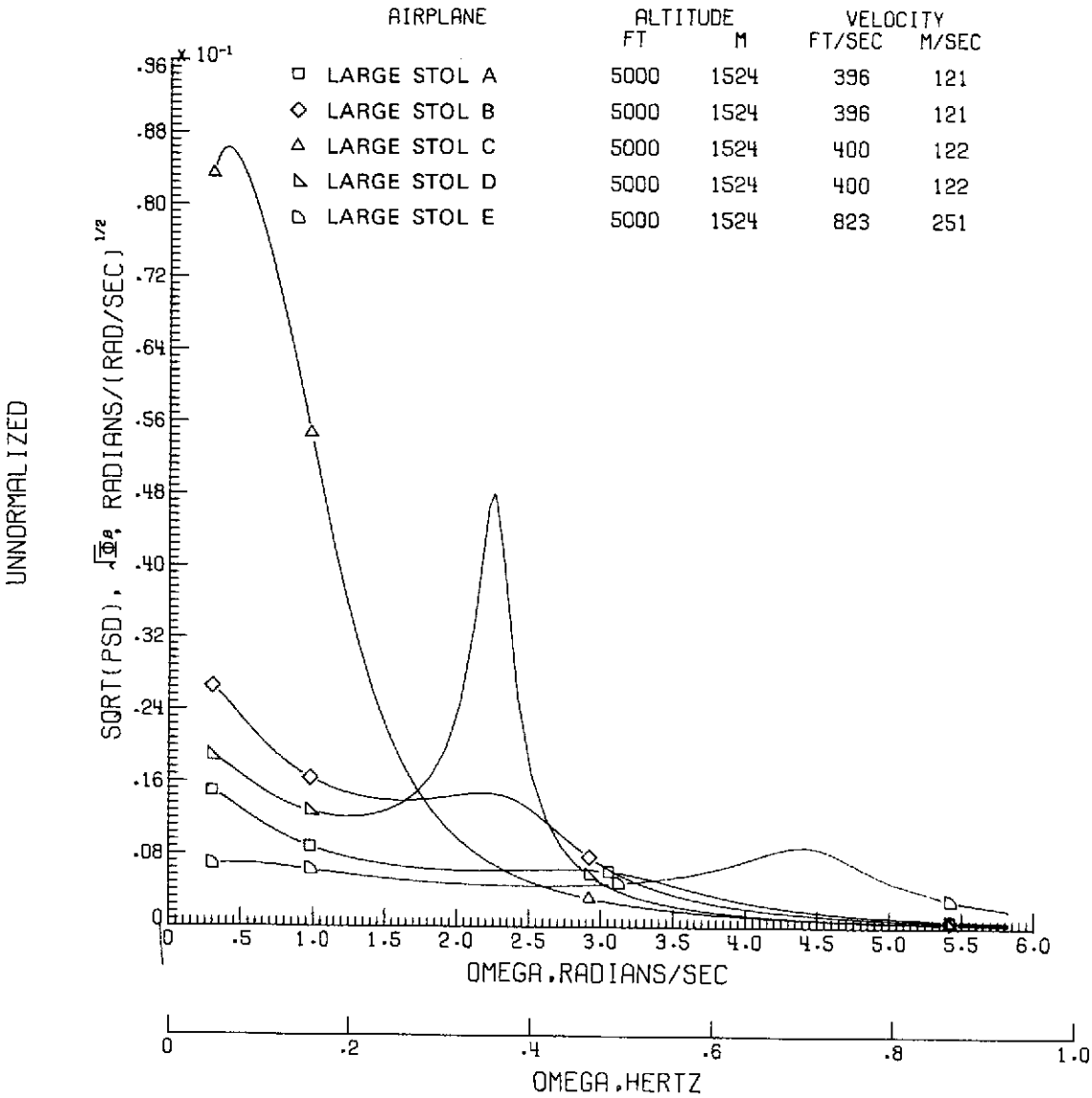

(c) Square root of sideslip angle power spectral density.

Figure 14.- Concluded.

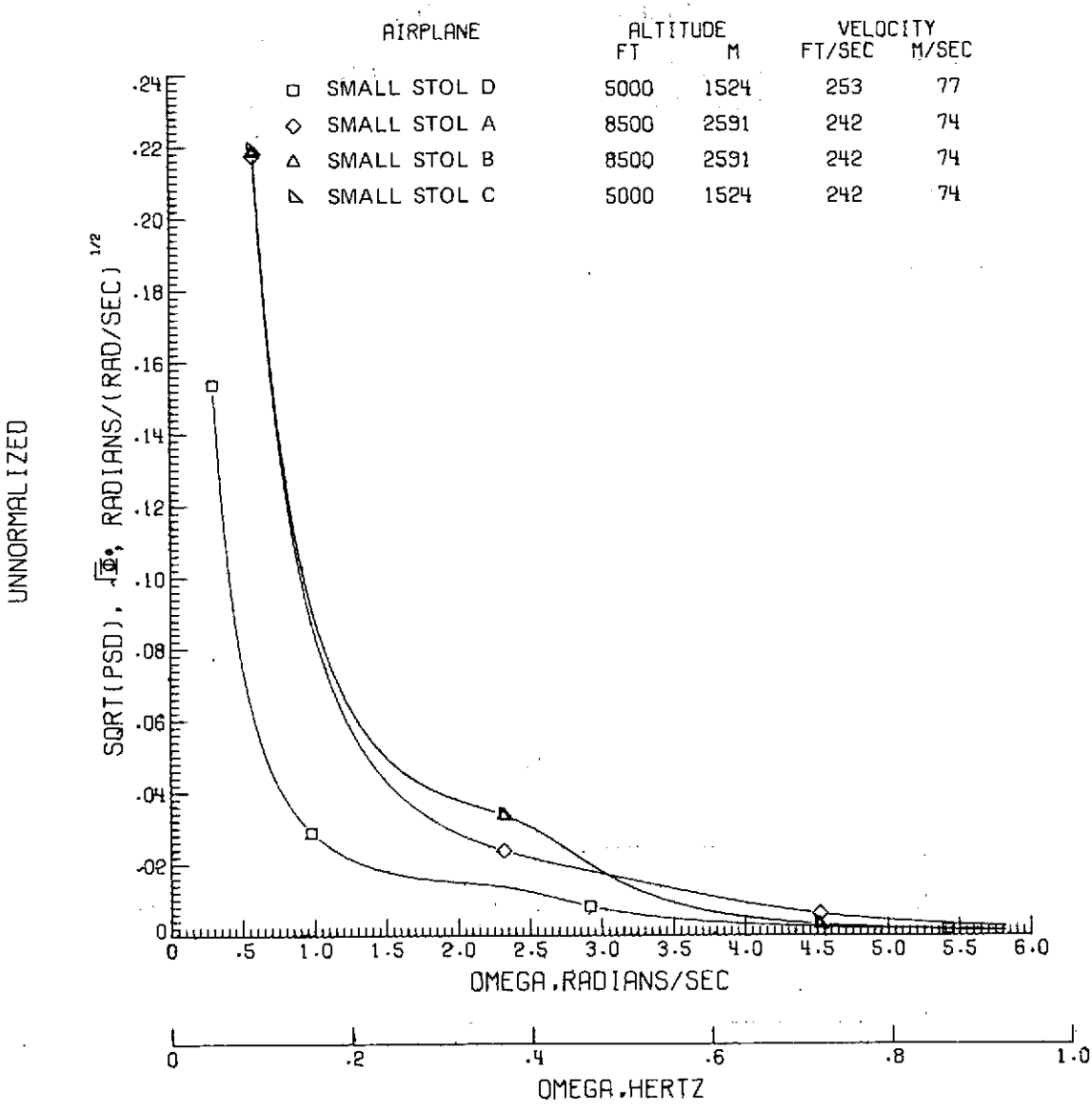

(a) Square root of roll angle power spectral density.

Figure 15.- Comparison of the square root of the power spectral density for "small STOL A, B, C, and D" airplanes. $\left(\sqrt{\overline{w_g{}^2}} = 1.83 \text{ m/sec (6 ft/sec)} \text{ and } L = 335.28 \text{ m (1100 ft)}.\right)$

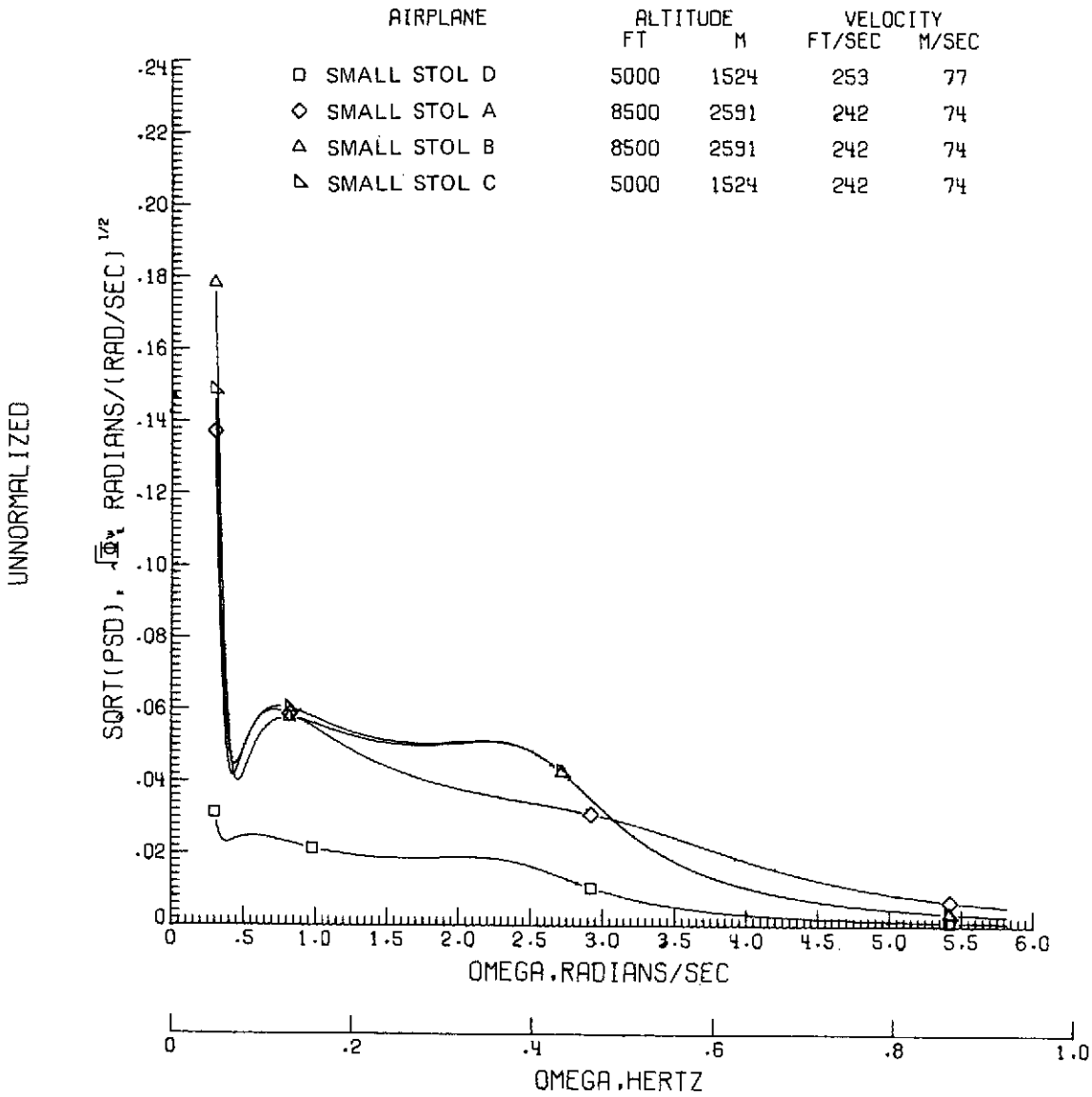

(b) Square root of yaw angle power spectral density.

Figure 15.- Continued.

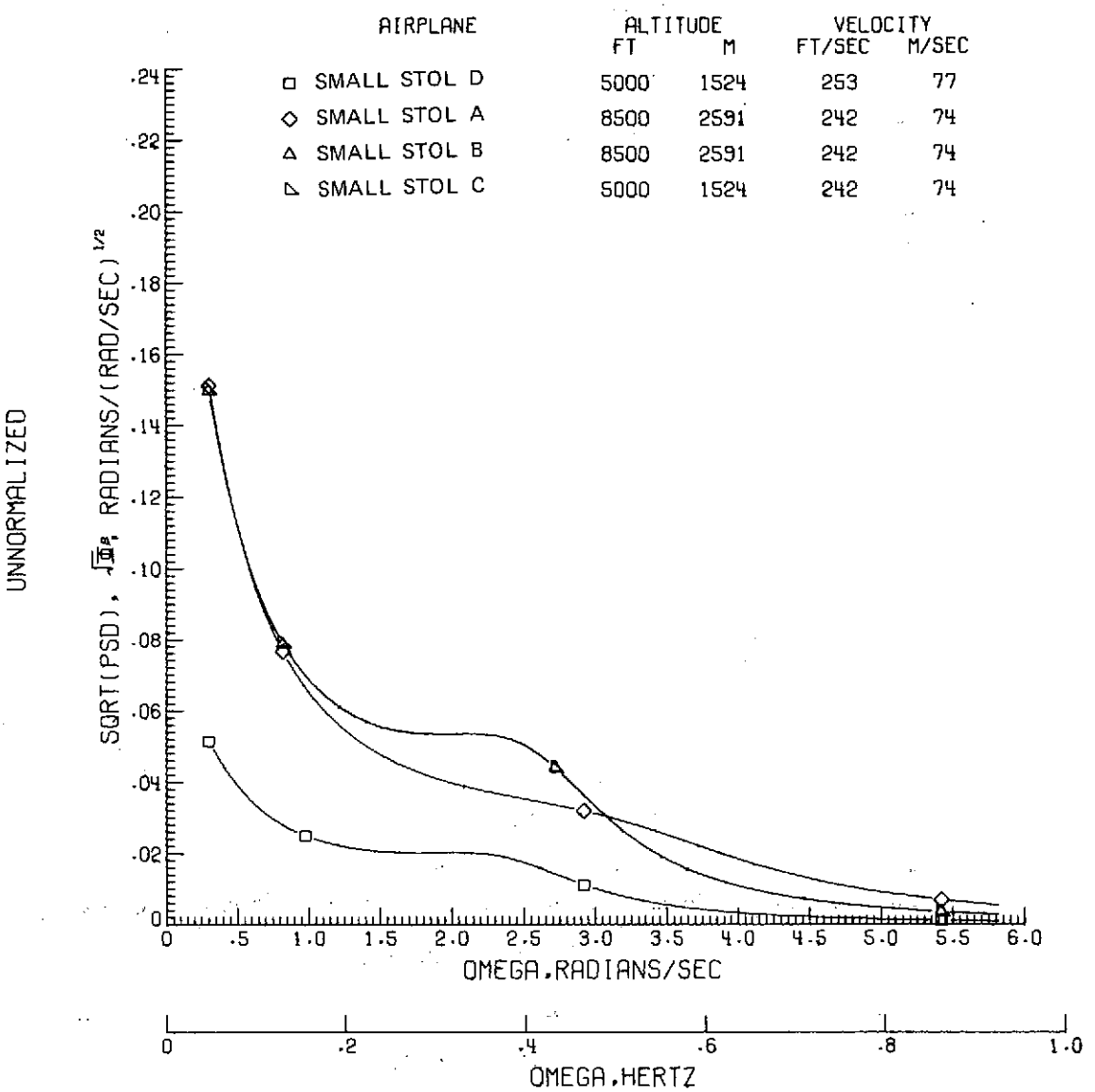

(c) Square root of sideslip angle power spectral density.

Figure 15.- Concluded.

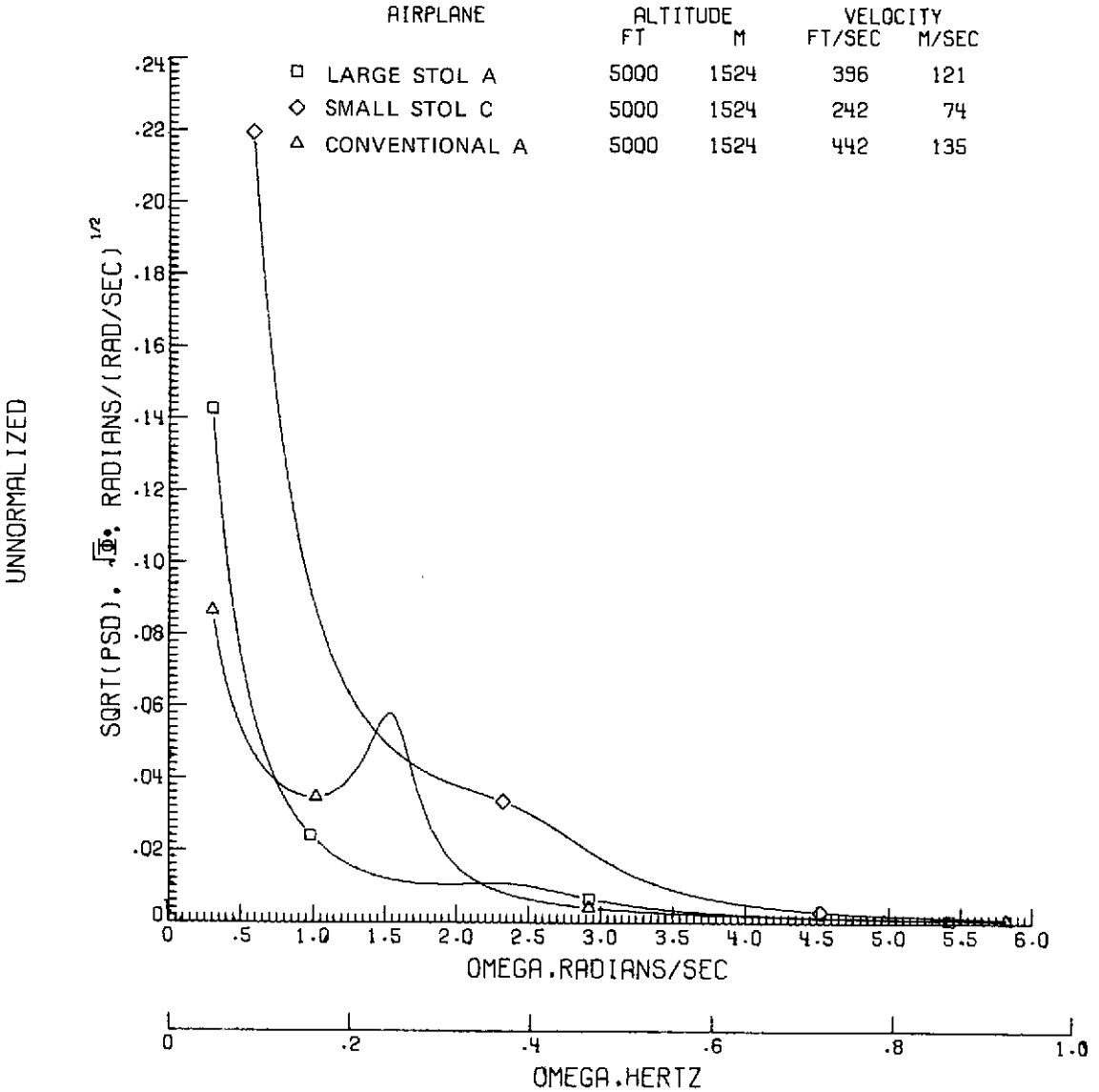

(a) Square root of roll angle power spectral density.

Figure 16.- Comparison of the square root of the power spectral density for a representative airplane from each of the groups.

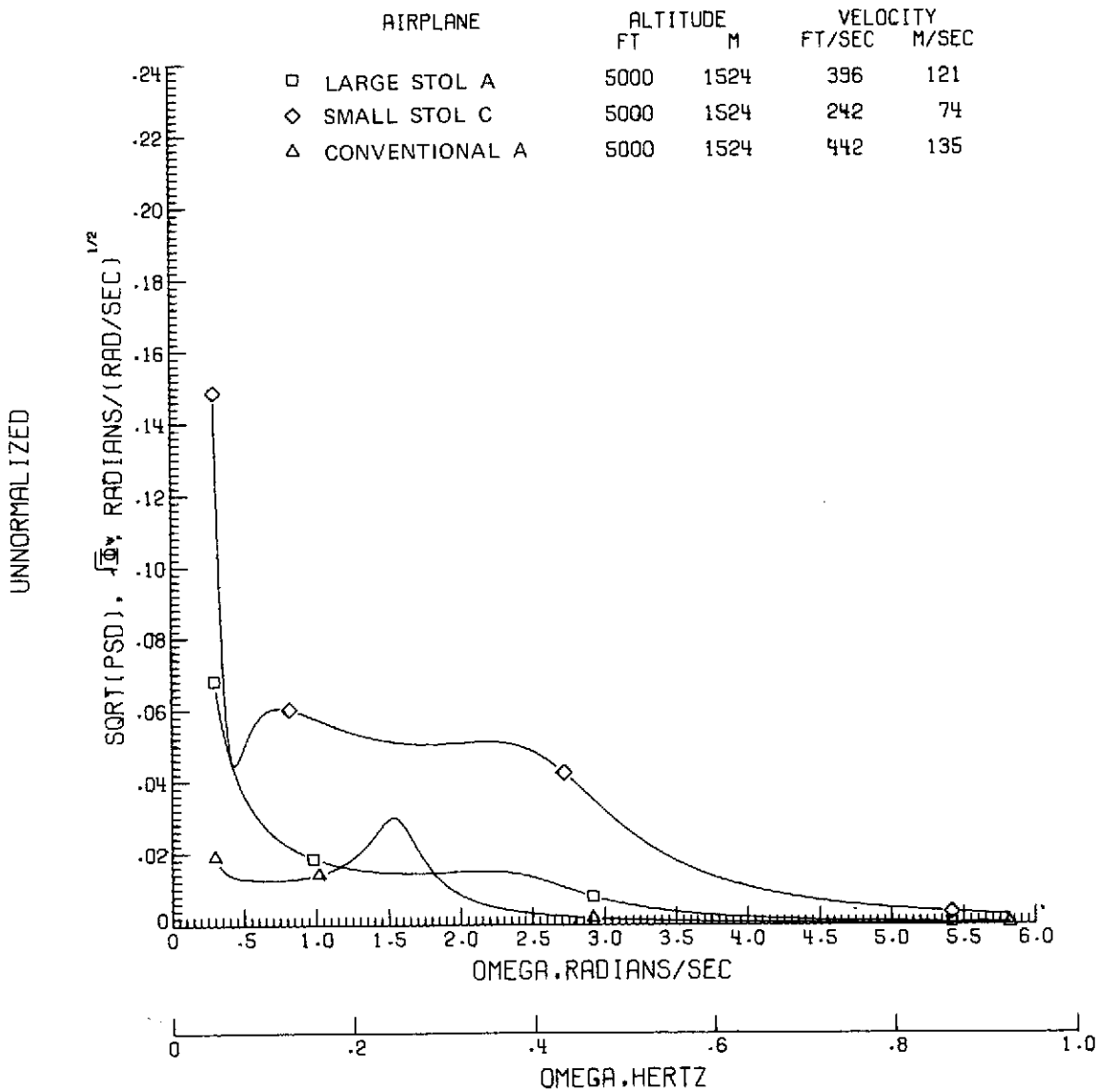

(b) Square root of yaw angle power spectral density.

Figure 16.- Continued.

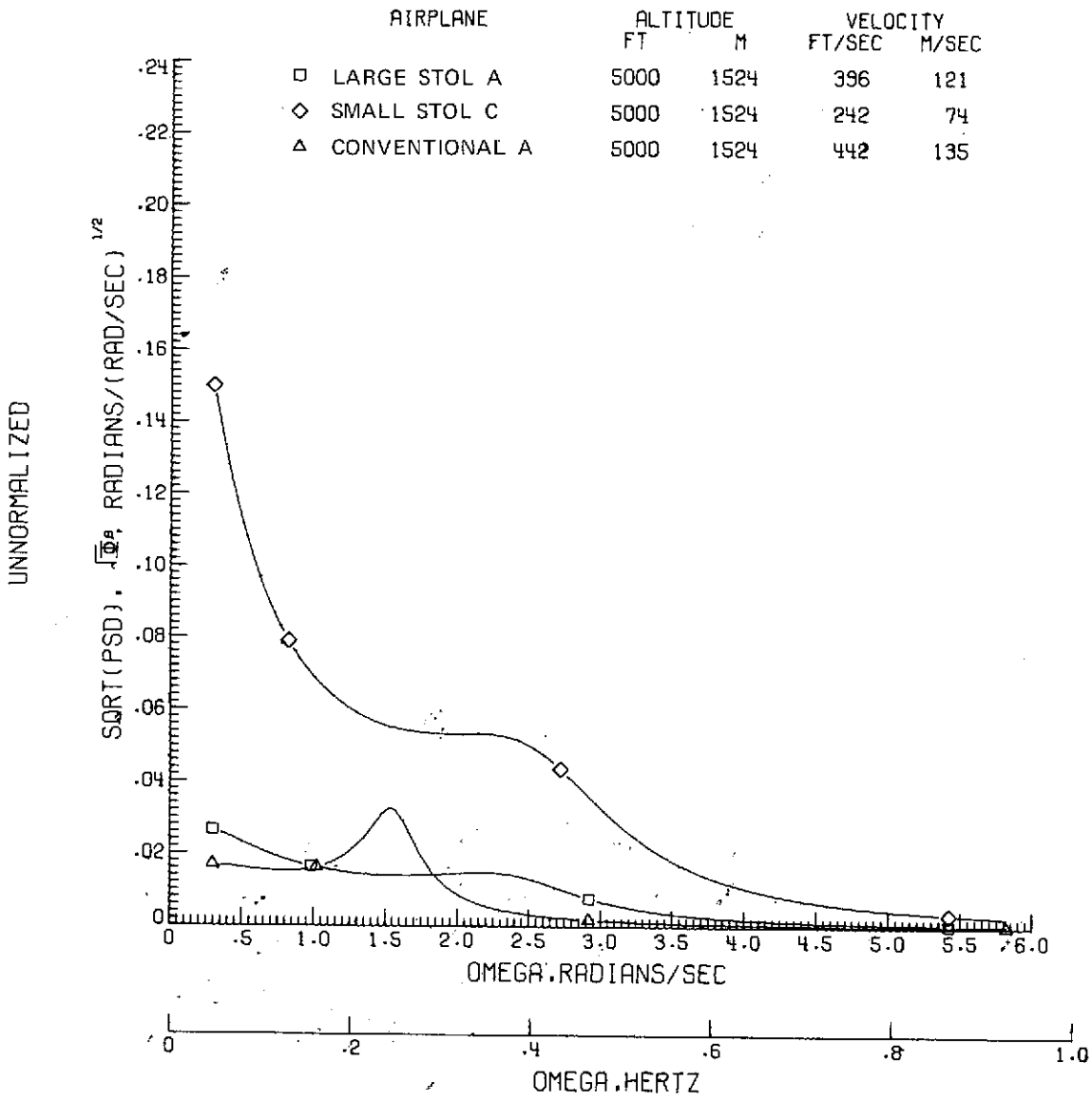

(c) Square root of sideslip angle power spectral density.

Figure 16.- Concluded.

NASA-Langley, 1974 L-9035